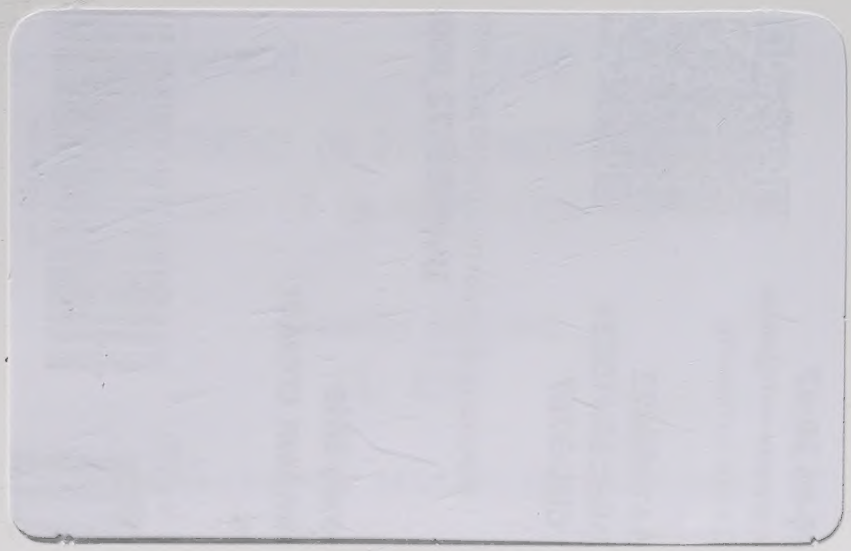

DEPARTMENT OF CHEMICAL ENGINEERING

AVDELNINGEN FÖR KEMISK APPARATTEKNIK

LUND INSTITUTE OF TECHNOLOGY
LUND – SWEDEN

CODEN: LUTKDH/(TKKA-1001)/1-10/(1980)

SOME STUDIES ON SIMULTANEOUS HEAT AND MASS TRANSFER IN ADSORPTION AND DRYING

KENNETH WERLING

DEPARTMENT OF CHEMICAL ENGINEERING
LUND INSTITUTE OF TECHNOLOGY
LUND
SWEDEN

DISSERTATION
APRIL 1980

Digitized by the Internet Archive
in 2026

https://archive.org/details/IA41553422_0012

SOME STUDIES ON SIMULTANEOUS HEAT AND MASS TRANSFER IN ADSORPTION AND DRYING

Kenneth Werling, Department of Chemical Engineering, Lund Institute of Technology, Lund, Sweden

This thesis consists of this summary and of the following papers, later referred to by Roman numerals:

I Werling K.
Adiabatic Drying of Hygroscopic Materials
First International Symposium on Drying, Science Press
Princeton 1978 36

II Werling K. and Wimmerstedt R.
A kinetic study of the adsorption and desorption process of two commercial molecular sieves
Accepted for publication in Chem. Engng Sci.

III Werling K.
On Non-Isothermal Adsorption and Desorption of Gases with Nonlinear Equilibria
Report LUTKDH/(TKKA-3005)/1-34/(1980), Dept. Chem. Eng., Lund Institute of Technology, 1980
(To be published in slightly revised form)

IV Werling K.
The Drying of a Crystalline Organic Material - A Case Study
Report LUTKDH/(TKKA-3004)/1-19/(1980), Dept. Chem. Eng., Lund Institute of Technology, 1980

INTRODUCTION

Adsorption and especially drying processes can be found in many industries. In adsorption, a component (or components) of a liquid or gas must diffuse into the usually porous adsorbent to the active surface. The adsorbate equilibrates with the matter on the internal surface and heat is generated. The equilibrium is normally considered to be reached very fast[1] so the adsorption kinetics is mainly controlled by the diffusional resistance in the pores. The generated heat raises the temperature of the adsorbent and because of that normally the adsorption rate is affected negatively. If the diffusion takes place in the opposite direction, the operation is known as desorption or regeneration. The gas-phase desorption is equivalent with the final drying of porous materials.

The knowledge of the kinetic behaviour of an adsorbent can be used for example to design a dehumidifying unit with regeneration of the saturated bed, and also to show how the unit may be controlled. However, the theory of nonisothermal sorption is maybe even more interesting in the case of final moisture removal in drying.

In many different types of industries, such as the chemical, food, agriculture and pulp industries, the operation of convective water removal from a solid matrix is of importance. The coupling between heat and mass transfer, when surface moisture is to be removed with hot air, is well-understood only if the surface of individual particles is available for the air stream. Less well-understood is the removal of internal moisture and the mass transport mechanisms which control the drying rate. Even if the amount of water, which is removed in the final stages of a drying operation, is comparatively small, the low drying rate determines the needed residence time of the material in the dryer and thus the size of the dryer and the capital costs. The temperature can in some cases be increased in order to increase the drying rate and thus decrease the size of the dryer. This often leads to pore utilization of the drying air and thus increasing energy costs. To find the optimum dryer design, a good knowledge of the diffusion-controlled removal of internal moisture is therefore essential. Sometimes such a knowledge can result in the design of two or more dryers in series. Each dryer is then optimized in a certain moisture content region.

If the rate of mass and heat transport can be formulated mathematically, the sorption behaviour in a specific type of contact equipment can be described by computer simulations. The unknown coefficients in the equations, which describe the process of the specific material, have to be determined in some small-scale experiments. Such computer simulations can also be used when designing control systems for a dryer. Frequently the direct continuous measurement of moisture content is not possible. If the coupling equations between heat and moisture transport are known, the temperature of the material or the temperature of the air in contact with the material can be measured and a good control-loop established.

Internal moisture can migrate to the surface in different ways. In one group of transport mechanisms, the rate is described by a gradient in moisture content. This group includes such mechanisms as liquid diffusion, surface diffusion and sometimes capillary movement. The transport coefficients are usually strongly temperature and moisture dependent, since they include such properties as viscosity and surface tension. In the investigations of molecular sieves (papers I-III), the other group of mechanisms, in which the rate is often described by a gradient in vapour pressure, has been found to be rate controlling. This group consists of ordinary vapour diffusion (Stefan diffusion) and Knudsen diffusion in the pores of the material. The vapour diffusion coefficient is almost unaffected by moisture content and temperature. Instead the equilibrium vapour pressure, and thus the driving force for mass transport, is strongly affected by both temperature and moisture content (for hygroscopic materials only).

Molecular sieves, which consist of small synthetic zeolites in a supporting material and which are strongly hygroscopic, have been studied during both adsorption and desorption of water. In desorption (drying), the heat, needed to release the adsorbed water, decreases the material temperature and thereby the equilibrium vapour pressure and desorption rate, compared to the isothermal case. In adsorption on the other hand, the adsorbed water releases heat and thereby increases the material temperature and vapour pressure. This results in lower adsorption rates than would have been expected in the isothermal case. The adsorption and desorption experiments together explain more about the internal mass transport process than only one type of experiments would have done. The heat and mass transport equa-

tions, which are coupled with the heat of sorption and the equilibrium relationship, form a system of partial differential equations. The unlinear equations can easily be integrated with the help of a computer.

During drying (or adsorption), a particle is always exposed to air of varying temperature and humidity, dependent on which type of contact-equipment it is processed in. One type, a through-circulated bed, has been investigated numerically for the cases of both adsorption and desorption.

The other investigated material, an organic non-hygroscopic crystalline material, was overdried in the industrial dryer in order to remove some remaining internal moisture, which was assumed to later migrate to the surface and cause clogging problems. Low heat efficiency was also found even when surface moisture was evaporated in the dryer. This was due to channelling in the bed. Possible means to get a better contact between individual particles and air were also investigated.

KINETICS OF MOLECULAR SIEVES

Molecular sieves are used for a variety of purposes involving the separation of both gases and liquids. Only their use as adsorbents for water in air will be discussed here. The commercial molecular sieve consists of small zeolite crystals, which are incorporated in a supporting material. The zeolite crystals are strongly hygroscopic and can in contrast to many other adsorbents dehumidify air at high temperatures. Two types of commercial molecular sieves have been investigated. One type, Union Carbide 4A, is in the form of pellets with diameter $3.18 \cdot 10^{-3}$ m and an average length of $6.17 \cdot 10^{-3}$ m. In the other investigated material, a corrugated, 10^{-4} m thick paper, arranged in a honeycomb structure, is the supporter for the 13X molecular sieve. A more thorough description of the structure and use of molecular sieves can be found in textbooks by Grubner et al[2] and Hersh[3].

Sorption properties

The most important property in adsorption-desorption processes is the equilibrium relationship between moisture of material, humidity of air and material temperature. In paper I a dynamic method for determining sorption isotherms is described. Air of a fixed humidity is produced by mixing one almost completely dry air stream with one fully saturated. The air is heated to the desired temperature level and blown through a sample of the material. The sample containers can easily be removed for weighing. Approximately 300 equilibrium data points were determined for each material in the vapour pressure range 20 - 2000 Pa and in the temperature range 20 - 400^{o}C.

The equilibrium data were fitted to a Clausius-Clapeyron expression:

$$\ln p^{*} = A(X) - \frac{\Delta H(X)}{R_o} \frac{1}{(T+273)}$$

where p^{*} is the equilibrium vapour pressure, R_o is the gas constant and T is the temperature (^{o}C). A(X) and $\Delta H(X)$ are polynomials with the moisture content X as argument. $\Delta H(X)$ describes how the heat of sorption (including heat of condensation) varies with moisture content. For both materials, six-parameter equations described the equilibrium relationship with a standard deviation less than 0.004 kg/kg in moisture content.

Next to the equilibrium relationship the heat of sorption is the most important sorption property as this affects the temperature change of material. It is directly given by the equilibrium function previously described. Later it was found that these functions had to be modified by approximately 10% to better correspond to the measured temperature change in the kinetic experiments.

The heat capacity level of the material is not so important except immediately after a sudden step change in boundary conditions has been made. This is due to the low time constant for heating compared with the time constant for adsorption. The results of the heat capacity determination for the two materials, in temperature and moisture range frequently encountered in practice, are also described in paper I.

Experimentals

In paper II and III some adsorption-desorption experiments are reported. The experiments were carried out in a new type of kinetic apparatus, which is described in detail in paper II. The method implies that the weight changes of a through-circulated bed after a step-change in humidity can be continuously measured by means of an electronic balance. In the experiments humidity and temperature changes in the through-circulated air were also measured. Fig. 1 shows the typical weight changes of a bed of pellets when the humidity is first raised (adsorption) and then lowered to the previous value (desorption).

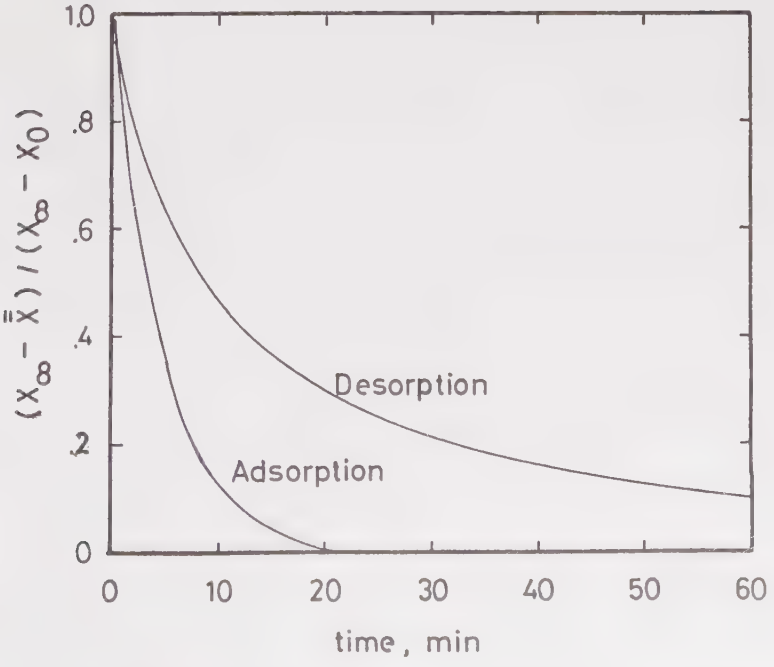

Fig. 1 Experimental sorption curves of a shallow bed of pellets after a step change in humidity

Although not fully tested, it also seems possible to simulate step changes in air temperature with a somewhat modified apparatus. To reduce any influences of natural convection forces upon the weight recording at changing temperatures, the whole bed of material is instead pushed into the hot air stream.

Mathematical modelling

In paper II a simple linear rate expression with an overall mass transfer coefficient was used to simulate the mass transfer of the adsorption-desorption experiments for both materials. Only external heat transfer resistance was considered. Mass and heat balances were also included to describe the changes of air temperature and humidity in the bed. The four equations were integrated numerically. By fitting the calculated results to the experimental, the overall mass transfer coefficient could be evaluated. Only the desorption experiments could be described satisfactorily for the pelletized material. In the desorption runs, the overall mass transfer coefficient was found to be approximately only five per cent of the theoretical film coefficient as determined from Gamson et al[4]. Both adsorption and desorption kinetics of the honeycomb molecular sieve were described well with a constant overall mass transfer coefficient. This coefficient was approximately 30% of the theoretical, as determined from Kays[5] and the analogy between heat and mass transfer. The difference in mass transfer rate between the two materials is easily explained by the difference in thickness.

The internal mass transport for the pelletized material has been investigated in paper III. Vapour diffusion in the individual particles has been found by others[6-8] to be the rate-controlling internal mass transport mechanism. To describe the transient behaviour of a single molecular sieve particle during both adsorption and desorption, both external and internal mass and heat transfer were included in the non-isothermal model. For molecular sieves, the isotherms have a curvature so that $\partial^2 p^*/\partial X^2$ is positive. This means that during adsorption, the equilibrium vapour pressure remains low and the driving force for adsorption thus remains high until the equilibrium moisture content is approached. In that way a sharp adsorption front was shown to recede into the particle. In desorption on the other hand, the equilibrium vapour pressure will decrease significantly after only a small change

in moisture content. Thus, the driving force is reduced faster in desorption than in adsorption and a rather flat moisture profile in the particle results. This also explains the found kinetic differences between desorption and adsorption in Fig. 1. The influence of internal temperature gradients was found to be negligible in the calculations.

Approximate rate equations were also formulated based on the calculated behaviour of one particle during adsorption and desorption. In adsorption, a "shrinking-core" model was formulated. In this model it is assumed that vapour has to diffuse through a saturated shell to an unaffected core. The diffusion length, i.e. the thickness of the saturated shell, can be determined from the average moisture content. The shrinking-core model was tested against the more complete model for both constant and varying boundary conditions. The shrinking-core model was found to follow the more complete model well. The model also gave a good description of the different adsorption experiments. A similar model has sometimes been used when describing drying rate curves[9-11]. In the drying of fertilizers[11], the isotherms have the opposite curvature, i.e. $\partial^2 p^*/\partial X^2$ is negative, compared to molecular sieves and consequently produce steep desorption fronts inside the particle of fertilizer during drying.

In paper II it was shown that some desorption experiments agreed well with the corresponding computor simulations, in which an approximate model with an overall or "lumped" mass transport coefficient was used to represent the desorption rate. The previous discussion about desorption explains why a "lumped" parameter model is successful in this case. The integration of the complete model for desorption showed that the steep moisture gradient remains close to the surface of the particle and the internal, rather flat, moisture profile is close to the average moisture content. The overall mass transfer expression now assumes vapour diffusion from a core of average moisture content through a thin outer shell of dry material and into the air bulk. The approximate desorption rate model was also compared to the more complete model for both constant and varying boundary conditions. The approximate model underestimates to a certain degree the desorption rate at higher moisture contents. As the regeneration time is determined by the lower desorption rates, the overall mass transfer coefficient was chosen so a good description at these rates was achieved. The same general difference was also found when comparing the desorp-

tion experiments with the results of the approximate model.

It can therefore be concluded that the difference between the adsorption and desorption curves of Fig. 1 is caused by the non-linear isotherms rather than any differences in mass transport mechanisms.

Calculated results of deep beds

The approximate mass and heat transport equations together with the mass and heat balances of a differential bed element were integrated numerically in the case of a 1.0 m bed of molecular sieve pellets during both adsorption and desorption (regeneration).

The molecular sieves have isotherms which during isothermal adsorption produce "constant-pattern" profiles. These types of isotherms are said to be "favourable". In isothermal desorption, on the other hand, the same isotherms produce "proportional-pattern" profiles i.e. the profiles become more and more extended. The same isotherms are said to be "unfavourable" for desorption. However, during non-isothermal adsorption the heat release deflects the real p^*-X path from that of the isotherm. An adsorption process was simulated and it was found that the bed quickly approached the constant-pattern behaviour. The regeneration was assumed to be performed by means of 200°C hot air. The high temperature deflects the non-isothermal p^*-X curve much from the isothermal. In the simulated example it was also shown that a region at low moisture contents existed, where the p^*-X curve was favourable. The role of the non-isothermal p^*-X curve has also been discussed by Vermeulen and Klein[12].

In both adsorption and desorption a two-front behaviour was noticed in the calculations. The first front is caused by the temperature change of material from the initial to an elevated temperature level. The velocity of this first front is determined by the ratio of heat capacity of air and material. The front is accompanied by a small change in humidity. The second, slower front is caused by the change in moisture content of material. The velocity of this front is therefore determined by the ratio of water capacity of air and material. The second front is accompanied by a change in temperature.

THE DRYING OF AN ORGANIC CRYSTALLINE MATERIAL - A CASE STUDY (PAPER IV)

The material, with an average particle diameter of $3 \cdot 10^{-4}$ m, was dried industrially from an initial moisture content of 0.15 - 0.20 kg/kg (dry basis) in a vibrated fluid bed dryer. In order to reduce the moisture content below 0.002 kg/kg the material temperature was raised over 100^{o}C before discharge. This was done as it was believed that remaining internal water later migrated to the surface of the particle and caused clogging problems in the transport of the dried material.

The drying kinetics was investigated in a small-scale drying apparatus under more constant conditions than could be achieved in the industrial dryer. Channelling immediately resulted if the air was blown from below through a stationary bed of wet material. By vibrating the whole apparatus good contact between particles and air was achieved. Other means employed to eliminate channelling, such as high kinetic energy of the air through the perforated plate, were not effective.

In the drying experiments it was found that only surface moisture existed down to the average moisture content of 0.006 kg/kg. The surface moisture was easily removed if the apparatus was vibrated. Even a bed of only 0.03 m in depth caused the inlet air of 110^{o}C to become fully saturated. After that the moisture content of 0.006 kg/kg was reached, the remaining "moisture" was removed only slowly and the material temperature was raised. All moisture contents so far had been determined by placing a sample of material in an oven at 105^{o}C for two hours. However, Karl-Fisher titration and liquid chromatography showed that a by-product called CMF also was present in the "moisture" analysis. Since the melting point of CMF is 60^{o}C, the presence of CMF is a more probable cause than migrating water of the clogging problems. The discovery also gave the guideline that the material and outlet air temperature should not exceed 60^{o}C, the melting-point of CMF. This necessitated careful control of the dryer. In the drying experiments it was also found that as the bed became drier the number of rising air bubbles and the entrainment rate of fine solids increased. Therefore a higher airflow can be used as long as the bed remains wet.

The importance of a good design of the distributor plate is also discussed in paper IV. Later contacts with the dryer manufacturer resulted in the replacement of the distributor plate with one which had a less

open area, and the drying efficiency was increased.

A literature review of some problems often encountered in the design of continuous fluid-bed dryers is also given.

ACKNOWLEDGEMENTS

This work has been carried out at the Department of Chemical Engineering, Lund Institute of Technology. The fourth paper of this thesis has been financed by the Swedish Board for Technical Development.

I wish to express my sincere gratitude to Professor Roland Wimmerstedt for his encouraging support throughout the course of this work.

I also wish to thank all my colleagues, of whom I would like to mention Anders Hallström especially, for stimulating discussions.

Many thanks are due to the technical staff of the department for their patience during many redesigns and reconstructions of different experimental equipment. I would also like to thank Hans-Olof Jönsson for skilful drawing and Sonja Dahlström for the excellent typing of my manuscripts.

REFERENCES

1. Dengler W. and Krückels W., *Chem. Ing. Techn.* 1970 42 1258

2. Grubner O., Jiru P. and Ralek M., *Molekularsiebe*, VEB Deutscher Verlag der Wissenschaften, Berlin 1968

3. Hersh C.K., *Molecular Sieves*, Reinhold Publishing Co., New York 1961

4. Gamson B.W., Thodos G. and Hougen O.A., *Trans. AIChE* 1943 39 1

5. Kays W.M., *Convective Heat and Mass Transfer*, 2nd ed. McGraw-Hill 1964

6. Kast W. and Jokisch F., *Chem. Ing. Techn.* 1973 45 538

7. Carter J.W., *Trans. Instn chem. Engrs* 1966 44 T253

8. Carter J.W. and Barret D.J., *Trans. Instn chem. Engrs* 1973 51 75

9. Schlünder E.U., *Chem. Ing. Techn.* 1976 3 190

10. Garside J., Lord L.W. and Reagan R., *Chem. Engng Sci.* 1970 25 1133

11. Hallström A., To be reported, Dept. of Chem. Eng., Lund Institute of Technology

12. Vermeulen T. and Klein G., *AIChE Symp. Ser. No. 117*, 1971 67 65

I

ADIABATIC DRYING OF HYGROSCOPIC MATERIALS

K. WERLING

Department of Chemical Engineering
Lund Institute of Technology
P.o.B. 740
S-220 07 LUND 7, Sweden

Paper presented at FIRST INTERNATIONAL
SYMPOSIUM ON DRYING, Montreal, Aug 3-5, 1978

ADIABATIC DRYING OF HYGROSCOPIC MATERIALS

K. Werling

Chemical Engineering, University of Lund, Sweden

ABSTRACT

This paper deals with the determination of material properties such as sorption isotherms and heat capacity, for a hygroscopic material. The hygroscopic agent, a molecular sieve, is impregnated in two different supporting materials. The report is the first from a research project investigating the drying process for hygroscopic materials.
The isotherms were determined with a kinetic method, where air was blown through a bed of material. The moisture content of the material was determined by weighing. From these isotherms the heat of sorption was calculated with the help of Clausius-Clapeyron's equation. It was found to vary between 3000 to 5000 kJ/kg.
The heat capacity measurements were made with a differential scanning calorimeter, where the samples were conditioned to different moisture content, estimated from the sorption isotherms.
A comparison between experimental fixed bed drying curves with those simulated on a computer gave satisfactory agreement, except for one of the materials. In this material a small discrepancy revealed a greater degree of internal mass transfer resistance.

NOMENCLATURE

a_v = specific area, m^2/m^3
c_p = specific heat, J/kgK
ΔH = heat of sorption, J/kg
$\dot{m}$ = mass flux of air, kg/m^2s
p = vapor pressure, N/m^2
R = water vapor gas constant, 460 J/kgK
s = standard deviation
T = temperature, K
t = time, s
w = solid moisture content, kg water/m^3 material
X = solid moisture content, kg water/kg dry material
Y = humidity, kg water/kg dry air
z = length coordinate, m
α = heat transfer coefficient, W/m^2K
β = mass transfer coefficient, kg/m^2s
ρ = density, kg/m^3
ρ_s = bulk density of solid, kg/m^3

Subscripts

g = gas
s = solid
v = vapor
w = liquid water
0 = beginning
1 = end

INTRODUCTION

This paper, describing the determintation and use of properties such as equilibrium data (i.e. sorption isotherms), heat of sorption and heat capacity, is the first report from a research project describing the kinetics of water adsorption and desorption of hygroscopic materials.
Water vapor adsorption and desorption from hygroscopic materials may be described by a mathematical model consisting of four differential equations. As a first part of the research project a solution routine was made for a computer. In these equations the properties, earlier mentioned, are needed. It was early on found that there was a need for more accurate knowledge about these properties than could be found in literature.
The specific selection of molecular sieves as the hygroscopic agent was made after taking such things as commercial use, availability, reproducability and available literature data, into consideration. The two materials investigated differ through the supporting material for the molecular sieves crystals. These two materials will therefore show different kinetic behaviour due to different properties and geometries.

DESCRIPTION OF MATERIALS

Molecular sieves are used for a variety of purposes involving the separation of both gases and liquids. They belong to a class of compounds known as zeolites. In contrast to other adsorbents, the

pores of any particular type of zeolite are uniform in size. Depending on the size of these pores, molecules may be adsorbed or completely excluded. They also have selective preference for polar or polarizable molecules.
The zeolite forms relatively large cavities connected with narrow pores. In the case of type 4A the diameter of the pores is appr. $3.5 \cdot 10^{-10}$ m. The water molecule has a length of appr. $2.8 \cdot 10^{-10}$ m and can therefore easily pass through these pores. The polar water molecule is relatively strongly bound and can be removed by heating. For most commercial applications the small crystals of zeolite (10^{-6} m) are mixed with a clay binder and are supplied in a pellet or bead form. A more thorough description of molecular sieves can be found in textbooks by Grubner et al (1) and Hersh (2).
The pelletized molecular sieve (Union Carbide 4A) contains appr. 23 % inert clay. The pellets have a diameter of $3.18 \cdot 10^{-3}$ m and an average length of $6.17 \cdot 10^{-3}$ m. The bulk density of the material is appr. 720 kg/m^3 and the external surface is 1120 m^2/m^3.
The other material investigated has a corrugated paper as the supporter for a 13X molecular sieve. The paper is arranged in a honeycomb structure with a flute size of appr. $1.8 \cdot 10^{-3}$ m. The bulk density is 220 kg/m^3 and the external surface area 2500 m^2/m^3.

DETERMINATION OF EQUILIBRIUM ISOTHERMS

General

There are at least two different methods of determining equilibrium isotherms, static methods and dynamic methods. In static systems the sample can be placed in a desiccator over a saturated salt or a sulphuric acid-water mixture. Climate test cabinets have also been used. This procedure gives equilibrium times ranging from one day to several weeks. A much faster procedure is to let the material equilibrate with pure water vapor at low pressure. One drawback with this method is the expensive high vacuum equipment needed. In the dynamic methods the air is blown over or through the material. This is the procedure used in this investigation. The method was chosen because of its relative speed and simplicity. One other advantage was that an equipment for generating air of different humidities and temperatures already existed. Great care should be taken when measuring the isotherms in the high humidity range. In this region the adsorption and desorption isotherms usually differ.
The measurements in this investigation were made in the adsorption mode, but tests in the investigated range of temperature and humidity show negligible difference between adsorption and desorption data. The heat released when water vapor is adsorbed (or heat demand when desorbed) results in a temperature rise (fall), which affects the equilibrium relationships. Therefore it is essential to take this amount into consideration when studying the kinetics. In this investigation the heat of sorption was predicted simply by using Clausius-Clapeyron equation.

$$\frac{d(\ln p)}{d(\frac{1}{T})} = -\frac{\Delta H}{R} \qquad (1)$$

If the heat of sorption could be regarded as independent of temperature, this equation claims a linear relationship between the logarithm of vapor pressure and the inverse of temperature.

Experimental

In the air conditioning equipment shown in Figure 1, two airstreams, one wet and the other dry, are mixed with each other to give air of different humidities.
In the humidifier temperature controlled water is recycled and sprayed over a packing material, which enables good contact between the two countercurrent streams. The maximum dewpoint reached is 330 K and the air leaving the humidifier is almost 100 % saturated. The dry air is produced in a drying tower filled with appr. 100 kg Union Carbide Molecular Sieves (4A, 1/8 in. pellets). From this tower air with a dewpoint less than 240 K is withdrawn. The drying agent can be regenerated with hot air from a heat coil.
With the help of a fan the air is sucked through the two towers. The proportion of wet to dry air is controlled manually with the help of a dewpoint meter (EG&G, Industrial Dew Point Hygrometer model 440) and two valves. The air stream is then splitted up into six, each having their own temperature controlled heater as shown in Figure 2. The maximum temperature used in this investigation was 675 K. The air is forced through the samples (weight from 0.03 to 0.06 kg) and flows down along the outer surface of the sample container, thus minimizing the radial temperature gradient in the material. The sample containers (diameters 0.07 and 0.10 m) are made of 0.5 mm sheet steel and the material rests on a thin wire net.
The superficial air velocity was appr. 0.2 m/s and the equilibrium time ranged from 1 to 40 hours. By weighing (Sartorius electronic balance model 3716) and comparing with a reference condition, with known moisture content, the moisture of the material could be estimated. Tests showed that uptake of water from the surroundings during weighing could be neglected. The influence of free convective airstreams on the warm container during weighing was estimated by tests and taken into account when calculating the moisture of the sample.
The fresh material showed a decrease in capacity when repeated adsorption-desorption cycles were performed. Before isotherm estimations were undertaken, the material was exposed to several such cycles until the capacity was proved to stabilize. To determine the dryweight, dry air at 673 K was passed through the material. Tests indicated that this assumedly bone-dry material contained less than 0.1 % of water. This water is only of importance when comparing different capacity data.
When comparing the water capacity of different samples of the honeycomb type, exposed to the same air condition, they seemed to contain different amounts of pure zeolite. A much better agreement was found when comparing the water capacity of the

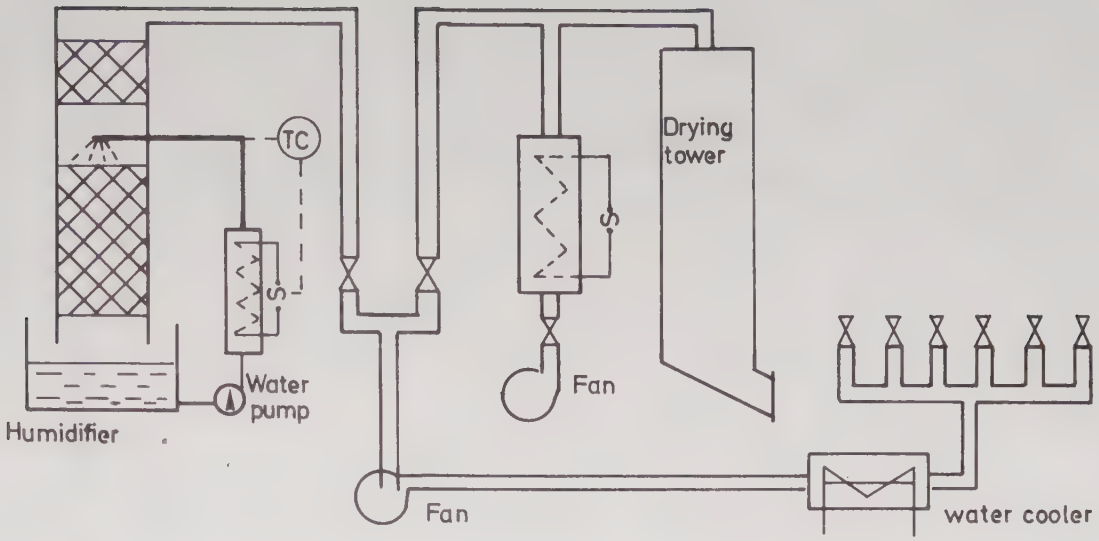

Figure 1 Air conditioning equipment

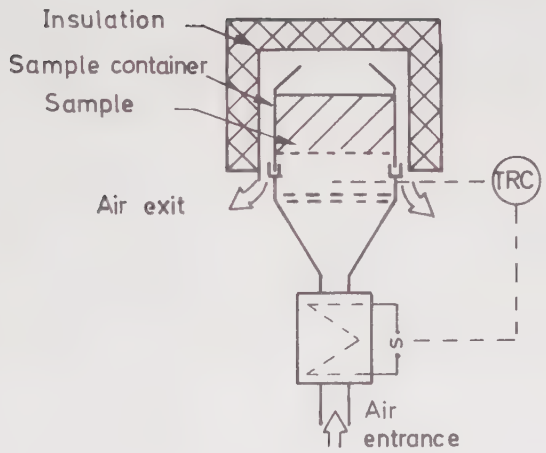

Figure 2 Sample conditioning equipment

samples as a volume based water concentration instead of mass based. The slight difference, which still remained was corrected by a concentration factor.

Results and discussions

For each material appr. 300 experimental points were found in the temperature range from 290 K to 510 K and dewpoint range 236 K to 294 K. The result is plotted in Figures 3 and 4 as moisture content of material versus partial pressure of water vapor with temperature as the parameter. A least square fit gave for the pellet type

$$\ln p = 23.43 + 28.39X - \frac{1000}{T}(2.738 + 48.69X + 0.1415X^{-1} - 149.8X^{2}) \quad (2)$$

with the standard deviation s = 0.0035 kg/kg. For the honeycomb type the corresponding expression became

$$\ln p = 29.06 - \frac{1000}{T}(5.981 + 0.1165w + 23.98w^{-1} - 0.003224w^{2} - 25.48w^{-2}) \quad (3)$$

with s = 0.32 kg/m^3

The heat of sorption was calculated from Clausius-Clapeyron's equation (Eq. 1) and the result is shown for the two materials in Figures 5 and 6. A comparison, in Figure 3, between two isotherms and corresponding values found in literature shows a good agreement. The considerable discrepancy between this isotherm and that found by Jury and Horng (4) can be explained by the previous discussion of bone-dry material. Jury and Horng regenerated their material with dry air at about 367 K. According to this investigation that condition means a moisture content equal to about 0.04 kg/kg. The pellet type model gives a standard deviation of about 0.0035 kg/kg. The major differences are located in those points were an error in measured dewpoint or temperature gives a substantial error in moisture content. For this type two runs gave a small discrepancy in moisture contents below 0.10, probably because of a small reduction in capacity. This error also affects the ΔH-curve in Figure 6. A more accurate estimation of ΔH in this region would be needed. A comparison with literature data is also given in Figure 5. The isotherms of the honeycomb type indicate an increased capacity at higher humidities than can be expected from a 13X molecular sieve. The reason for this is probably the presence of other hygroscopic compounds in the impregnating agent.

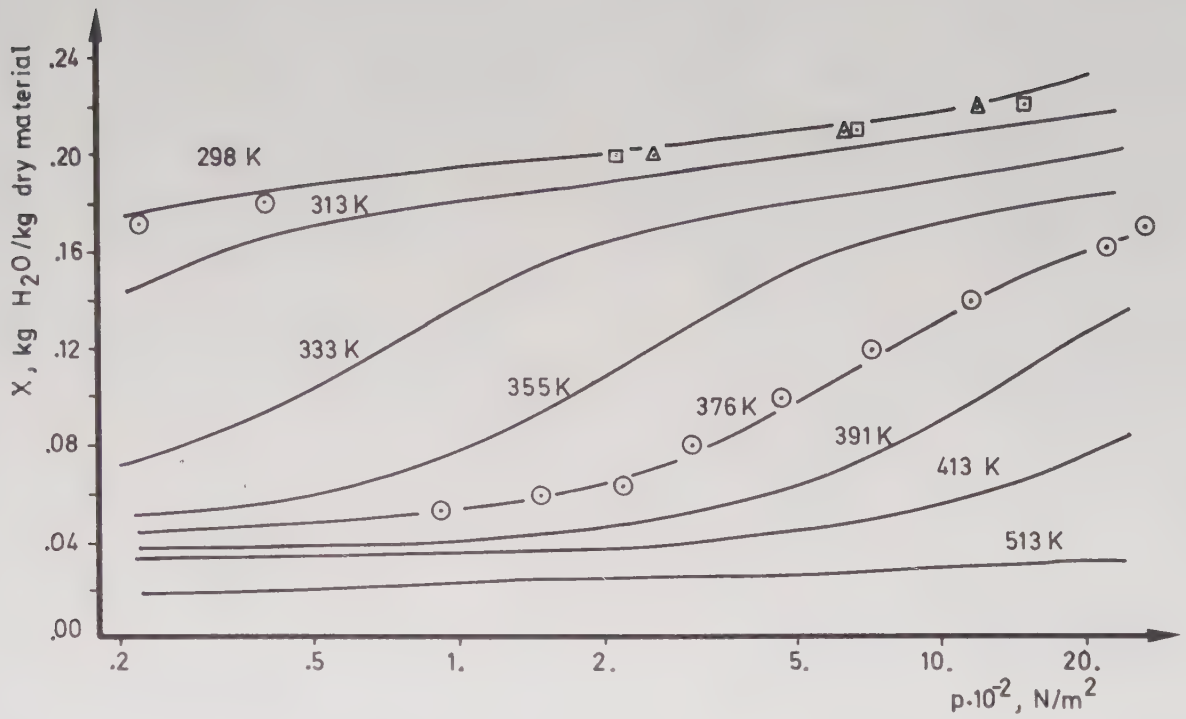

Figure 3 Sorption isotherms for the pellet type (4A)
○ = Grubner et al (1), ◘ = Hersh (2), Δ = Linde Co (3)

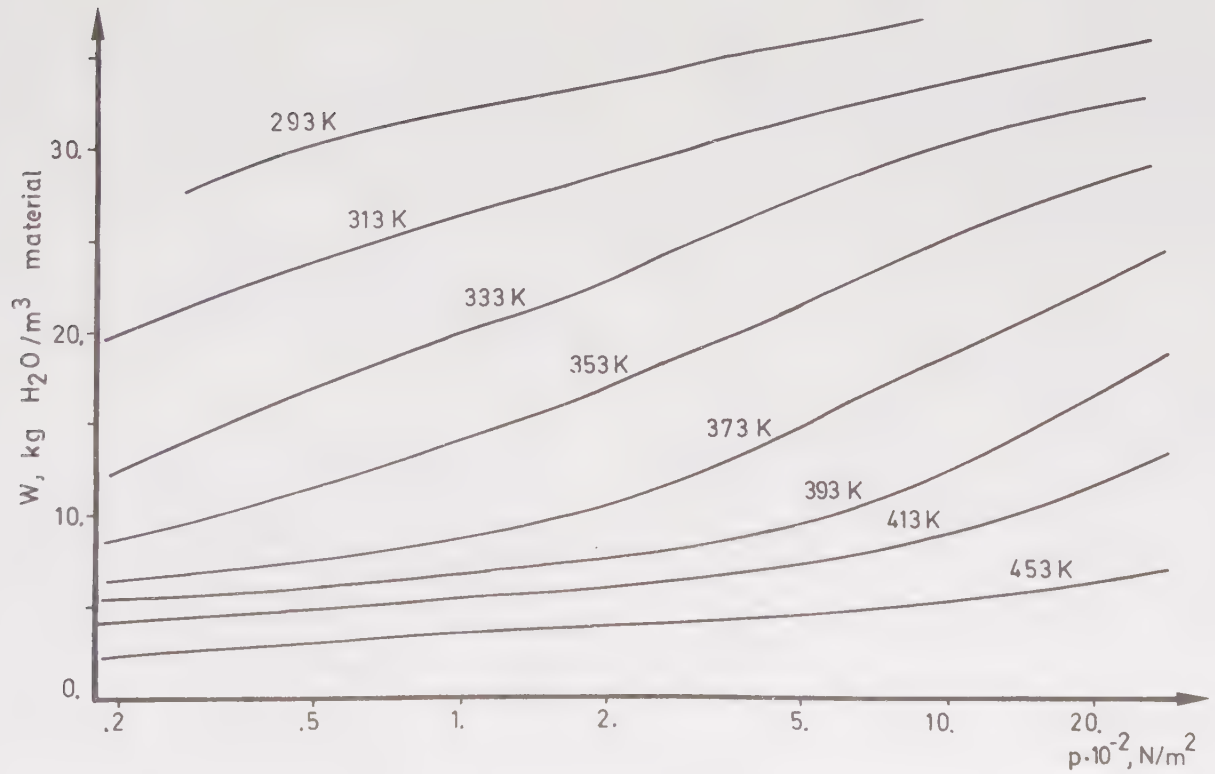

Figure 4 Sorption isotherms for the honeycomb type

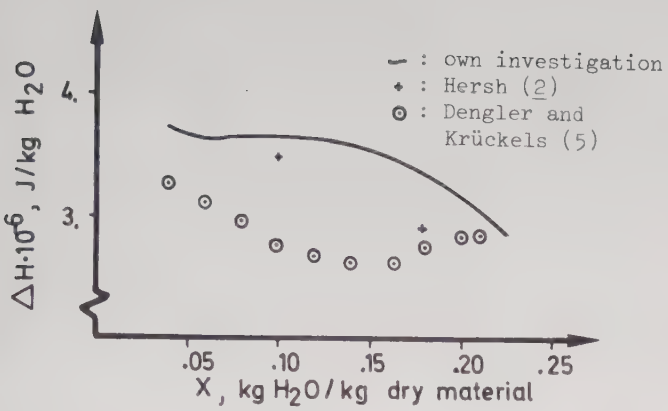

Figure 5 Heat of sorption for the pellet type

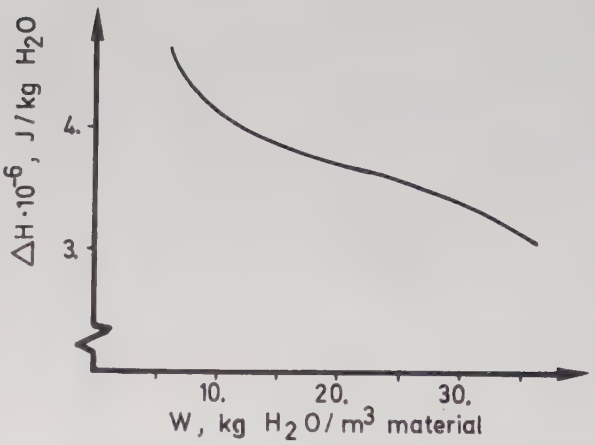

Figure 6 Heat of sorption for the honeycomb type

DETERMINATION OF HEAT CAPACITY

Introduction

Heat capacity data for molecular sieves have been reported (6, 7). These measurements have been made on pure compounds without supporting material and at temperatures and moisture contents not generally used in practice. This investigation presents data in the temperature range from 290 K to 475 K and with moisture contents frequently encountered in practice.

Experimental

Samples, as packed cylinders of appr. $3.4 \cdot 10^{-3}$ m in diameter and $1.6 \cdot 10^{-3}$ m in height, were prepared. They were then equilibrated in blowing air of known temperature and humidity. The final moisture content of the samples were estimated from the isotherms described previously.
After equilibrium was reached the samples were packed in hermetically sealed ampoules in order to prevent adsorption or desorption of water vapor during the specific heat measurements. A differential scanning calorimeter (Perkin-Elmer model DSC-2) was used for the measurements, made in five degree intervals.

Result

The heat capacity was taken as the average of two runs with equal moisture contents. The evaporation of water, during the temperature rise, was taken into account, using the isotherms and heat of sorption previously described. Figures 7 and 8 show the result and Equations 4 and 5 give the least square fit for the two materials. The result for the pellet type can be compared with the constant value of 800 J/kgK at 313 K frequently encountered in literature (3).
Pellet type: (s = 23 J/kgK)

$$c_p(1 + X) = 980.4 + 0.3361T - 1.79 \cdot 10^{7}T^{-2} + X(8.55 \cdot 10^{3} - 8.438T - 1.5 \cdot 10^{8}T^{-2}) \qquad (4)$$

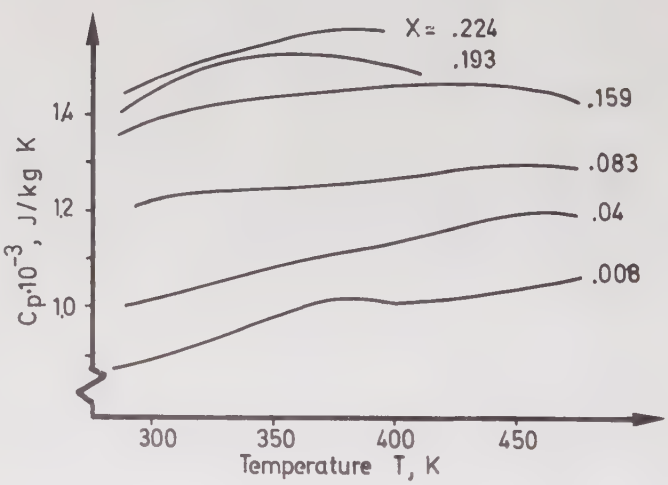

Figure 7 Heat capacity curves for the pellet type

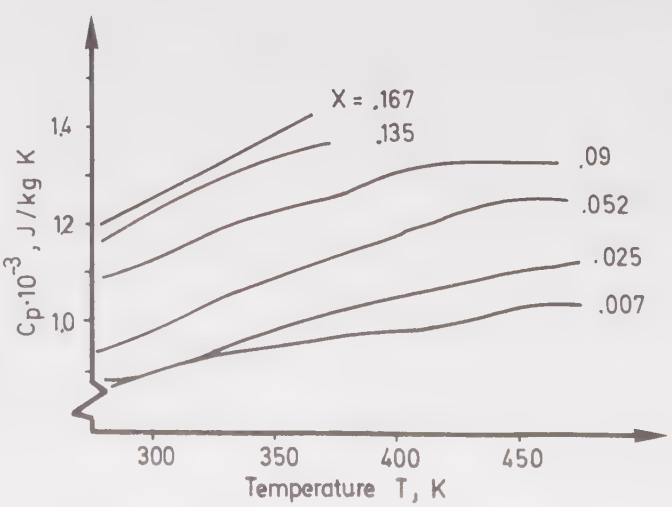

Figure 8 Heat capacity curves for the honeycomb type

Honeycomb type: (s = 22 J/kgK)

$$c_p(1 + X) = 1084.3 + 0.0817T - 2.32 \cdot 10^7 T^{-2} + X(2.684 \cdot 10^3 + 6.3717T - 7.1835 \cdot 10^7 T^{-2}) \quad (5)$$

DRYING CURVES; SIMULATED - EXPERIMENTAL

This part of the paper tries to examplify the use of the properties in simulating a drying process. A more detailed report of this work will be published later.
To describe the adiabatic adsorption-desorption behaviour of a fixed bed Eq. 6 to 9 may be derived.

$$\dot{m}\left(\frac{\partial Y}{\partial z}\right) = -\rho_s\left(\frac{\partial X}{\partial t}\right) - \varepsilon\rho_g\left(\frac{\partial Y}{\partial t}\right) \quad (6)$$

$$-\rho_s\left(\frac{\partial X}{\partial t}\right) = \beta a_v(Y_s - Y) \quad (7)$$

$$\rho_s(\Delta H + c_{p,v}T_g - c_{p,w}T_s)\left(\frac{\partial X}{\partial t}\right) = \dot{m}(c_{p,g} + Yc_{p,v})\left(\frac{\partial T_g}{\partial z}\right) + \rho_s(c_{p,s} + Xc_{p,w})\left(\frac{\partial T_s}{\partial t}\right) \quad (8)$$

$$\dot{m}(c_{p,g} + Yc_{p,v})\left(\frac{\partial T_g}{\partial z}\right) = \alpha a_v(T_s - T_g) \quad (9)$$

The severe limitation of this model appears in Eq. 7. The only significant mass transfer resistance is said to be of stagnant film type. However, using a so called "lumped" mass transfer coefficient has often proved to describe the drying process satisfactorily.
Using the isotherms, heat of sorption and heat capacity data these sets of equations can be solved simultaneously with the help of a finite difference computer program. The experiments were conducted in an equipment where air of constant temperature and humidity was blown from below through a fixed bed. When equilibrium was reached, a step change in the humidity was made. The change in weight of the bed could be continuously recorded and when equilibrium was reached a new change in the humidity, back to previous, was made. Repeated cycles showed good reproducability.
Figure 9 compares experimental with simulated runs for each material. The curves show that the honeycomb type can satisfactorily be simulated with a lumped mass transfer coefficient. For comparison an isothermal run is also pictured, showing the importance of adiabatic simulation. For the pellet type a certain discrepancy between experiment and simulation indicates a greater degree of internal mass transfer resistance. This effect is more pronounced when comparing adsorption curves. This kinetic behaviour of a fixed bed is studied at present at our department for later use in a research project regarding design and dimensioning of industrial dryers.

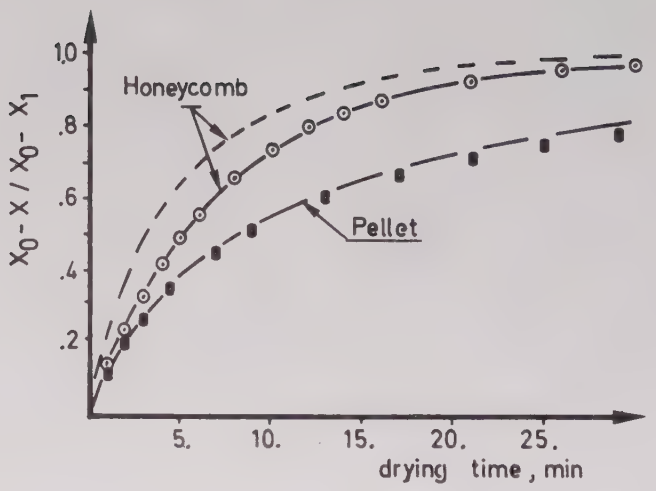

Figure 9 Drying curves for the two materials
— = adiabatic simulation
o,● = experimental
-- = isothermal simulation

ACKNOWLEDGEMENT

The author wish to thank Dr. A.S. Zelepuga for the help with the c_p-measurements. (Present address: Heat and Mass Transfer Institute, Minsk, USSR).

REFERENCES

1. Grubner, O. et al., Molekularsiebe, VEB Deutsher Verlag der Wissenschaften, Berlin 1968
2. Hersh, C.K., Molecular Sieves, Reinhold Publishing Co., New York 1961
3. Information Brochure on Linde Molecular Sieve
4. Jury, S.H. and Horng, J.S., The Molecular Sieve 4-A Water Vapor Sorption Therm, AIChE Journal, Vol. 19, No. 2, p. 371-372 1973
5. Dengler, W. and Krückels, W, Chemie-Ing.-Techn., 42. Jahrg., Nr. 21, p. 1332-1336 1970
6. Barrer, R.M. and Bratt, G.C., J. Phys. Chem. Solids, Vol. 12, p. 130-145 1959
7. Berezin, G.I. et al., Trans. Faraday Soc., Vol. 19, p. 614-619 1959

II

A KINETIC STUDY OF THE ADSORPTION AND DESORPTION PROCESS OF TWO COMMERCIAL MOLECULAR SIEVES

KENNETH WERLING AND ROLAND WIMMERSTEDT

DEPARTMENT OF CHEMICAL ENGINEERING
LUND INSTITUTE OF TECHNOLOGY
LUND
SWEDEN

Abstract

A mathematical model and its numerical solution is presented to describe adiabatic adsorption-desorption processes in a fixed bed when the mass and heat transfer can be described by external film transfer coefficients only, which is especially interesting in the case of non-uniform, irregular particles. A new method to measure such rates is presented, based on continuous weighing of a through-circulated bed. The measured rates can be checked against the difference in humidity and temperature between the outlet and inlet air in order to minimize errors.

The comparison between experimental results and calculations showed that the adsorption process in a bed of molecular sieve pellets can not be described with a constant mass transfer coefficient; the desorption process is better described although not entirely satisfactorily. In the case of a honeycomb molecular sieve, a constant mass transfer coefficient described both the adsorption and desorption processes satisfactorily.

Inroduction

The main objectives of this work have been to develop a technique for measuring adsorption and desorption rates of water vapour in a fixed bed and to evaluate a mathematical model and its numerical solution to simulate these processes. It should also be possible to use the technique in describing the drying process of granular materials in a fixed bed.

In this work, two types of molecular sieves have been studied. Both types are of great interest as air drying agents. One of the materials, cylindrical pellets of small molecular sieve crystals of 4A-type supported on clay, has previously been studied in the literature. The kinetics of the other material - with paper supporting the 13X-molecular sieve crystals - has to our knowledge not been described in the literature. The determination of sorption isotherms, heat of sorption and heat capacity of the two materials have been presented earlier[1].

Mathematical model

In this work a model based on a film transfer coefficient, has been used to simulate the mass transfer in a through-circulated bed.

$$\rho_b \frac{\partial \bar{X}}{\partial t} = - \beta a_v (Y_s - Y) \qquad (1)$$

In this case β must be regarded as a "lumped" transfer coefficient, i.e. a coefficient which includes all possible mass transfer resistances, internal as well as external. This type of rate equation, with a moisture dependent β-value, has often been used in describing drying processes.

Such a model has been tested by Uhlman and Krückels[2] on silica gel. They presented a conversion formula for an effective diffusivity to a β-value, and the method appears to give sufficient accuracy for practical purposes.

Some other works using "lumped" mass transfer coefficients are found in references[3-5].

Besides Eq. (1), equations needed to describe the whole process in a differential bed are: a mass balance, a heat balance, and a heat transfer equation

$$- \dot{m}_g \frac{\partial Y}{\partial z} = \rho_b \frac{\partial \bar{X}}{\partial t} + \varepsilon_b \rho_g \frac{\partial Y}{\partial t} \qquad (2)$$

$$\rho_b (\Delta H_o + c_{p,v} T_g - c_{p,\ell} T_s) \frac{\partial \bar{X}}{\partial t} = \dot{m}_g c_{p,g} \frac{\partial T_g}{\partial z} +$$

$$\varepsilon_b \rho_g c_{p,g} \frac{\partial T_g}{\partial t} + \rho_b c_{p,s} \frac{\partial T_s}{\partial t} \qquad (3)$$

$$\dot{m}_g c_{p,g} \frac{\partial T_g}{\partial z} = \alpha a_v (T_s - T_g) \qquad (4)$$

In addition, functions describing vapour pressure equilibrium and thermodynamic data are needed:

$$Y_s = f_1(X, T_s) \qquad \Delta H_o = f_2(X) \qquad (5,6)$$

$$c_{p,g} = f_3(Y, T_g) \qquad c_{p,s} = f_4(X, T_s) \qquad (7,8)$$

together with the appropriate initial and boundary conditions.

To simplify the solution, the pore-volume terms in Eqs. (2) and (3) were neglected as corresponding solid phase terms are of the order of 10^4 times greater.

To solve the set of differential equations, a predictor-corrector method in a two-dimensional grid system was used.

Experimental

Different experimental techniques have been used in the literature to determine the kinetics of water vapour adsorption and desorption. Some authors have studied a single particle in a controlled air atmosphere[6-10] or in pure water vapour[11]. Both discontinuous and continuous weighing methods have been reported. Usually, isothermal adsorption or desorption has been assumed in the above-mentioned techniques.

Methods based on a through-circulated shallow bed are of two categories: one measuring the difference in outlet and inlet humidity and the other measuring the change in weight of the material.

An interesting technique of the first kind is that of Barschdorff[12]. In this method the outlet humidity is measured by IR-absorption, which has the advantage - in contrast to many other humidity measuring devices - of being very fast. For example, this method has been used for determining drying rates in a fluidized bed with drying times of a few seconds.

The other principle, measuring the weight change of a bed of material, is probably the most common. Most techniques are based on a discontinuous weighing, where the bed is removed from the air-stream. Far less common is the continuous weighing of a through-circulated bed. Schicketanz[13] has described such equipment. Another technique in this category is described in this paper.

The whole apparatus, as presented in Fig. 1, is suspended on a sharp-edged knife. Most of the weight of the equipment is counter-balanced by a moveable mass, and the rest is taken up by an electronic balance (Sartorius 3716). Air, electrical power and thermocouples are connected in the vertical plane along the axis of the suspension point. This arrangement minimizes the influence of these connections and flow forces in the equipment upon the weight recording.

Air of controlled humidity is produced in an air conditioning equipment, which has been presented earlier[1]. Two separate air-streams, each having its own controlled humidity, are drawn to a four-way valve. The valve makes it possible to switch airstreams to produce step changes in humidity. From the valve, the air passes a flow rate meter and enters the kinetic

equipment through a flexible plastic tube. Before entering the bed the air is heated by a thermostatted electrical heater. The temperature difference over the bed is measured with thermocouples and the weight is continuously recorded by the electronic balance. The balance is so constructed that a weight increase does not alter the level of its pan. This is important, as the connections would otherwise affect the weight recording. The balance was calibrated before each new series of experiments. The weight proved to be linear with respect to the calibration masses, but its value was a few percent smaller. The humidity of the outlet air is measured with a dew-point meter of the condensing mirror type (EG&G mod. 440). With the help of another sampling line occasional checks were made on the humidity of the inlet air. The readings from thermocouples, balance and dew-point meter were recorded with a pen-recorder as well as via a data acquisition system on a paper tape. Not shown in Fig. 1 are some additional thermocouples, the electrical wirings, and the insulation layer around the bed.

From the weight curve, the sorption rate is derived. This is directly proportional to the difference in outlet and inlet humidity. However, mixing of the air and the relative slowness of the dew-poing meter, compared to that of the balance, makes the humidity curve more "smoothened".

The procedure for the experiments was as follows. The bed of material was kept in an air stream of constant humidity Y_o and temperature T_g until equilibrium was attained. A step change in humidity was then made from Y_o to Y_{in} at time $t = 0$ and the change in the parameters described earlier was measured. The bed of material was left in this air stream until the new equilibrium was reached. After that a new step change in humidity, back to the original, was made and the reverse process was studied. This procedure was carried out for different air flows, temperatures, and humidity steps.

Description of materials

In this work the adsorption and desorption kinetics have been studied for two molecular sieves of commercial interest for air drying or dehumidification.

The sorption isotherms, heat capacity and heat of sorption of the two materials have been determined earlier over a wide range of moisture contents and temperatures[1]. Figure 2 shows the sorption isotherms used in the evaluation of the experiments and in the calculations.

The pelletized molecular sieve (Union Carbide 4A) has a pellèt diameter of $3.18 \cdot 10^{-3}$ m, an average length of $6.2 \cdot 10^{-3}$ (with the standard deviation $1.8 \cdot 10^{-3}$ m) supported on clay (≃23%). In the experiments a bed height of 0.0175 m was used. The bulk density and external surface area were 720 kg/m^3 and 1120 m^2/m^3 respectively.

The other material investigated has a corrugated paper (≃40%) to support the 13X molecular sieve crystals. The paper, with the thickness of $1.3 \cdot 10^{-4}$ m, is arranged in a honeycomb structure with a flute size av ca. $1.8 \cdot 10^{-3}$ m. A bed height of 0.1 m was used in the experiments. The bulk density and external surface area were 220 kg/m^3 and 2500 m^2/m^3 respectively. In the calculations a ten percent reduction of ΔH_o, as determined in ref. 1, gave a better fit to the experimental results and was therefore used.

Results

Figure 3 shows some adsorption runs for the two materials. Run P-1 reveals that a constant β-value can not describe the adsorption kinetics of the pelletized material satisfactorily. The adsorption rate is much faster in the beginning and slower toward the end. The same phenomenon was found in other adsorption runs with this material.

Three desorption runs of the pellet type are presented in Fig. 4. It seems possible to simulate the desorption kinetics satisfactorily with a constant β - value. However, also these experiments show an initially higher mass transfer rate, but for a shorter period of time. This is more clearly revealed in the temperature difference curves, which have a higher value for the first minute compared with the calculated value, and also when studying the amount of water desorbed. For the first half minute, the amount was about 40% higher in the experiments, and only a few percent higher for the second half. Also, at the end, the experimental desorption rates were found to be smaller than those calculated.

In the honeycomb structure the experimental flow rates will give a laminar flow inside the small channels and the external heat and mass transfer resistance can therefore be described by a constant film transfer coefficient independent of flow rate.

As seen from run H-1, 2 and 3 in Fig. 3 the adsorption process seems to be described fairly well by a constant β-value. Fig. 3 also reveals the difference in adsorption rate, due to different "thickness", between the two materials. The plateau in the adsorption rate curves indicates that the whole mass transfer zone (MTZ) is within the height of the bed. This was also shown to be approximately true in the computer calculations.

The results of some desorption runs of the honeycomb type are presented in Fig. 5. The number of experiments is too low to judge whether one β-value can describe all experiments, but a certain variation was found.

Discussions and conclusions

The better fit between experiments and calculations in the desorption runs of the pelletized material is probably due to the nonlinear shape of the isotherm ($\partial^2 Y_s / \partial X^2 > 0$).

In the case of adsorption, the high driving force at the beginning will create an outer shell in near-equilibrium with the ambient air and a relatively steep moisture gradient is formed inside the shell. A β-function, which includes both external and internal diffusion resistances and which is decreasing with increasing moisture content, appears to fit the adsorption runs much better. The type of β-function needed is at present under investigation.

In the case of desorption, the steep moisture gradient remains close to the surface. Also, the internal moisture profile is rather flat and is close to the average moisture content. Therefore a constant β-value will be more appropriate in this case.

The same difference in describing the adsorption and desorption process was not found with the honeycomb material; probably because of the shorter diffusion path and the deeper bed in this case.

It can therefore be concluded that the adsorption process in a bed of molecular sieve pellets can not be described with a constant mass transfer coefficient; the desorption process seems, for any practical purpose, to be satisfactorily described. In the case of a honeycomb molecular sieve, a constant mass transfer coefficient described both the adsorption and desorption behaviour satisfactorily.

References

1 Werling K., First International Symposium on Drying, Science Press Princeton, 1978.

2 Uhlmann H.J. and Krückels W., Verfahrenstechnik 1975 9 19.

3 Garg D.R. and Ruthven D.M., AIChE J. 1975 21 200.

4 Chi C.W. and Wasan D.T., AIChE J. 1970 16 23.

5 Nordon P., Int. J. Heat Mass Transfer 1964 7 639.

6 Kast W. and Jokisch F., Chem. Ing. Tech. 1972 44 556.

7 Marcussen L., Chem. Engng Sci. 1970 25 1487.

8 Punwani D., Chi C.W. and Wasan D.T., Ind. Eng. Chem. Process Design Develop. 1968 7 410.

9 Krischer O. and Mahler K., Chem. Ing. Tech. 1959 31 88.

10 Gerstenberg H., Chem. Ing. Tech 1960 32 613.

11 Dengler W. and Krückels W., Chem. Ing. Tech. 1970 42 1258.

12 Barschdorff D., Messen-Steuern-Regeln 1969 12 119.

13 Schicketanz W., Chem. Ing. Tech. 1971 43 245.

Notation

a_v	interfacial area	m^2/m^3
c_p	specific heat	J/K (kg dry material)
$\dot{m}_g$	mass flux of air	kg/m^2 s
t	time coordinate	s
T	temperature	^oC
$\bar{X}$	average moisture content	kg/kg dry material
Y	humidity	kg/kg dry air
z	axial length coordinate	m
α	heat transfer coefficient	W/m^2 K
β	mass transfer coefficient	kg/m^2 s
ΔH_o	heat of sorption	J/kg
ε	porosity	
ρ	density	kg/m^3

Subscripts:

b	bed
g	gas
in	inlet
ℓ	liquid
out	outlet
s	surface or solid
v	vapour
o	initial

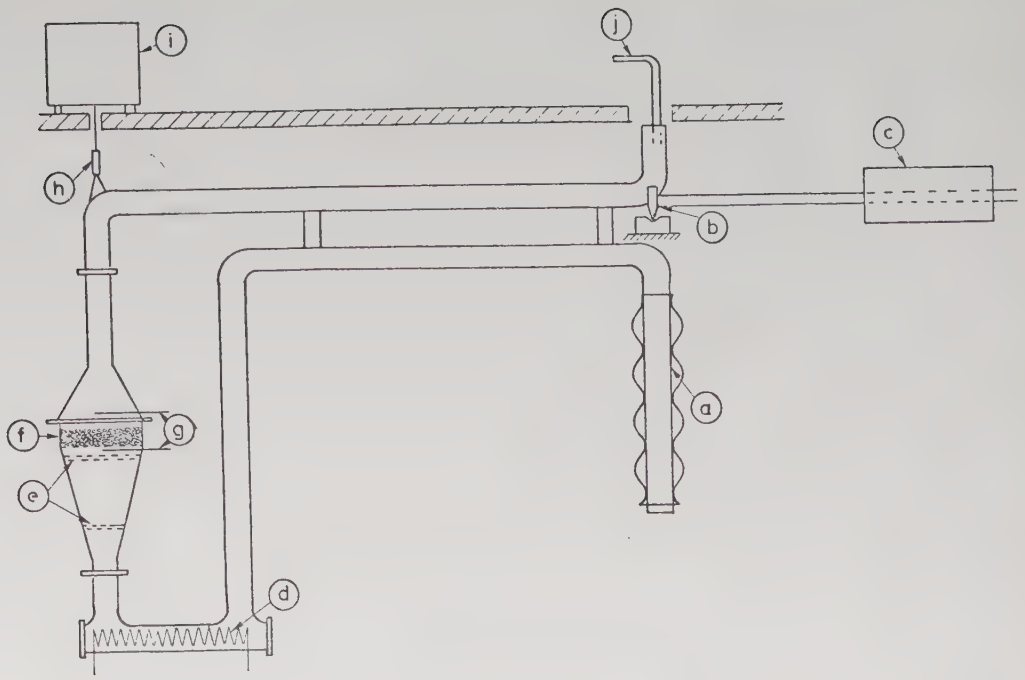

Fig. 1. The kinetic adsorption-desorption equipment

a: flexible plastic tube	f: bed of material
b: sharp-edged knife	g: thermocouples
c: moveable mass	h: suspension mounting
d: electrical air heater	i: balance
e: distribution plates	j: sampling line to dew-point meter

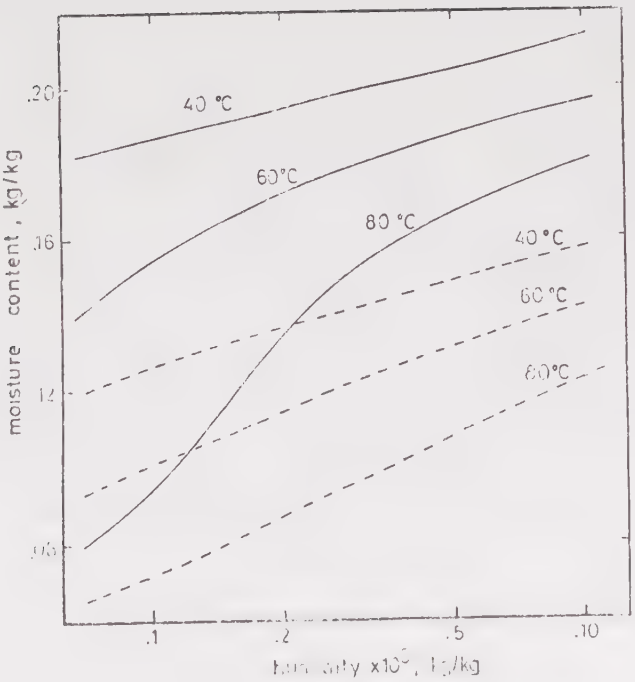

Fig. 2. Sorption isotherms of the pelletized (—) and honeycomb (-----) material.

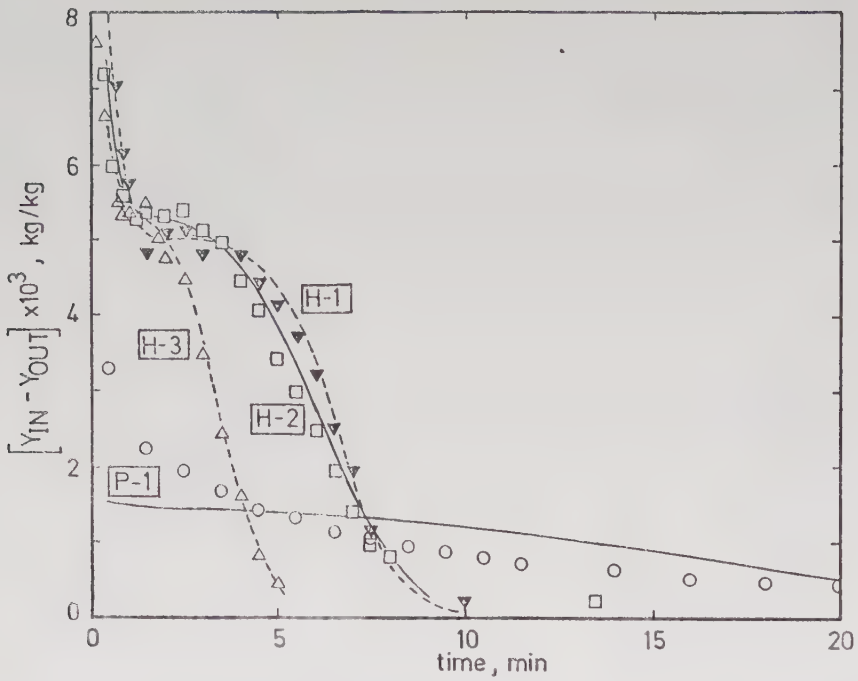

Fig. 3. Experimental (▼□△○) adsorption runs compared to simulated (----) for pelletized (P) and honeycomb (H) material.

(H-1: $\dot{m}_g$=0.38, Y=.0011→.0092, T_G=60, α=60, β=0.02
H-2: $\dot{m}_g$=0.52, Y=.0010→.0092, T_G=83, α=60, β=0.02
H-3: $\dot{m}_g$=0.76, Y=.0009→.0092, T_G=60, α=60, β=0.02
P-1: $\dot{m}_g$=0.52, Y=.0012→.0092, T_G=81, α=114, β=0.006)

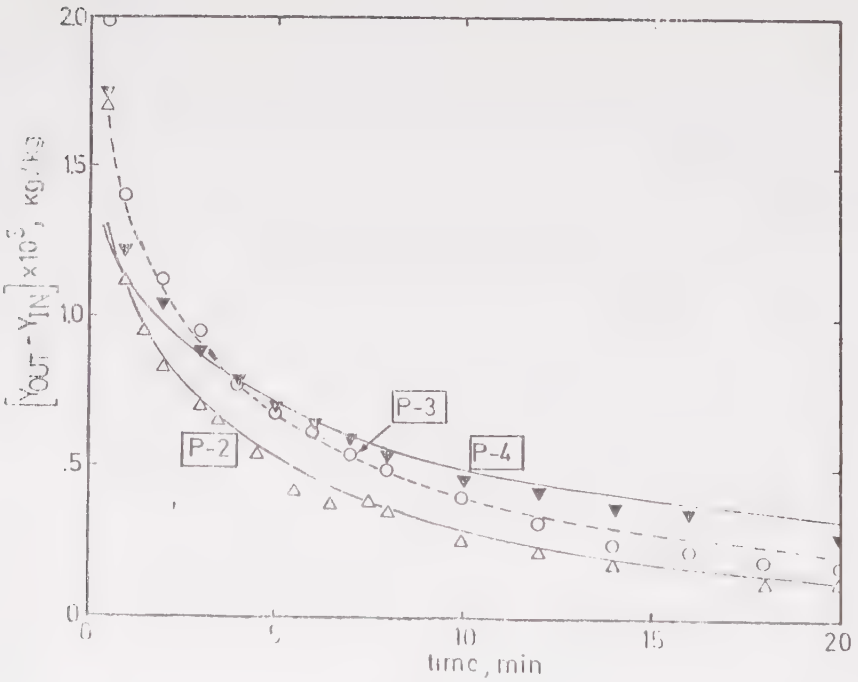

Fig. 4. Experimental (▽○△) desorption runs compared to simulated (----) for pelletized material.

(P-2: $\dot{m}_g$=0.52, Y=.0101→.0010, T_G=40, α=114, β=0.006
P-3: $\dot{m}_g$=0.52, Y=.0103→.0010, T_G=60, α=114, β=0.006
P-4: $\dot{m}_g$=0.52, Y=.0101→.0010, T_G=81, α=114, β=0.006)

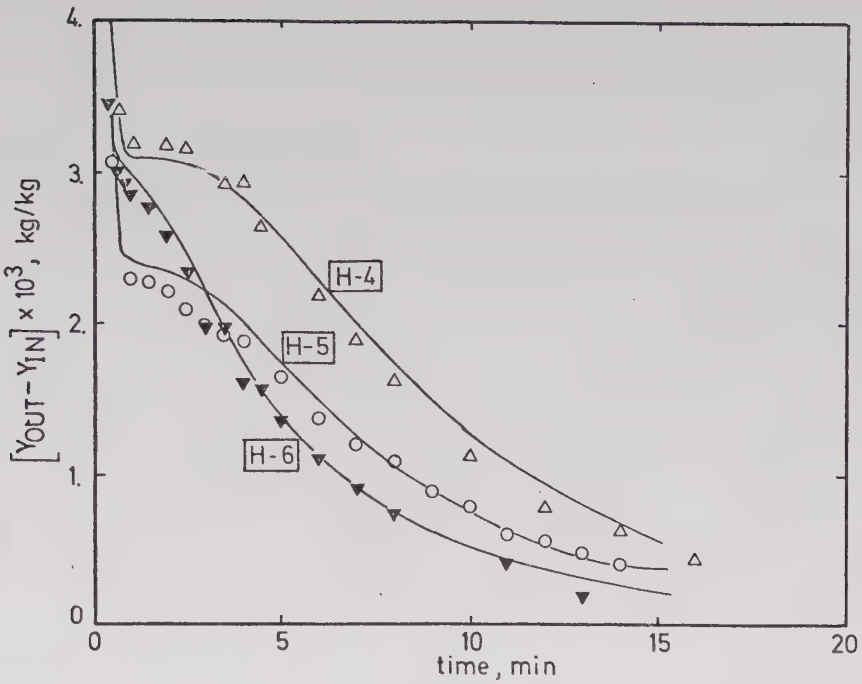

Fig. 5. Experimental (▼○△) desorption runs compared to simulated (———) for honeycomb material.
(H-4: $\dot{m}_g$=0.52, Y=0.0092→0.0011, T_G=83, α=60, β=0.02
H-5: $\dot{m}_g$=0.52, Y=0.0066→0.0011, T_G=59, α=60, β=0.02
H-6: $\dot{m}_g$=0.76, Y=0.0092→0.0011, T_G=60, α=60, β=0.02)

III

CODEN: LUTKDH/(TKKA-3005)/1-34/(1980)

ON NON-ISOTHERMAL ADSORPTION AND DESORPTION OF GASES WITH NON-LINEAR EQUILIBRIA

KENNETH WERLING

DEPARTMENT OF CHEMICAL ENGINEERING
LUND INSTITUTE OF TECHNOLOGY
LUND
SWEDEN

Dokumentutgivare
Lund Institute of Technology
Department of Chemical Engineering

Dokumentnamn
Report

Dokumentbeteckning
LUTKDH/(TKKA-3005)
/1-34/(1980)

Handläggare
R. Wimmerstedt

Utgivningsdatum
February 1980

Ärendebeteckning

Författare
K. Werling

Dokumenttitel och undertitel

On Non-Isothermal Adsorption and Desorption of Gases with Non-Linear Equilibria

Referat (sammandrag)

Abstract (III)

The non-isothermal adsorption-desorption kinetics of gases with nonlinear equilibria was studied theoretically and experimentally. The simultaneous heat and mass transfer equations were solved for both adsorption and desorption of water vapour in a molecular sieve particle, when vapour diffusion in pores is rate-controlling. When the equilibrium isotherms have a curvature, so that $\partial^2 p^*/\partial X^2$ is positive, a relatively sharp adsorption zone recedesinto the particle. In desorption, the same isotherms cause a rather flat moisture profile in the particle. Approximate rate models for both adsorption and desorption were derived and the models were tested against experiments with good results. The behaviour of deep beds during adsorption and "thermal-swing" regeneration was also investigated.

Referat skrivet av
author

Förslag till ytterligare nyckelord

pore diffusion

Klassifikationssystem och -klass(er)

Indextermer (ange källa)

Omfång
43 pages

Övriga bibliografiska uppgifter

Språk
English

Sekretessuppgifter

ISSN

ISBN

Dokumentet kan erhållas från
Department of Chemical Engineering
Chemical Center, POB 740,
S-220 07 LUND 7, Sweden

Mottagarens uppgifter

Pris

DOKUMENTDATABLAD enligt SIS 62 10 12

SIS
DB 1

Blankett LU 11:25 1976--07

Abstract

The adsorption-desorption kinetics of gases with non-linear equilibria has been studied theoretically and experimentally. The simultaneous heat and mass transfer equations were solved for adsorption and desorption of water in a molecular sieve particle. Vapour diffusion in the pores was assumed to be the only internal mass transfer resistance.

When the equilibrium isotherms have the curvature so that $\partial^2 p^*/\partial X^2$ is positive, as is the case for molecular sieves, it was shown that during adsorption the particle is made up of an almost saturated outer shell and a decreasing unaffected core. This led to the formulation of a "shrinking-core" model for adsorption. In this model it is assumed that a sharp adsorption front recedes into the particle and that the mass transport rate is determined by the diffusional resistance from the air bulk to the receding adsorption front. The internal mass transport for a sphere is thus defined by the following coefficient:

$$\frac{3\, D_{vap}}{R^2 a_{v,p}(R/R_c - 1)} = \frac{\beta_i}{(R/R_c - 1)}$$

R_c/R is here the relative radius of the unaffected core (sphere). The internal mass transfer coefficient β_i of molecular sieve pellets was determined by experiments to be $6.6 \cdot 10^{-4}$ m/s (at 20^oC).

In desorption, the same type of isotherm influences the mass transport differently. The core of the particle is now almost immediately affected and a steep moisture gradient remains at the surface. The magnitude of desorption rate will therefore also be lower than that of adsorption. A simple linear rate expression, which assumed vapour diffusion from a particle at average moisture content to the air bulk, had earlier proved to describe some desorption experiments fairly well. However, the approximate rate expression underestimates the desorption rate at higher moisture contents and somewhat overestimates the rate at lower moisture contents. Since the lower desorption rates determine the time needed for regeneration, the "lumped" β-value (0.0035 m/s) was chosen so a good description of this region was achieved.

The applicability of the two approximate models was shown in examples where the concentration and temperature profiles in a 1.0 m bed were cal-

culated during both adsorption and desorption. In adsorption the "constant-pattern" behaviour soon became prevalent. The regeneration was assumed to be carried out by means of hot air. As the temperature raises the equilibrium vapour pressure of the material, the drawbacks of this type of isotherm during desorption are partly neutralized, and rather sharp profiles result. In both adsorption and desorption a two-front behaviour was found. The first front is caused by the temperature change of material from the initial to an elevated temperature level. The second, much slower, front arises from the change in moisture content of material.

CONTENTS

1 INTRODUCTION 1

2 COMPLETE MODEL FOR MASS AND HEAT TRANSPORT IN A PARTICLE 5

2.1 Water transport 5

2.2 Heat transport 7

2.3 Numerical solution 8

3 THE ADSORPTION OF WATER VAPOUR ON A MOLECULAR SIEVE PARTICLE 10

3.1 The simplified adsorption model - the shrinking-core model 11

3.2 Influence of variations in geometry and particle size 16

3.3 A comparison between experimental and calculated adsorption runs 18

3.4 Calculated concentration and temperature profiles in a bed during adsorption 24

4 THE DESORPTION OF WATER VAPOUR FROM A MOLECULAR SIEVE PARTICLE 25

4.1 Simplified desorption kinetic model 25

4.2 A comparison between experimental and calculated desorption runs 27

4.3 Calculated concentration and temperature profiles in a bed during desorption 29

5 CONCLUSIONS 33

NOTATION

REFERENCES

1 INTRODUCTION

In previous work[1,2] the adiabatic adsorption (and desorption) of water vapour in a fixed bed of two commercial molecular sieves has been studied. Equilibrium data, heat capacity and heat of sorption have been determined experimentally[1]. The technique of continuously measuring the weight change of a through-circulated bed was developed and a number of adsorption-desorption experiments were carried out[2]. A simple linear rate expression proved to describe the desorption experiments fairly well but failed to do so for the adsorption experiments of the pelletized molecular sieve.

This report tries to treat the adsorption-desorption process, both in a single molecular sieve particle and in a through-circulated bed of particles, more theoretically. The importance of the shape of the isotherms is discussed. Although only experimentally determined material properties for a molecular sieve have been used, much of the analysis should apply for any hygroscopic material.

The investigated material (1/8-in. pellets of Linde Molecular Sieve 4A) consists of small synthetic zeolite crystals ($\simeq 10^{-6}$m) and a clay binder ($\simeq$23%). Due to the bidisperse pore structure, the water vapour has to overcome resistances both in the macropores of the pellet and in the micropores of the zeolite itself. In a number of articles[3-6], Garg and Ruthven have reported studies of the mass transport process in commercial molecular sieves. Their analysis is restricted to a Langmuir isotherm and components other than water, but shows a concentration dependence for the micropore diffusivity and an isotherm gradient dependence for the macropore diffusivity.

Kast and Jokisch[7] found that vapour diffusion was the dominant mass transport mechanism in molecular sieves at relative humidities less than 95%.

The local change in moisture content of a spherical particle can thus approximately be represented by:

$$\rho_p \frac{\partial X}{\partial t} + \varepsilon_p \frac{M_w}{R_o T} \frac{\partial p}{\partial t} = \frac{M_w}{R_o T} D_{vap} \left(\frac{\partial^2 p}{\partial r^2} + \frac{2}{r} \frac{\partial p}{\partial r}\right) \qquad (1.1)$$

In this equation isothermal sorption is assumed. Often this diffusion expression is transformed to one based on a concentration gradient in the

adsorbed phase. This implies that vapour in the gas phase is in equilibrium with moisture in the adsorbed phase. The equation then becomes:

$$\frac{\partial X}{\partial t} = \frac{D_{vap}}{\varepsilon_p+\gamma(X)} \left| \frac{\partial^2 X}{\partial r^2} + \frac{2}{r}\frac{\partial X}{\partial r} \right| + \frac{D_{vap}\ \delta(X)}{\varepsilon_p + \gamma(X)} \left(\frac{\partial X}{\partial r}\right)^2 \qquad (1.2)$$

where

$$\gamma(X) = \frac{\rho_p R_o T}{M_w} \left(\frac{dX}{dp^*}\right) \qquad (1.3)$$

$$\delta(X) = \left(\frac{d^2 p^*}{dX^2}\right) / \left(\frac{dp^*}{dX}\right) \qquad (1.4)$$

In many cases the last term of Eq. (1.2) has been neglected and the equation reduced to:

$$\frac{\partial X}{\partial t} = D_{eff} \left| \frac{\partial^2 X}{\partial r^2} + \frac{2}{r}\frac{\partial X}{\partial r} \right| \qquad (1.5)$$

Kast and Jokisch found in four adsorption experiments with spherical molecular sieve 4A that D_{vap}/ε_p of Eq. (1.2) was almost constant ($2.5 \cdot 10^{-6}$ - $2.75 \cdot 10^{-6}$ m^2/s), whereas the D_{eff} of Eq. (1.5) varied much more ($0.8 \cdot 10^{-10}$ - $2 \cdot 10^{-10}$ m^2/s).

The accumulation of vapour in the pores is negligible in comparison to the accumulation in the liquid phase, and thus Eq. (1.1) can also be written as:

$$\frac{\partial X}{\partial t} = \frac{1}{r^2} \frac{\partial}{\partial r} \left(r^2 D_{eff}(X) \frac{\partial X}{\partial r}\right) \qquad (1.6)$$

where

$$D_{eff}(X) = \frac{M_w D_{vap}}{R_o T \rho_p} \left(\frac{dp^*}{dX}\right) \qquad (1.7)$$

Dengler and Krückels[8] have for a silica gel particle determined an apparent or effective diffusivity, D_{eff}, according to Eq. (1.5), which varied both with moisture content and temperature. The diffusivity was found to vary between $0.3 \cdot 10^{-10}$ and $4 \cdot 10^{-10}$ m^2/s in their experiments. Later Krückels[9] showed that this variation in diffusivity could be explained by a concentration- and concentration gradient dependence.

Carter[10,11] has used an equation similar to Eq. (1.5) to calculate adsorption rates for four types of 4A molecular sieves. D_{eff} was experimentally found to vary between $1.5 \cdot 10^{-10}$ and $10 \cdot 10^{-10}$ m^2/s. The main resistance for mass transport was found to be in the macropores of the particles.

It is a well-known fact that "favourable" isotherms, as those of Fig. 1, result in self-sharpening or constant-pattern profiles in an adsorption

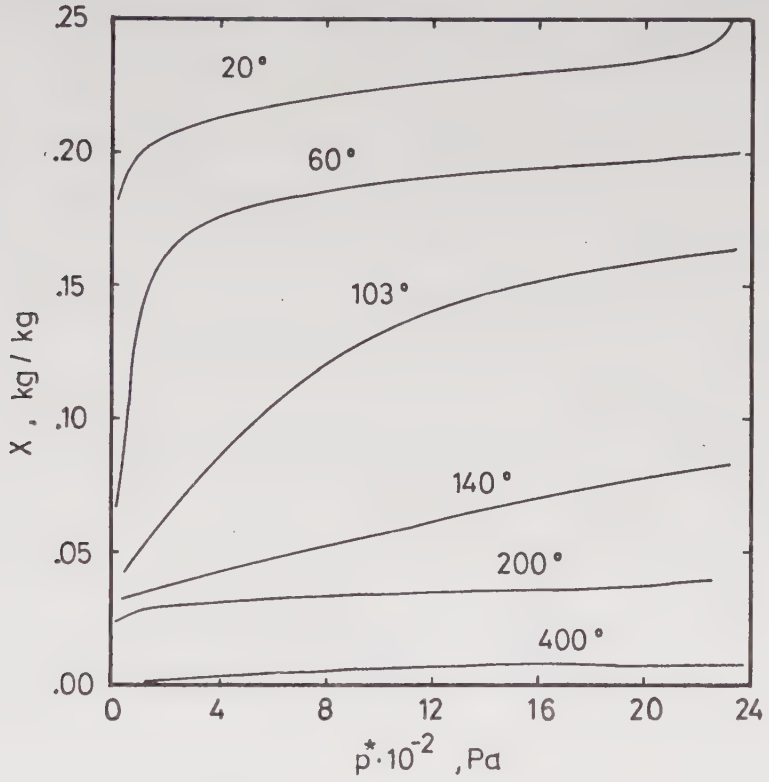

Fig. 1 Some sorption isotherms for the molecular sieve 4A[1]

bed (see for example ref. 12). It is also well-known that an isotherm which is "favourable" during adsorption is "unfavourable" during desorption. This means much lower desorption rates, and the constant pattern profile in the bed is never developed. Instead the profile becomes flatter and flatter. The reason for this is that the driving force for desorption, $p^* - p_{air}$, is reduced quickly as the moisture content is reduced. The influence of a non-linear isotherm on fixed bed behaviour during isothermal adsorption-desorption has been shown by several authors[13-15].

The above discussion is applicable for isothermal adsorption-desorption processes. Vermeulen and Klein[16] showed how the heat release during adiabatic adsorption raises the temperature of the material so that the real curve describing the moisture-equilibrium vapour pressure becomes more

"unfavourable" for adsorption. Nordon[17] described how the moisture profile moves in a through-circulated bed of wool. Wool has an isotherm which is slightly "unfavourable" for adsorption at relative humidities above 25%. The author showed that constant-pattern profiles are developed during desorption, whereas the profiles during adsorption become flatter and flatter. However, at lower moisture contents it can be seen that the constant-pattern approach doesn't hold completely. The reason for constant-pattern profiles is probably a combination of the favourable isotherm for desorption and the fact that the temperature decrease makes the real equilibrium curve even more "favourable" for desorption.

Carter[18] has experimentally and theoretically studied a bed of activated alumina during adsorption and "thermal-swing" regeneration (i.e. hot air is used for regeneration).

2 COMPLETE MODEL FOR MASS AND HEAT TRANSPORT IN A PARTICLE

To understand the limitations of existing drying and adsorption models (and to develop new ones), they have to be compared with a more complete model. Both heat and mass transport must be included, since the temperature of a particle can change drastically during water vapour sorption processes and the sorption properties, such as equilibrium values and diffusivities, usually are strongly temperature-dependent.

2.1 Water transport

In this more complete model it is assumed that the internal water transport is accomplished by either (or both) so-called liquid diffusion or vapour diffusion. Liquid diffusion is here defined as a mass transport proportional to a moisture gradient, whereas vapour diffusion is proportional to a vapour concentration gradient.

The one-dimensional flow of liquid water can then be written as:

$$\dot{m}_{liq} = - \rho_p D_{liq} (X, T_s) \frac{\partial X}{\partial r} \qquad (2.1)$$

D_{liq}, an effective liquid diffusivity, often varies both with moisture content and temperature. A material balance over a differential shell of the particle gives:

$$\rho_p \frac{\partial X}{\partial t} + \varepsilon_p \frac{M_w}{R_o T_s} \frac{\partial p}{\partial t} = - \frac{1}{r^n} \frac{\partial}{\partial r} (r^n \dot{m}_{liq}) \qquad (2.2)$$

For a sphere n equals 2, for an infinite cylinder 1 and for an infinite flat plate 0. The second term of Eq. (2.2), the change in vapour content of the pores, can be neglected as the vapour content normally is approximately 10^{-4} times smaller than the liquid content. Equation (2.1) inserted into Eq. (2.2) gives after some rearrangements:

$$\frac{\partial X}{\partial t} = \frac{1}{r^n} \frac{\partial}{\partial r} (r^n D_{liq} (X, T_s) \frac{\partial X}{\partial r}) \qquad (2.3)$$

By introducing the dimensionless radius, η of Eq. (2.4), into Eq. (2.3), Eq. (2.5) results.

$$\eta = (r/R)^{m+1} \qquad (2.4)$$

$$\frac{\partial X}{\partial t} = \frac{(m+1)^2}{R^2} \eta^{\frac{m-n}{m+1}} \frac{\partial}{\partial \eta} \left(D_{liq} \eta^{\frac{m+n}{m+1}} \frac{\partial X}{\partial \eta}\right) \tag{2.5}$$

To describe the vapour diffusion, the vapour pressure everywhere in the particle must be assumed to be in equilibrium with the local moisture content at the local temperature of the particle. The vapour pressure is found from the sorption isotherms. The equations for vapour diffusion corresponding to Eqs. (2.1), (2.3) and (2.5) then become:

$$\dot{m}_{vap} = -\frac{M_w P_{tot}}{R_o T_s} \frac{D_{vap}}{(P_{tot} - p)} \left(\frac{\partial p}{\partial r}\right) \tag{2.6}$$

$$\frac{\partial X}{\partial t} = \frac{M_w}{R_o \rho_p} \frac{1}{r^n} \frac{\partial}{\partial r} \left(\frac{P_{tot}}{P_{tot} - p} \frac{D_{vap}}{T_s} r^n \left(\frac{\partial p}{\partial r}\right)\right) \tag{2.7}$$

$$\frac{\partial X}{\partial t} = \frac{M_w}{R_o \rho_p} \frac{(m+1)^2}{R^2} \eta^{\frac{m-n}{m+1}} \frac{\partial}{\partial \eta} \left(\frac{P_{tot}}{P_{tot} - p} \frac{D_{vap}}{T_s} \eta^{\frac{m+n}{m+1}} \left(\frac{\partial p}{\partial \eta}\right)\right) \tag{2.8}$$

The effective vapour phase diffusivity, D_{vap}, is assumed to change with temperature as the normal water vapour diffusivity does[19].

$$D_{vap} = D_{vap,o} \left(\frac{T}{T_o}\right)^{1.81} \tag{2.9}$$

Inserted into Eq. (2.8) this gives:

$$\frac{\partial X}{\partial t} = \frac{M_w}{R_o \rho_p} \frac{(m+1)^2}{R^2} \frac{D_{vap,o}}{T_o^{1.81}} \eta^{\frac{m-n}{m+1}} \frac{\partial}{\partial \eta} \left(\frac{P_{tot} T_s^{0.81}}{P_{tot} - p} \eta^{\frac{m+n}{m+1}} \left(\frac{\partial p}{\partial \eta}\right)\right) \tag{2.10}$$

Eqs. (2.5) and (2.10) can then be solved with the following boundary conditions.

$$\eta = 0; \quad \frac{\partial X}{\partial \eta} = \frac{\partial p}{\partial \eta} = 0 \tag{2.11}$$

$$\eta = 1; \quad \dot{m}_{liq} + \dot{m}_{vap} = -\frac{m+1}{R} \rho_p D_{liq} \left(\frac{\partial X}{\partial \eta}\right) - \frac{m+1}{R} \frac{M_w P_{tot}}{R_o T_s} \frac{D_{vap}}{(P_{tot} - p)} \left(\frac{\partial p}{\partial \eta}\right) =$$

$$= \frac{M_w P_{tot}}{R_o T_s} \beta_e \ln \left(\frac{P_{tot} - p_{air}}{P_{tot} - p_i}\right) \tag{2.12}$$

An alternative boundary condition to Eq. (2.12) is

$$X_i = \text{constant} \tag{2.13}$$

2.2 Heat transport

A heat balance over a differential shell of the particle means that the rate of accumulation of energy within this shell equals the net transport of energy to the shell. The rate of energy accumulation is given by:

$$\frac{\partial}{\partial t}\{\varepsilon_p \frac{pM_w}{R_o T_s}(\Delta H_o(X) + c_{p,v} T_s) + \varepsilon_p \frac{(P_{tot}-p)M_{air}}{R_o T} c_{p,air} T_s +$$

$$\rho_p c_{p,s}(X) T_s\} \tag{2.14}$$

where $c_{p,s}(X)$ is a linear function of X. ΔH_o, the sorption heat, includes both heat of condensation and wetting. The net transport of heat to the shell is given by the following equation:

$$-\frac{1}{r^n}\frac{\partial}{\partial r}\{r^n | \dot{m}_{vap}(\Delta H_o(X) + c_{p,v} T_s) + \dot{m}_{liq} c_{p,w} T_s - \lambda \frac{\partial T_s}{\partial r}|\} \tag{2.15}$$

In this case the vapour in the pores has to be assumed to be in equilibrium with the material. It is also assumed that the temperature of the vapour in the pores equals that of the particle. The reference state for enthalpy of water is chosen as adsorbed water of 0^oC. If the terms for accumulated energy in vapour and air of pores are neglected, since they are small compared to the terms for the adsorbed phase, Eqs. (2.1), (2.6), (2.14) and (2.15) can be combined to:

$$\frac{\partial T_s}{\partial t} = \frac{1}{c_{p,s}(X)}\left|- c_{p,w} T_s \frac{\partial X}{\partial t} + \frac{1}{r^n}\frac{\partial}{\partial r}\{r^n | \frac{M_w P_{tot}}{\rho_p R_o T_s}\frac{D_{vap}}{P_{tot}-p}(\Delta H_o(X) +\right.$$

$$\left. c_{p,v} T_s)\frac{\partial p}{\partial r} + D_{liq} c_{p,w} T_s \frac{\partial X}{\partial r} + \frac{\lambda}{\rho_p}\frac{\partial T_s}{\partial r}|\}\right| \tag{2.16}$$

By introducing η of Eq. (2.4) the following equation results:

$$\frac{\partial T_s}{\partial t} = \frac{1}{c_{p,s}(X)} \left| - c_{p,w} T_s \frac{\partial X}{\partial t} + \frac{(m+1)^2}{R^2} \eta^{\frac{m-n}{m+1}} \frac{\partial}{\partial \eta} \{ \eta^{\frac{m+n}{m+1}} \cdot \right.$$

$$\left| \frac{M_w P_{tot} D_{vap}}{\rho_p R_o T_s} \frac{(\Delta H_o(X) + c_{p,v} T_s)}{(P_{tot} - p)} \frac{\partial p}{\partial \eta} + D_{liq} c_{p,w} T_s \frac{\partial X}{\partial \eta} + \right.$$

$$\left. \left. \frac{\lambda}{\rho_p} \frac{\partial T_s}{\partial \eta} | \} \right| \right. \qquad (2.17)$$

Equation (2.17) can then be solved together with following boundary conditions:

$$\eta = 0; \quad \frac{\partial T_s}{\partial \eta} = 0 \qquad (2.18)$$

$$\eta = 1; \quad \alpha(T_{air} - T_{s,i}) = \frac{m+1}{R} \lambda \frac{\partial T_s}{\partial \eta} + \dot{m}_{liq} (\Delta H_o(X) + (c_{p,v} - c_{p,w}) T_s) +$$

$$(\dot{m}_{liq} + \dot{m}_{vap}) c_{pv} (T_{air} - T_s) \qquad (2.19)$$

In cases where the external resistance for heat transfer dominates, Eqs. (2.17)-(2.19) can be replaced by:

$$\alpha(T_{air} - \bar{T}_s) = \frac{\rho_p R}{n+1} c_{p,s}(X) \frac{\partial \bar{T}_s}{\partial t} + (\dot{m}_{liq} + \dot{m}_{vap})(\Delta H_o(X) + c_{p,v} T_{air} -$$

$$c_{p,w} \bar{T}_s) \qquad (2.20)$$

2.3 Numerical solution

The set of equations (2.5), (2.10) and (2.17) together with (2.11), (2.12), (2.18) and (2.19) are solved numerically by the application of a Crank-Nicolson finite-difference technique. The length coordinate can be divided either as equal-length intervals or equal-volume intervals. A predictor-corrector method is used to calculate the temperature and concentration profiles at a new time level. The difference between predicted and corrected values are always checked against a maximum and a minimum error. If the maximum error is exceeded, the time step is reduced and if the differences everywhere in the particle are

below the minimum error - and have been so for some time steps - the time step is increased.

The length coordinate η was normally divided into 20 intervals. The use of only 10 intervals generally did not change the calculated profiles to any significant extent, but calculated sorption rates and average moisture contents at the very beginning were affected.

It was found that one of the demands for stability in the numerical calculations is that:

$$\text{Max} \left| \frac{\lambda}{\rho_p \, c_{p,s}} \frac{\Delta t}{\Delta r^2} , \; D_{liq} \frac{\Delta t}{\Delta r^2} , \; D_{vap} \frac{M_w}{R_o \rho_p \, T_s} \left(\frac{\partial p^*}{\partial X}\right) \frac{\Delta t}{\Delta r^2} \right| < 0.5 \qquad (2.21)$$

This demand automatically restricts the size to which the time interval may be increased during the calculations.

The numerical solution was tested against reported analytical solutions[20,21] for the case of constant λ, D_{liq} and $D_{vap} \left(\frac{\partial p^*}{\partial X}\right)_T$. The numerical solution was also tested against other numerical solutions and mass and heat balances have also been checked against each other. The length step, time step and allowable maximum error have been reduced and the results checked against one another. All these tests gave sufficient reason to believe that the numerical solution is reliable.

3 THE ADSORPTION OF WATER VAPOUR ON A MOLECULAR SIEVE PARTICLE

The complete diffusion equations were solved for a sphere of molecular sieve ($R = 1.59 \cdot 10^{-3}$ m). In the calculations, the particle density ρ_p was set to 1213 kg/m^3. The choice of initial and boundary conditions corresponds to the experiments later described. Some of the used equilibrium data are plotted in Fig. 1 as isotherms with their characteristic curvature. The $c_{p,s}$- and ΔH_o-functions, which were used in the calculations, are described by the following equations:

$$c_{p,s}(X) = 1029 + 2500\ X \qquad |J/kg\ K| \tag{3.1}$$

$$\Delta H_o(X) = 3.44 \cdot 10^6 + 1.19 \cdot 10^7\ X - 5.89 \cdot 10^7\ X^2 \qquad |J/kg| \tag{3.2}$$

As Bi_h is low ($\simeq 0.2$) and the heat capacity of a particle is small, the internal temperature gradient becomes small, and the simpler Eq. (2.20) (assuming $Bi_h \to 0$) can be used to describe the heat transport. This also reduces the computation time for reasons described earlier (see Eq. (2.21)). Figure 2 presents the calculated concentration profiles at two different

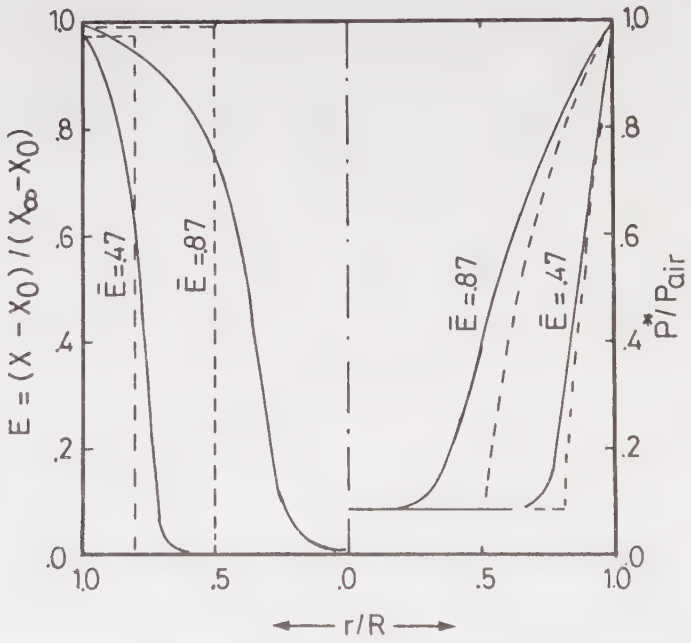

Fig. 2 Adsorption: Calculated concentration profiles in a molecular sieve sphere under constant boundary conditions.

$\bar{X}_o = 0.161$ kg/kg, $T_{s,o} = 60^oC$, $p_{air} = 2540$ Pa, $T_{air} = 60^oC$

$R = 1.59 \cdot 10^{-3}$ m, $D_{vap} = 1.1 \cdot 10^{-6}$ m^2/s, $\beta_e = 0.1$ m/s, $\alpha = 114$ W/m^2 K

times for a spherical particle. Due to the shape of the isotherms relatively sharp moisture profiles occur. If the term $(X - X_o)$ had been greater, which is the normal case for adsorption on regenerated material, the profiles would have been even sharper.

3.1 The simplified adsorption model - the shrinking-core model

In Fig. 2 it was shown that the isotherms produced an almost saturated outer shell and a decreasing unaffected core during adsorption. In the simplified model, the extreme case of a fully saturated outer shell is assumed. The dotted lines in Fig. 2 represent the assumed profiles in a shrinking-core model. According to the notations of Fig. 3, the vapour transport to the surface of a particle can be expressed as:

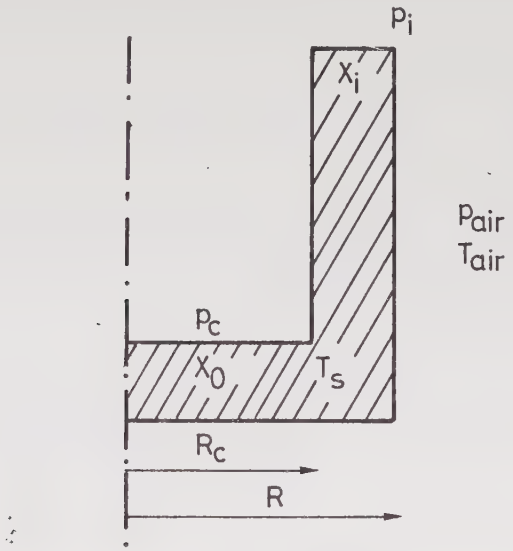

Fig. 3 The simplified adsorption kinetic model

$$r = R;\ \dot{m}_{vap} = -\frac{M_w P_{tot}}{R_o T}\ \beta_e \ln\left(\frac{p_{tot} - p_i}{p_{tot} - p_{air}}\right) \qquad (3.3)$$

The vapour transport from the surface to the core (through an inert spherical shell) is given by:

$$R_c \leq r \leq R;\quad \dot{m}_{vap} = -\frac{M_w P_{tot}}{R_o T}\ \frac{D_{vap}}{P_{tot} - p}\left(\frac{\partial p}{\partial r}\right) \qquad (3.4)$$

If the vapour pressure is assumed to be unaffected by the moisture content in the spherical shell (which holds completely only for extremely "favourable" isotherms) and if the product $\dot{m}_{vap} \cdot r^2$ is con-

sidered constant, Eq. (3.4) can be integrated between R_c and R. The result is given by the following equation:

$$r = R;\quad \dot{m}_{vap} = -\frac{M_w P_{tot}}{R_o T}\,\frac{D_{vap}}{R\,(R/R_c-1)}\,\ln\left(\frac{P_{tot}-p_c}{P_{tot}-p_i}\right) \qquad (3.5)$$

Eliminating p_i in Eqs. (3.3) and (3.5) gives:

$$r = R;\ \dot{m}_{vap} = -\frac{M_w P_{tot}}{R_o T}\,\frac{1}{\frac{1}{\beta_e}+\frac{R\,(R/R_c-1)}{D_{vap}}}\,\ln\left(\frac{P_{tot}-p_c}{P_{tot}-p_{air}}\right) \qquad (3.6)$$

As

$$\rho_p \frac{\partial \bar{X}}{\partial t} = -\frac{3}{R}\,\dot{m}_{vap,r=R} \qquad (3.7)$$

the average moisture content change can be written as:

$$\frac{\partial \bar{X}}{\partial t} = \frac{M_w P_{tot}}{R_o T}\,\frac{3}{R\rho_p}\,\frac{1}{\frac{1}{\beta_e}+\frac{R\,(R/R_c-1)}{D_{vap}}}\,\ln\left(\frac{P_{tot}-p_c}{P_{tot}-p_{air}}\right) \qquad (3.8a)$$

In the equations above R_c is unknown. It can be calculated, if X_i is known, since

$$R/R_c = \left|(X_i - X_o)/(X_i - \bar{X})\right|^{1/3} \qquad (3.9a)$$

X_i is a function of both p_i and $T_{s,i}$ (from equilibrium data). p_i can be calculated through Eq. (3.3) after a first estimate of vapour flow rate has been made. This procedure must then be repeated until a constant $\partial\bar{X}/\partial t$ is reached.

If the internal diffusion dominates, p_i can be assumed to approximately equal p_{air} and the calculations become simpler.

The corresponding equations for an infinite cylinder with radius R become:

$$\frac{\partial \bar{X}}{\partial t} = \frac{M_w P_{tot}}{R_o T}\,\frac{2}{R\rho_p}\,\frac{1}{\frac{1}{\beta_e}+\frac{R}{D_{vap}}\ln(R/R_c)}\,\ln\left(\frac{P_{tot}-p_c}{P_{tot}-p_{air}}\right) \qquad (3.8b)$$

$$R/R_c = |(X_i - X_o)/(X_i - \bar{X})|^{1/2} \qquad (3.9b)$$

and for an infinite flat plate with thickness 2R:

$$\frac{\partial \bar{X}}{\partial t} = \frac{M_w P_{tot}}{R_o T} \frac{1}{R\rho_p} \frac{1}{\frac{1}{\beta_e} + \frac{R - R_c}{D_{vap}}} \ln\left(\frac{P_{tot} - p_c}{P_{tot} - p_{air}}\right) \qquad (3.8c)$$

$$R/R_c = (X_i - X_o)/(X_i - \bar{X}) \qquad (3.9c)$$

The heat transport is assumed to be affected only by external heat resistance ($Bi_h \to 0$). Then the change in temperature of a spherical particle can be described by:

$$\frac{\partial T_p}{\partial t} = \frac{1}{c_{p,s}(X)} \{(\Delta H_o - c_{p,w} T_p + c_{p,v} T_{air}) \frac{\partial \bar{X}}{\partial t} - \frac{3\alpha}{R\rho_p} (T_p - T_{air})\} \qquad (3.10)$$

The adsorption rate versus the moisture content is compared for the two models in Fig. 4. The sorption rate of the shrinking-core model

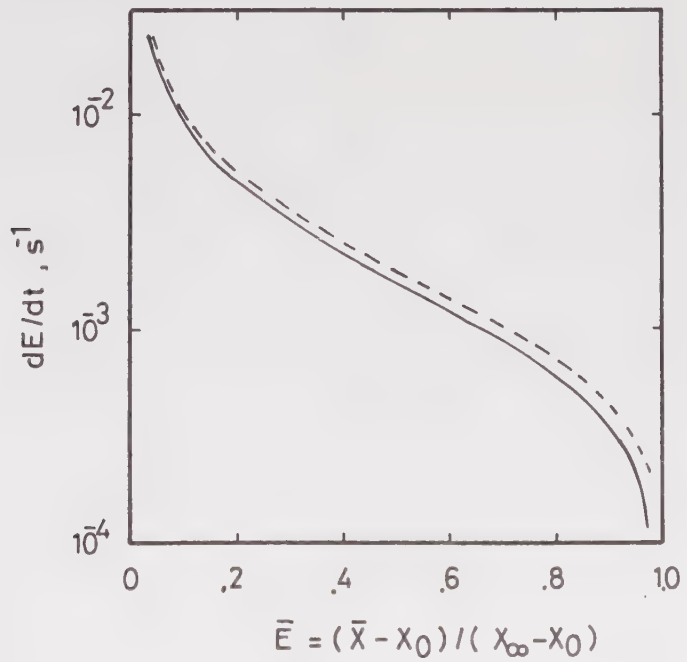

Fig. 4 Adsorption rates of the simplified model (---) compared to the more complete model (——). Constant boundary conditions $\beta_i = 6.9 \cdot 10^{-4}$ m/s. Other data given in text of Fig. 2

follows the more complex model well, although it is a little bit higher.

In an adsorption tower, a particle is exposed to varying air conditions. To be reliable the simplified model must react in accordance with the more complex model even for this case. If the external vapour pressure is always increasing, as is the case during adsorption in an adsorption tower, there is reason to believe that the model can be used. Figure 5 describes a possible way in which the air temperature and humidity can change with time in an adsorption tower. The two models are compared in Fig. 6 with respect to adsorption rate for the varying boundary conditions of Fig. 5. Even here the two models follow each other fairly well. The adsorption rate seems to be the most important kinetic parameter to study in adsorption as this directly affects the degree of dehumidification. It must however be observed that there is no reason to believe that the model can be used with good results if the increase in external vapour pressure stops half-way for any longer period of time or if the vapour pressure is reduced.

The assumption of negligible temperature gradient inside the particles and its eventual effect upon adsorption rate has been tested for the two examples described in Figs. 4 and 6. Due to low internal heat transport resistance and the low heat capacity of the simulated sphere (Bi_h is low and Fo_h high), most of the heat flow is caused by the heat release at the adsorption front and little heat is used for changing the temperature of material. In the example of Fig. 4, the complete model was also solved with $Bi_h = \alpha R/\lambda = 0.18$. In the example a step change in humidity was made and of course temperature gradients occured in the beginning. However, the difference in average moisture content between the two models was less than 0.0002 kg/kg already after a couple of seconds. In the example described by Figs. 5 and 6, the boundary conditions are changing with time and the adsorption rate is slower than in the beginning of the previous example. In a similar way to the shrinking-core model for mass transfer, a heat transfer expression can be formulated. Since all heat is released in a thin shell, there must be a gradient between this shell and the outer surface of the particle. The following equations approximately represent the case:

$$\alpha_i (T_{cent} - T_{surf}) = \alpha_e (T_{surf} - T_{air}) \qquad (3.11)$$

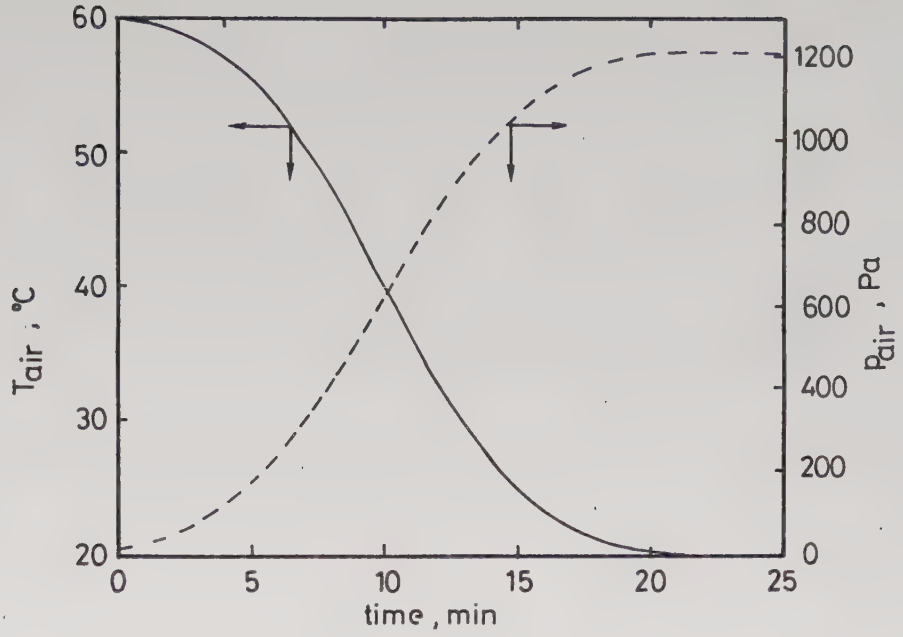

Fig. 5 Assumed varying boundary conditions for a particle in an adsorption tower.

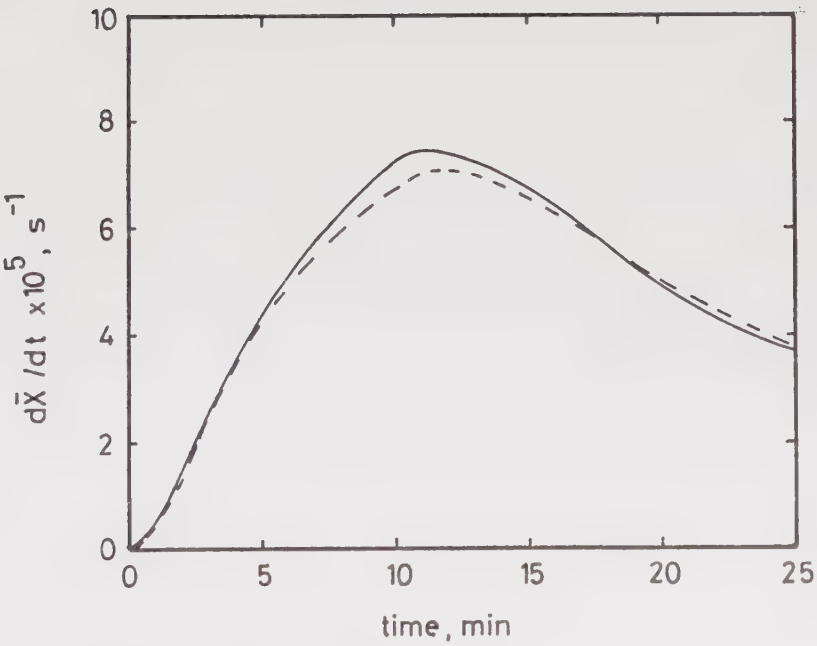

Fig. 6 Adsorption rates of the simplified model (---) compared to the more complete model (——). Varying boundary conditions.

$\bar{X}_o$ = 0.0731 kg/kg, $T_{s,o}$ = 60 °C, R = $1.59 \cdot 10^{-3}$ m,

D_{vap} = $1.1 \cdot 10^{-6}$ m^2/s, β_e = 0.1 m/s, β_i = $6.9 \cdot 10^{-4}$ m/s, α = 114 W/m^2K

where

$$\alpha_i = \frac{\lambda}{R(R/R_c - 1)} \qquad (3.12)$$

Since $\alpha_i >> \alpha_e$, the term $(T_{cent} - T_{surf})$ is less than 0.04^oC during the whole simulation. Thus the internal temperature gradient and its effect upon the internal mass transport can be neglected.

Similar types of mass transport models have sometimes been used to explain drying rate curves. Schlünder[22] and Zabeschek[23] found that a similar model can to some extent explain experimentally found drying rate curves of spheres of alumina silicate, which is weakly hygroscopic. A "receding-plane" model has been used by Keey and Suzuki[24] to describe theoretically the drying curve of a porous, non-hygroscopic slab.

For the drying of granular fertilizers, Garside et al[25] used a simple shrinking-core model to determine an effective vapour-phase diffusivity. The fertilizers were hygroscopic and the isotherms had a curvature opposite that of molecular sieves, i.e. $\frac{\partial^2 p}{\partial X^2} < 0$. Hallström[26] has recently extended the model and shown its practicality for such materials.

3.2 Influence of variations in geometry and particle size

The molecular sieve pellets have a cylinder diameter of $3.2 \cdot 10^{-3}$ m and an average length of $6.2 \cdot 10^{-3}$ m. The standard deviation in lenght was found to be $1.8 \cdot 10^{-3}$ m. It is clear that neither the shrinking-core model for a sphere or that for an infinite cylinder would describe the mass transfer rates of a pellet correctly. In Eq. (3.8a) β_e must act on the real external surface area $a_{v,p}$. The equation can therefore be rewritten to:

$$\frac{\partial \bar{X}}{\partial t} = \frac{M_w P_{tot}}{R_o T} \frac{a_{v,p}}{\rho_p} \frac{1}{\frac{1}{\beta_e} + \frac{R^2(R/R_c - 1) \cdot a_{vp}}{3 \cdot D_{vap}}} \ln\left(\frac{P_{tot} - p_c}{P_{tot} - p_{air}}\right) \qquad (3.13)$$

or

$$\frac{\partial \bar{X}}{\partial t} = \frac{M_w P_{tot}}{R_o T} \frac{a_{v,p}}{\rho_p} \frac{1}{\frac{1}{\beta_e} + \frac{R/R_c - 1}{\beta_i}} \ln\left(\frac{P_{tot} - p_c}{P_{tot} - p_{air}}\right) \qquad (3.14)$$

The corresponding equation for the cylinder then becomes:

$$\frac{\partial \bar{X}}{\partial t} = \frac{M_w P_{tot}}{R_o T} \frac{a_{v,p}}{\rho_p} \frac{1}{\frac{1}{\beta_e} + \frac{\ln(R/R_c)}{\beta_i}} \ln\left(\frac{P_{tot} - p_c}{P_{tot} - p_{air}}\right) \qquad (3.15)$$

The constant β_i is then determined experimentally. The question arises which of the two models would best describe the adsorption of water vapour on the pelletized molecular sieve. In Fig. 7 the two models are

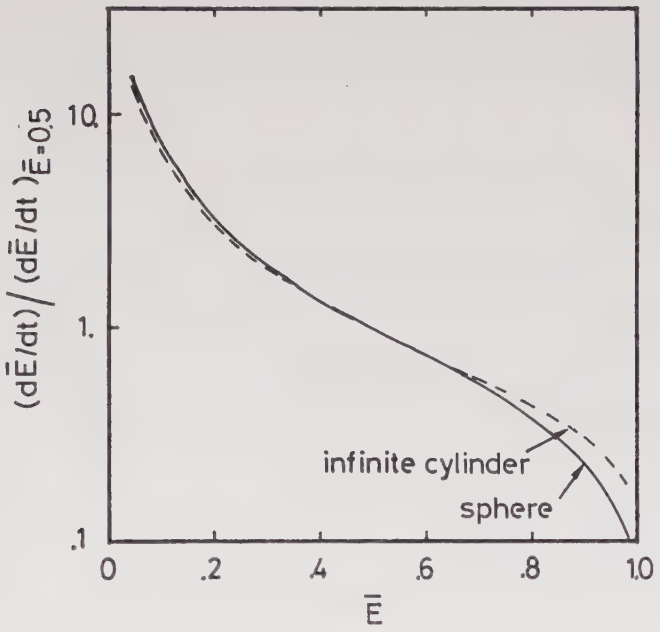

Fig. 7 A comparison of relative adsorption rates between two shrinking-core models.

compared for the case of no external mass transfer resistance. The deviation between the two models is small, except for higher degrees of saturation. If a shrinking-core model for a finite cylinder is derived and if it is assumed that the length-diameter ratio of the core equals the same ratio of the particle, the same type of equation as in (3.14) results (see also Eq. (3.16)). A similar expression, where the reduction in length of the core cylinder equals the reduction in core diameter, gives a curve that closely follows the curve for the sphere of Fig. 7. For these reasons the shrinking-core model for a sphere has been assumed to best describe the changing mass transport resistance in the particles.

The effect of varying cylinder lengths on the total adsorption rate has also been investigated. If the external mass transfer is neglected the rate equation for a finite cylinder becomes:

$$\frac{\partial \bar{X}}{\partial t} = \frac{M_w P_{tot} D_{vap}}{R_o T \rho_p} \left(\frac{1}{L^2} + \frac{2}{R^2}\right) \frac{1}{(1-\bar{E})^{-1/3}-1} \ln\left(\frac{P_{tot} - p_c}{P_{tot} - p_{air}}\right) \quad (3.16)$$

where

$$\bar{E} = (\bar{X} - X_o)/(X_i - X_o) \quad (3.17)$$

The length of the cylinder is here 2L and L_c/L equals R_c/R. This equation can be integrated over time to:

$$1.5 - \bar{E} - 1.5\ (1-\bar{E})^{2/3} = \frac{M_w P_{tot} D_{vap}}{R_o T \rho_p} \left(\frac{1}{L^2} + \frac{2}{R^2}\right) \frac{t}{(X_i - X_o)} \ln\left(\frac{P_{tot} - p_c}{P_{tot} - p_{air}}\right) \quad (3.18)$$

The variation in cylinder length is assumed to follow a normal distribution curve with the experimentally determined standard deviation of $1.8 \cdot 10^{-3}$ m. The distribution curve was divided into nine intervals and for each interval $\bar{E}$ and $d\bar{E}/dt$ were calculated at different times with the help of Eqs. (3.16) and (3.18). The weight fraction of each interval and the weight-average of $\bar{E}$ and $d\bar{E}/dt$ could then be calculated. At no time value did the weight-averaged $\bar{E}$ or $d\bar{E}/dt$ differ more than 0.5% from the $\bar{E}$ and $d\bar{E}/dt$ calculated at the average length-cylinder ratio.

For these reasons it can be concluded that the shrinking-core model of a sphere, together with the real specific surface area and particle density, should be able to describe the adsorption kinetics of the pellets.

3.3 A comparison between experimental and calculated adsorption runs

In the experiments, the weight changes of a through-circulated bed (0.017 m in height), the outlet temperature and humidity were continuously measured, when the inlet air humidity was suddenly raised. The inlet air temperature remained constant. More details of the experimental equipment and technique can be found elsewhere[2]. Figures 8 and 9 describe the results from one adsorption experiment. The shrinking-core model was now applied to describe the local rate of adsorption. The following equations were integrated to describe the adsorption process of the whole bed.

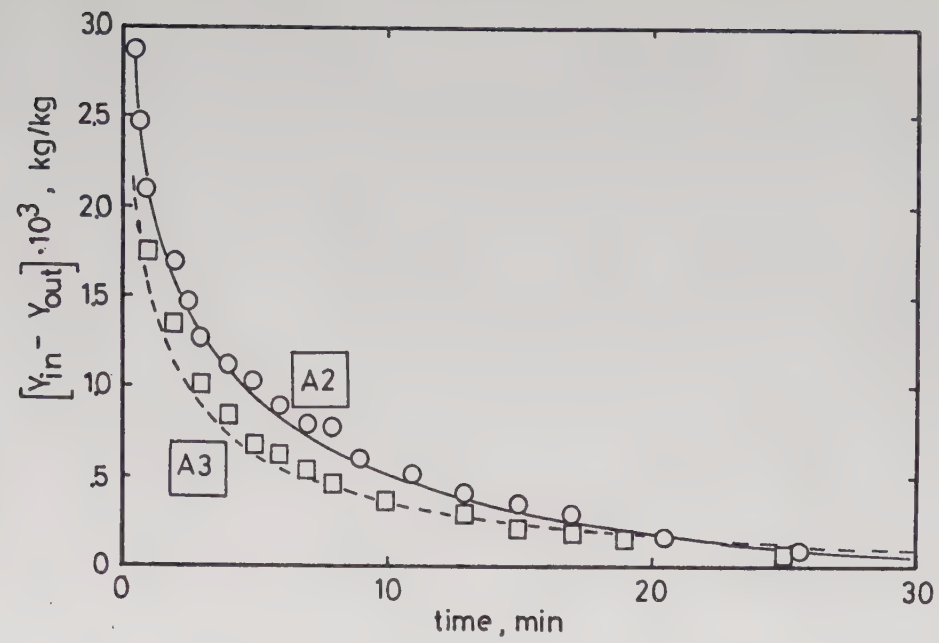

Fig. 10 Experimental (○,□) adsorption runs compared with calculated runs (——). Varying air fluxes. $T_{air} = 60^{o}C$, $\beta_i = 6.6 \cdot 10^{-4}$ m/s
Run A2: $\bar{X}_o = 0.163$ kg/kg, $p_{air} = 1440$ Pa, $\dot{m}_{air} = 0.38$ kg/m^{2}s, $\beta_e = 0.11$ m/s, $\alpha = 106$ W/m^{2}K
Run A3: $X_o = 0.148$ kg/kg, $p_{air} = 1470$ Pa, $\dot{m}_{air} = 0.76$ kg/m^{2}s, $\beta_e = 0.13$ m/s, $\alpha = 130$ W/m^2 K

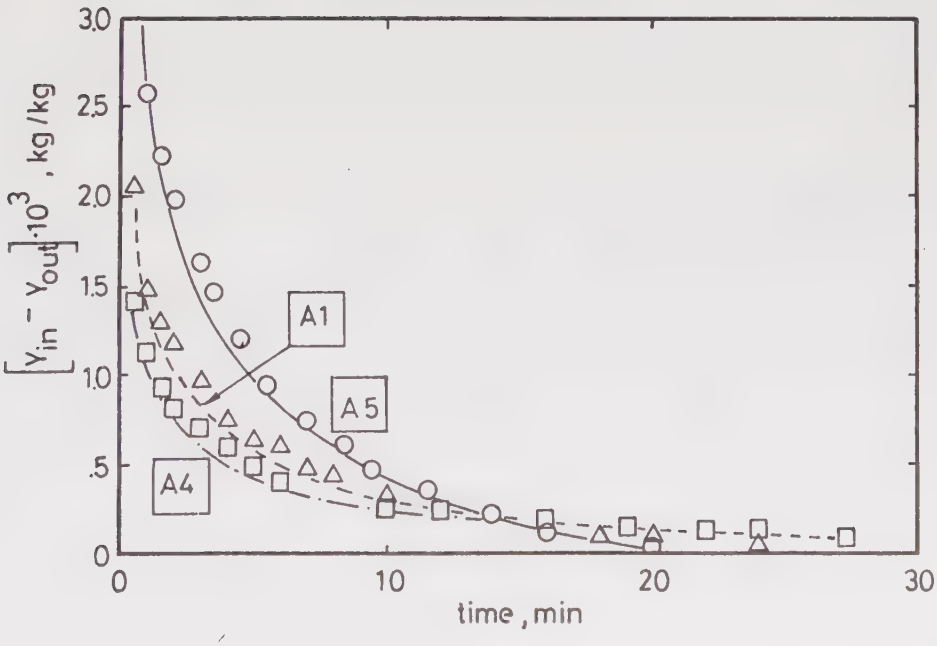

Fig. 11 Experimental (○,△,□) adsorption runs compared with calculated runs (——). Varying air humidities.
$X_o = 0.168$ kg/kg, $\dot{m}_{air} = 0.52$ kg/m^{2}s, $T_{air} = 60^{o}C$
$\beta_e = 0.12$ m/s, $\beta_i = 6.6 \cdot 10^{-4}$ m/s, $\alpha = 114$ W/m^{2}K
Run A4: $p_{air} = 940$ Pa; Run A1: $p_{air} = 1320$ Pa;
Run A5: $p_{air} = 2540$ Pa

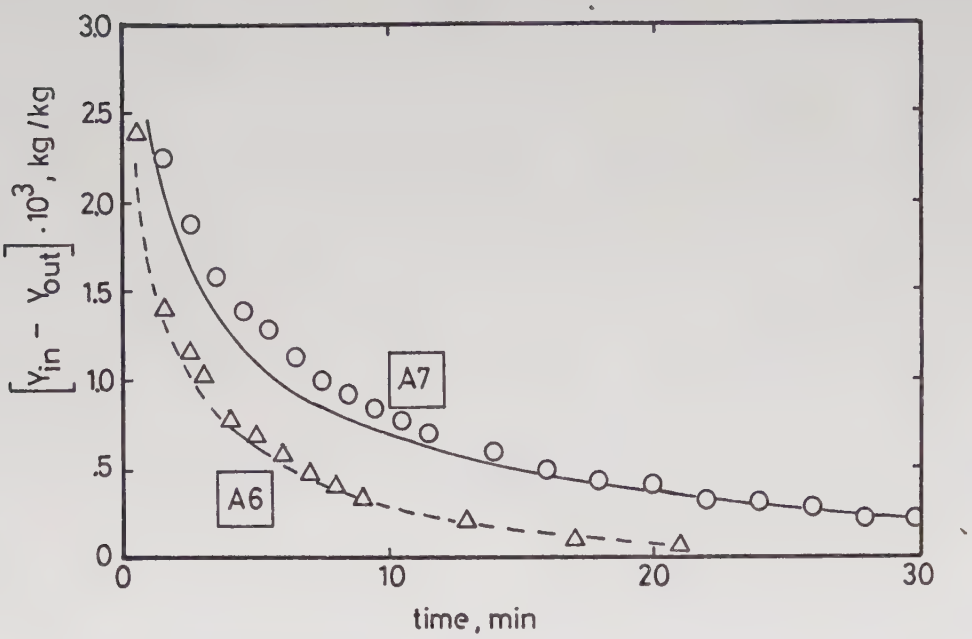

Fig. 12 Experimental (○,△) adsorption runs compared with calculated runs (═══). Varying temperatures.

β_e = 0.12 m/s, β_i = $6.6 \cdot 10^{-4}$ m/s, α = 114 W/m^{2}K, $\dot{m}_{air}$ = 0.52 kg/m^{2}s

Run A6: $\bar{X}_o$ = 0.187 kg/kg, p_{air} = 1630 Pa, T_{air} = 40°C

Run A7: $\bar{X}_o$ = 0.117 kg/kg, p_{air} = 1490 Pa, T_{air} = 81°C

follow the experimental rather well. In Figs. 10 to 12 some more runs are presented. Only the difference between outlet and inlet humidities versus time is presented, since this gives a direct measure of the capability of the material to reduce the air humidity. The difference has in comparison to Fig. 9 been calculated from the weight change, which continuously was measured by an electronic balance. A rather good fit between calculations and experiments is found in all runs.

Therefore it seems possible to approximately describe the adsorption process of the pellets as the saturation of an increasing outer shell of a sphere. In this model the mass transfer is described by Eqs. (3.21), (3.23) and (3.24). β_i has been found from experiments to be approximately $6.6 \cdot 10^{-4}$ m/s.

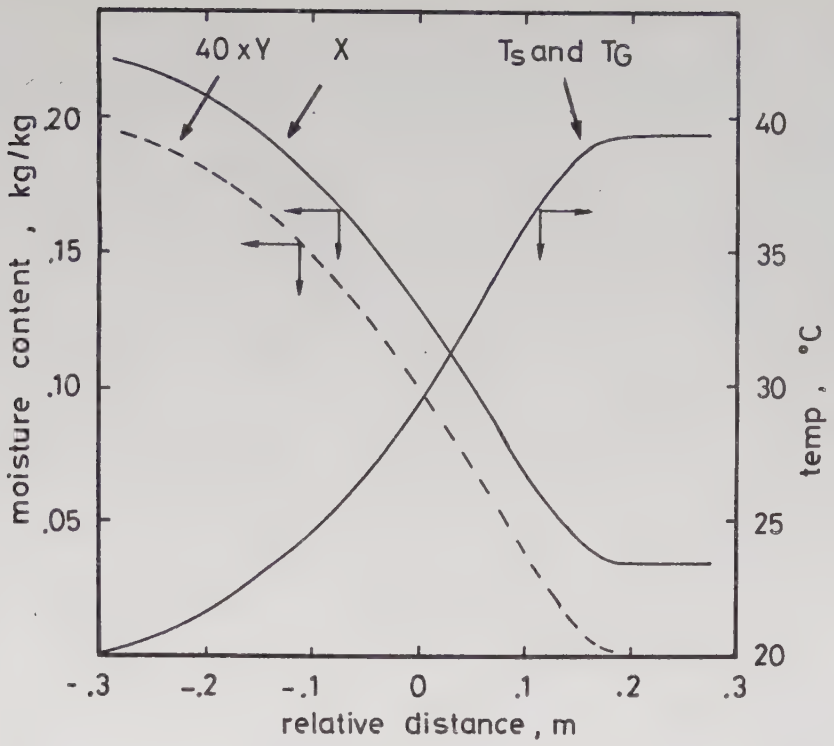

Fig. 13 Adsorption: Calculated moisture, humidity and temperature profiles in a fixed bed of particles. The location of the relative distance 0 is given by: 0.02 + 0.0654 × hours (m).
$\bar{X}_o$ = 0.034 kg/kg, $T_{s,o}$ = 20°C, T_{air} = 20°C, Y_{in} = 0.005 kg/kg
$\dot{m}_{air}$ = 0.5 kg/m^{2}s, β_e = 0.1 m/s, β_i = 6.6·10^{-4} m/s, α = 114 W/m^{2}K

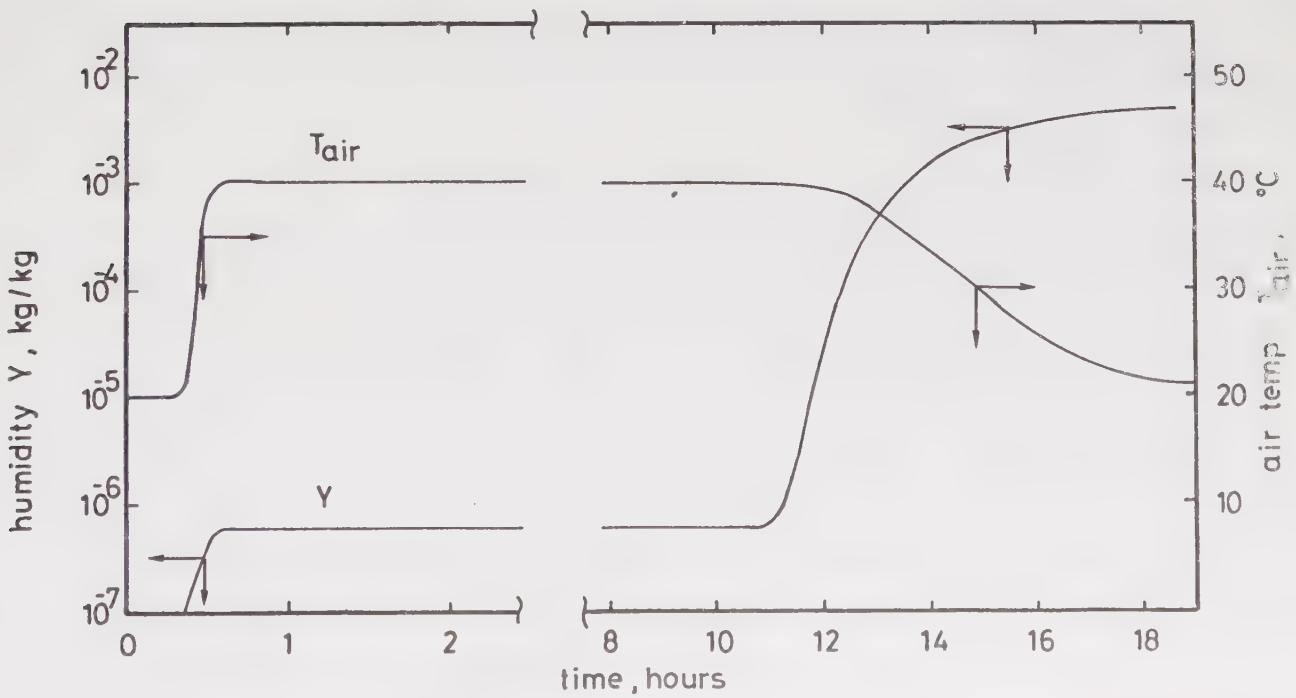

Fig. 14 Adsorption: Calculated outlet air conditions from a 1.0 m bed. See also text of Fig. 13.

3.4 Calculated concentration and temperature profiles in a bed during adsorption

During adsorption the moisture profile of the bed approaches the "constant-pattern" behaviour. Figure 13 gives the calculated moisture, humidity and temperature profiles progressively through a deep bed of pellets. As $\dot{m}_{air}$ appears in all length derivates, the same curve results at other air flow rates if the corresponding change in distance parameter is made. The front in Figure 13 is preceded by another front. This is clearly revealed in Figure 14, which gives the outlet air condition versus time for a 1.0 m bed. The whole process can be seen as two fronts moving at different velocities through the bed. The velocity of the first front is determined by the rate at which the material can reach the elevated temperature level from its initial temperature. This rate will be determined by the ratio of heat capacity of air and material. The front consists of a temperature change and a small accompaning vapour concentration change. Normally the material is regenerated at an elevated temperature and therefore has a high temperature at the beginning of the adsorption cycle. If so the first front will appear as a cooling front, where the material is cooled down. This change in temperature is also accompanied by a corresponding change in air humidity.

The second, much slower, front is caused by the adsorption of water vapour on the material and its rate is determined by the water holding capacity of the material.

The calculated two-front behaviour in both adsorption and desorption has also been shown experimentally and theoretically by others[16,27,28].

Axial dispersion has been neglected in the calculations. Garg and Ruthven[29] have analysed the combined effects of mass transfer and longitudinal diffusion in molecular sieve adsorption columns. They conclude that the effect of axial dispersion may be significant at low Reynolds numbers but only if intraparticle resistance is small. If the conditions of the present simulations are applied to their analysis it is shown that the effect of axial dispersion on the break-through curve is negligible.

4 THE DESORPTION OF WATER VAPOUR FROM A MOLECULAR SIEVE PARTICLE

The mass transport mechanism, the assumption of no internal temperature gradients, and the influence of variations in geometry and shape upon mass transport were discussed under the description of adsorption. Much of those discussions are applicable even to desorption and will therefore not be discussed here.

4.1 Simplified desorption kinetic model

It has earlier been shown[2] that a simple linear kinetic expression seemed to describe the desorption process relatively well. The rate expression was:

$$\rho_b \left(\frac{\partial \bar{X}}{\partial t}\right) = - \beta a_v \rho_{air} (Y_s^* - Y) \qquad (4.1)$$

where $Y_s^* = f(\bar{X}, T_s)$ and β is a "lumped" mass transfer coefficient. Such coefficients include both external and internal mass transfer resistances. Eq. (4.1), which is valid at low vapour pressures, is the approximate form of:

$$\rho_b \left(\frac{\partial \bar{X}}{\partial t}\right) = - \beta a_v \frac{M_w P_{tot}}{R_o T} \ln \frac{P_{tot} - p_s^*}{P_{tot} - p_{air}} \qquad (4.2)$$

where $p_s^* = f(\bar{X}, T_s)$. In this work Eq. (4.2) has been used throughout.

Figure 15 shows the concentration profiles in a molecular sieve particle during desorption. The profiles have been calculated from the complete model of mass transfer, as was earlier described in sect. 2 and with the material properties given in sect. 3. In contrast to the adsorption process (see Fig. 2), the moisture content in the center of the particle is affected rather early and a steep moisture gradient is maintained close to the surface of the particle. In Fig. 15 it can also be seen how a reduction in average moisture content strongly affects the vapour pressure gradient. Not surprisingly, the magnitude of the desorption rate is lower than that for adsorption. This is also shown when comparing the solid lines of Figs. 4 and 16.

The simplified kinetic model of Eq. (4.2) now claims that vapour is diffusing from an internal core, with moisture content $\bar{X}$, through a

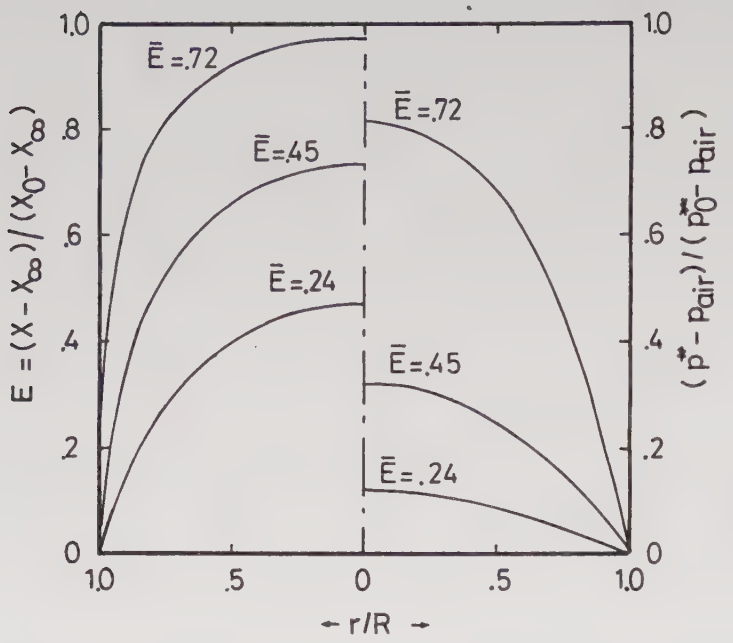

Fig. 15 Desorption: Calculated concentration profiles in a molecular sieve sphere. Constant boundary conditions.

$\bar{X}_o$ = 0.200 kg/kg, p_{air} = 206 Pa, T_{air} = 60°C

R = $1.59 \cdot 10^{-3}$ m, D_{vap} = $1.1 \cdot 10^{-6}$ m^2/s, β_e = 0.1 m/s, α = 114 W/m^2K

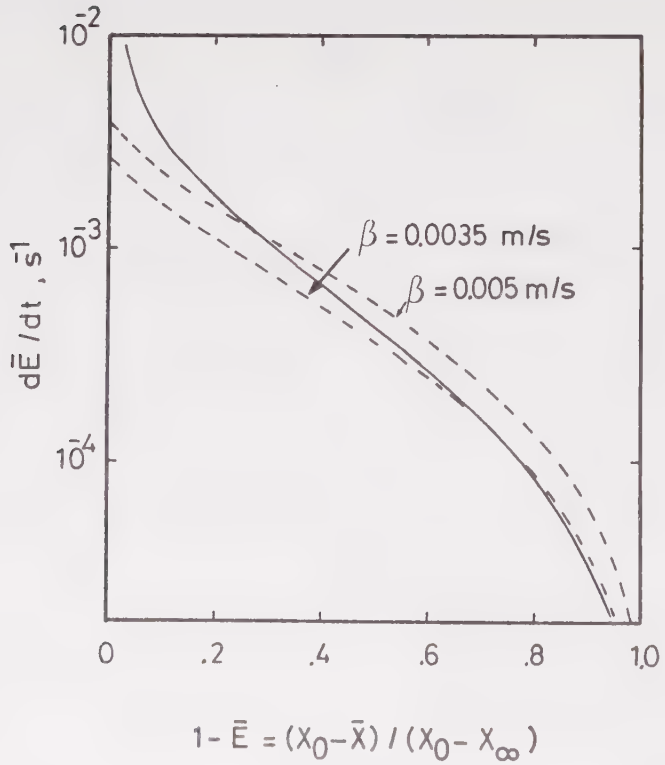

Fig. 16 Desorption rates of the simplified model (----) compared to those of the more complete model (——). See also text of Fig. 15.

shell of dry material and through an external boundary layer to the air bulk. That this is not fully true can be seen in Figs. 15 and 16. However, the approximation gives some description of how the desorption rate varies. There is also reason to believe that the approximation is better when the moisture content is reduced more than was the case in the example of Figs. 15 and 16. Some difference between reality and model can also be accepted, at high desorption rates, only if the lower rates are well described. This due to the fact that in desorption, the curve describing the moisture content versus time is interesting, not the desorption rate in itself. Therefore the lower β-value has been used in the following calculations.

The two models have also been tested at varying boundary conditions. The assumed conditions correspond to the calculated outlet air condition of a 0.5 m bed, initially with a moisture content of 0.23 kg/kg and which is regenerated with air of 200°C. With $\beta = 0.0035$ m/s, the discrepancy between the two moisture content curves was generally negligible and never over 0.008 kg/kg.

In the desorption calculations, the equilibrium vapour pressure exceeds the region in which the sorption isotherms were determined. However, it is assumed that the isotherms at higher temperature levels have the same shape as was found at lower temperatures and consequently that Eq. (3.25) still is valid. Equation (3.25) was also extended so that at relative humidities over 80% the isotherms are bended upwards as is indicated by the 20°-isotherm in Fig. 1.

4.2 A comparison between experimental and calculated desorption runs

Figure 17 shows the moisture content - time curves of two experiments together with the calculated curves of two different β-values. The slow process is very well revealed by the curves. (Compare for example with adsorption in Fig. 10 and observe the different time scales.) Figure 18 describes two other experiments. The two experiments have been made at different temperatures. At 80°C the curvature of the isotherm is more pronounced than in the case at 40°C which is revealed by the desorption rates. The comparison between the two mass transport models in Fig. 16 showed that the more complete model gave lower desorption rates towards the end. The results of the desorption experiments also show this tendency.

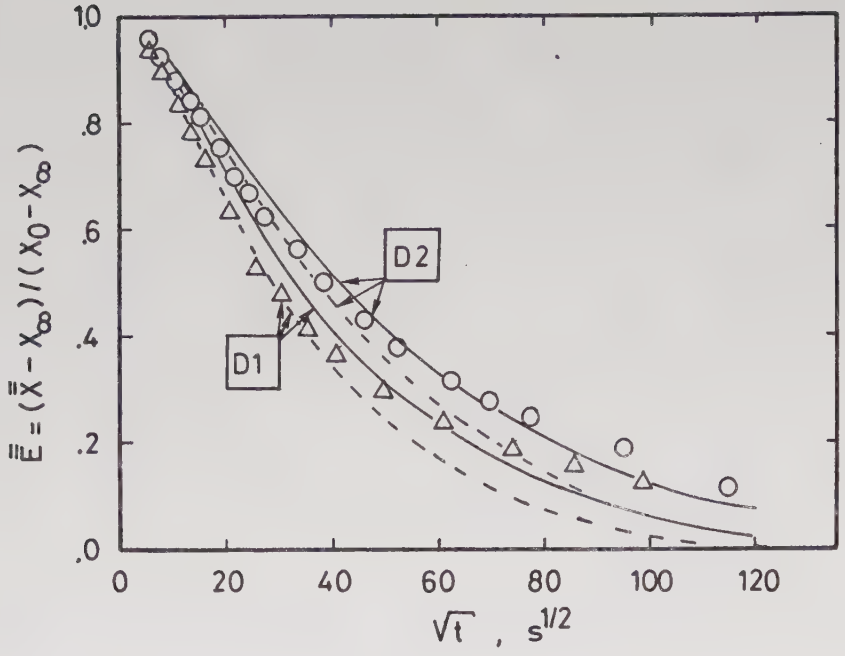

Fig. 17 Experimental (0,Δ) desorption runs compared with calculated runs. Varying air fluxes.

β = 0.005 m/s (---), β = 0.0035 m/s (——), T_{air} = 60°C

Run D1: $\bar{X}_o$ = 0.200 kg/kg, $\dot{m}_{air}$ = 0.52 kg/m^{2}s, p_{air} = 150 Pa, α = 114 W/m^{2}K

Run D2: $\bar{X}_o$ = 0.194 kg/kg, $\dot{m}_{air}$ = 0.38 kg/m^{2}s, p_{air} = 120 Pa, α = 105 W/m^{2}K

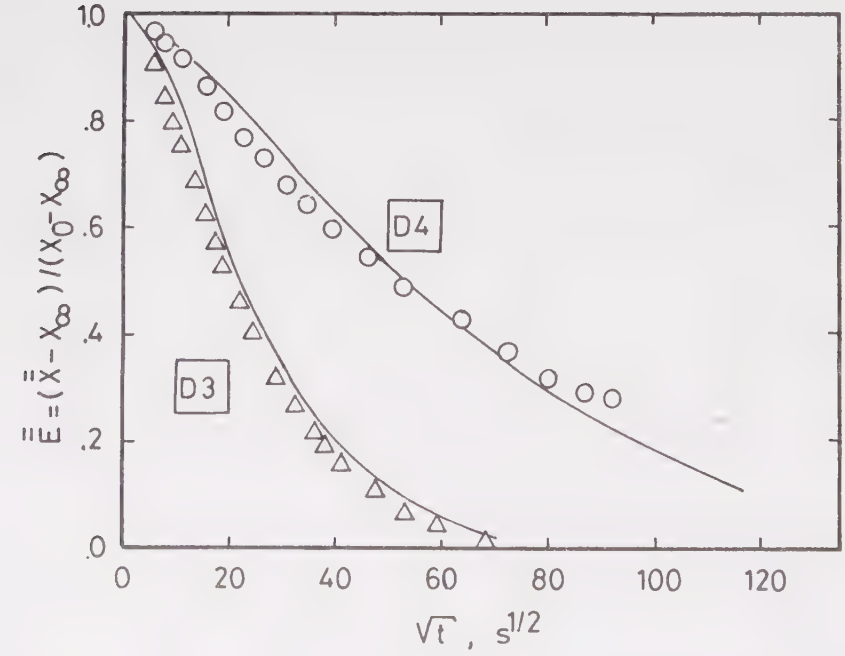

Fig. 18 Experimental (0,Δ) desorption runs compared with calculated runs (——).

β = 0.0035 m/s, α = 114 W/m^{2}K, $\dot{m}_{air}$ = 0.52 kg/m^{2}s, p_{air} = 163 Pa

Run D3: $\bar{X}_o$ = 0.214 kg/kg, T_{air} = 40°C

Run D4: $\bar{X}_o$ = 0.179 kg/kg, T_{air} = 81°C

Unfortunately most experiments were, due to the slow deosprtion rate, interrupted before the equilibrium moisture content was reached. The final moisture content can of course be found from the isotherms and the experimentally-determined air humidities and temperatures. However, at low air humidities the isotherms are rather steep which makes it difficult to exactly determine the final moisture content. This, together with the fact that there was a small drift in the weight recordings, made the moisture content determination towards the end less accurate.

However, it must be concluded that the simplified model describes the desorption experiments rather well.

4.3 Calculated concentration and temperature profiles in a bed during desorption

The bed can either be regenerated with hot air or with air of extremely low vapour pressure. In twin-tower applications the regeneration must also be completed before break-through is reached in the adsorption tower.

Air of low vapour pressure is used in some cases when dehumidifying compressed air. The dried compressed air is then expanded and used as air for regeneration. Such procedure is often called "pressure-swing" regeneration. Compared to the compressed air the expanded air can contain more water as the total pressure is lower and thus less air is needed. In these simulations, atmospheric total pressure has been assumed so the low vapour pressure regeneration would here be rather hypothetical. However, to illustrate the behaviour a calculation was made for a 0.5 m bed originally with $T_s = 20^oC$ and $\bar{X} = 0.22$ kg/kg. The bed was regenerated with air of 20^oC and 0.015 Pa in vapour pressure. This vapour pressure is approximately the equilibrium vapour pressure of a pellet at $\bar{X} = 0.034$ kg/kg and $T_s = 20^oC$. It was shown before that the magnitude of the desorption rate was much lower than that of adsorption and this is also clearly revealed in the calculations. The break-through of a 0.5 m bed in the previously described adsorption simulation occurs after approximately 8 hours. After 8 hours of regeneration the moisture content at the inlet has only been reduced from 0.22 to 0.17 kg/kg. The shape of the isotherms also makes the moisture profiles in the bed become flatter and flatter in contrast to adsorption.

In thermal regeneration, also called "thermal-swing" regeneration, hot air raises the temperature of the material and consequently the equilibrium vapour pressure. The increase in temperature also means that the air can contain more water. Figure 19 presents the calculated result of how the moisture profiles in a bed can change during regeneration with hot air of 200°C. In these calculations the vapour pressure relation has been extended over the region originally determined. As high relative humidities occur and other mass transport processes such as liquid capillary flow are neglected, the true moisture profiles will probably differ from those calculated at higher moisture contents. At the beginning of the thermal regeneration the first layers of particles approach such high equilibrium vapour pressures that the total pressure P_{tot} inside the particle probably would be affected. If so, the flow of vapour would also be caused by a total pressure gradient in the particle. The vapour will then also be transported in laminar flow to the surface. This has not been considered in the model. None the less some interesting things can be derived from the calculations.

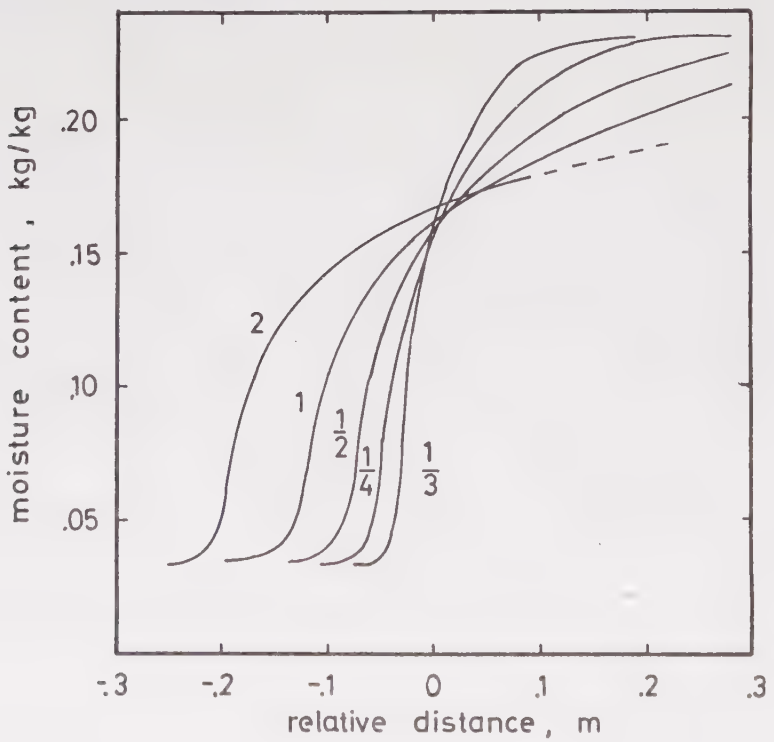

Fig. 19 Desorption: moisture profiles in a 1.0 m bed. The location of the relative distance 0 is given by: 0.452 × hours (m).
Parameter: time in hours

$\bar{X}_o$ = 0.22 kg/kg, $T_{s,o}$ = 20°C, $T_{air,in}$ = 200°C, Y_{in} = 0.005 kg/kg

$\dot{m}_{air}$ = 0.5 kg/m^{2}s, α = 114 W/m^{2}K, β = 0.0035 m/s

Compared with the low vapour pressure regeneration, the moisture profiles in Fig. 19 are much steeper. The constant pattern behaviour is not found here either, although at low moisture contents a constant pattern seems to have developed. The isotherms are highly unfavourable for "constant-pattern" profiles in desorption. However, in thermal regeneration the particle is heated during the desorption and the real p^* - $\bar{X}$ curve does not follow an isotherm. The calculations gave the relation between p^* and $\bar{X}$ as presented in Fig. 20. The actual curve has a part at lower moisture content where $\partial^2 p^*/\partial X^2 < 0$, i.e. this part is favourable for desorption and will therefore produce constant pattern profiles.

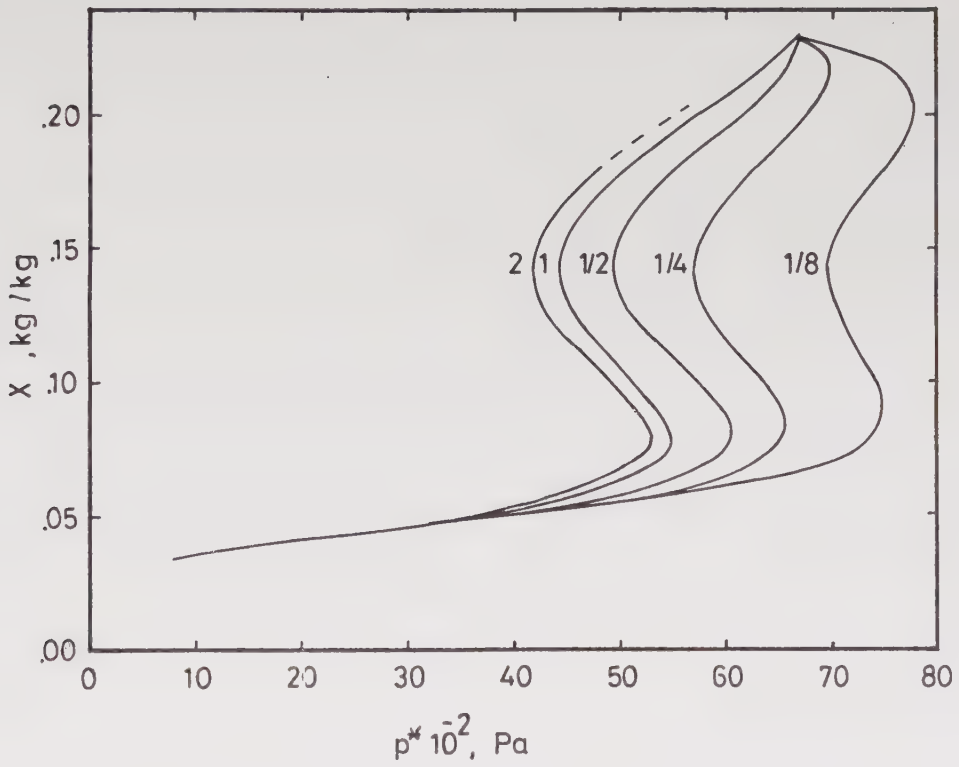

Fig. 20 Desorption: The real p^* - $\bar{X}$ curves in the calculated run shown in Fig. 19.

The changes in outlet air condition with time for a 1.0 m bed during desorption are presented in Fig. 21. The two-front behaviour as discussed earlier for adsorption in sect. 3.4 can also be seen here.

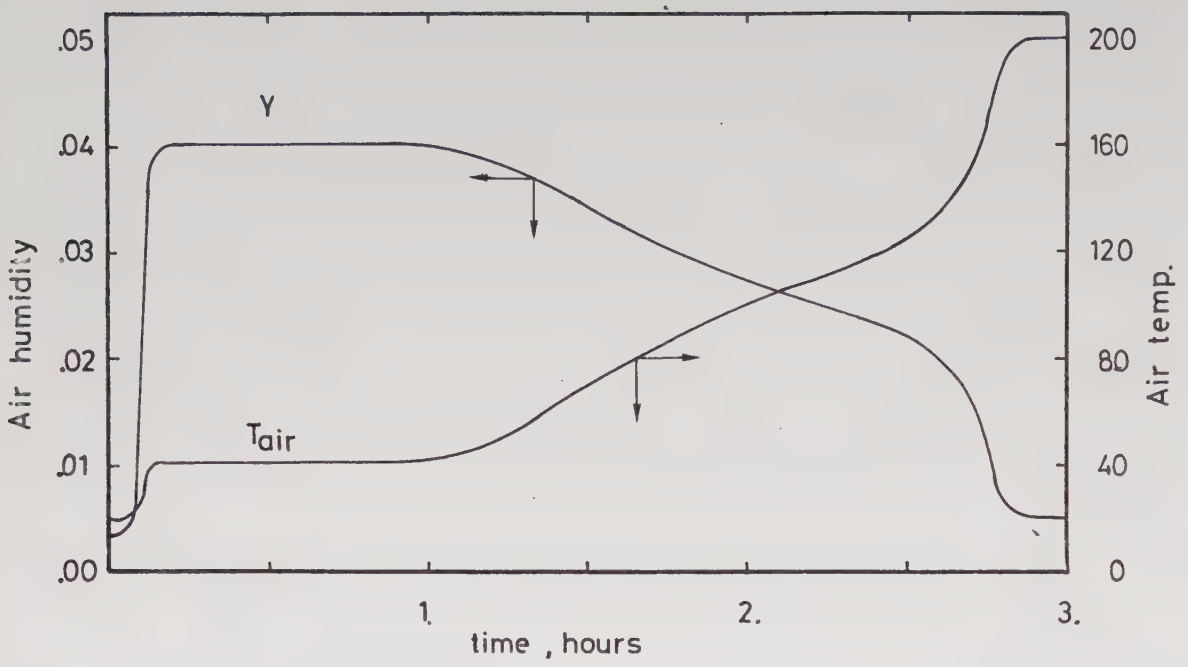

Fig. 21 Desorption: The outlet air condition from a 1.0 m bed. See also text of Fig. 19.

5 CONCLUSIONS

A number of adsorption experiments and calculations show that the adsorption kinetics of water vapour on molecular sieve particles can approximately be described by a shrinking-core model. The reason for this is the non-linear equilibrium function ($\partial^2 p^*/\partial X^2 > 0$), which during adsorption causes sharp moisture profiles in the particle. The internal mass transport coefficient β_i of Eq. (3.23) was determined by experiments to $6.6 \cdot 10^{-4}$ m/s (at 20°C) for the investigated molecular sieve pellets.

In desorption, the shape of the isotherms results in a rather steep moisture profile near the surface of the particle while rather flat inside the particle. This also means that the magnitude of the desorption rate is less than the adsorption rate for corresponding humidity changes. The approximate desorption model (Eq. (4.2)) assumes vapour diffusion from a core of average moisture content through a hypothetical shell of dry material to the air bulk. In experiments and calculations it has been shown that the approximate model underestimates the desorption rate at high moisture contents and overestimates it a little at lower moisture contents. Since the lower desorption rates (at lower moisture contents) determine the time of regeneration, the mass transfer coefficient has been chosen so a good description of this region was achieved. The "lumped" β-value was determined to 0.0035 m/s (at 20°C).

The equilibrium function is favourable for adsorption i.e. "constant-pattern" profiles are developed in a bed during adsorption. In a bed during isothermal desorption, the moisture profiles become flatter and flatter since the same isotherms are unfavourable for desorption. If, however, hot air is used for regeneration, the temperature rise of the particle increases the equilibrium vapour pressure and consequently the desorption rate. At lower moisture contents of the real p^*-X curve in the non-isothermal desorption, $\partial^2 p^*/\partial X^2$ is less than zero. A constant-pattern behaviour was also found in this moisture region.

The comparison between calculations and experiments also show that the difference between adsorption and desorption behaviour is caused by the non-linear isotherms rather than by any differences in the mass transport mechanisms.

In this investigation, only macropore diffusional resistance has been considered. If diffusional resistance in the micropores of the zeolites had also been important this would have caused a greater difference between calculations and experiments. However, if only micropore diffusional resistance is rate-controlling approximately the same sorption curves would have been obtained. Other investigations[11] with different sizes of pellets, however, show that vapour diffusion in the macropores is rate-controlling.

NOTATION

a_v	specific surface area	m^2/m^3
Bi_h	Biot number for heat transfer, $\alpha R/\lambda$	
c_p	specific heat	J/kg K
D	diffusivity	m^2/s
D_{liq}	effective adsorbed phase diffusivity	m^2/s
D_{vap}	effective vapour phase diffusivity	m^2/s
E	degree of saturation or dryness	
Fo_h	Fourier number for heat transfer, $\lambda t/(\rho c_p R^2)$	
L	cylinder length	m
$\dot{m}$	mass flux	kg/m^2s
$\dot{m}_{liq}$	mass flux of water in the adsorbed phase	kg/m^2s
$\dot{m}_{vap}$	mass flux of water in the vapour phase	kg/m^2s
m	exponent in Eq. (2.4)	
M	molecular weight	kg/kmole
n	exponent in Eq. (2.2)	
p	water vapour pressure	Pa (N/m^2)
p_{air}	water vapour pressure in the external air bulk	Pa (N/m^2)
P_{tot}	total gas pressure	Pa (N/m^2)
r	length coordinate in particle	m
R	characteristic length of particle	m
R_o	gas constant	J/kmole K
t	time coordinate	s
T	temperature	^oC
T_{air}	temperature of the external air bulk	^oC
X	moisture content (dry basis)	kg/kg
Y	air humidity (dry basis)	kg/kg

α	heat transfer coefficient	W/m^2K
β	mass transfer coefficient	m/s
ΔH_o	heat of sorption	J/kg
Δr	length step	m
Δt	time step	s
ε	porosity	
η	dimensionless length coordinate in particle, see Eq. (2.4)	
λ	heat conductivity	W/m K
ρ	density	kg/m^3

Subscripts

b	bed
c	core
e	external
i	interface or internal
o	initial or reference
p	particle
s	solid
v	vapour
w	adsorbed water
∞	infinite

Superscripts

*	equilibrium
-	average in particle
=	average in bed

REFERENCES

1. Werling K., *First International Symposium on Drying*, Science Press Princeton 1978

2. Werling K. and Wimmerstedt R., Accepted for publication in *Chem. Engng Sci.* 1980

3. Ruthven D.M., Garg D.R. and Crawford R.M., *Chem. Engng Sci.* 1975 30 803

4. Garg D.R. and Ruthven D.M., *Chem. Engng Sci.* 1973 28 791

5. Garg D.R. and Ruthven D.M., *Chem. Engng Sci.* 1973 28 799

6. Garg D.R. and Ruthven D.M., *AIChE Journal* 1975 21 200

7. Kast W. and Jokisch F., *Chem. Ing. Techn.* 1973 45 538

8. Dengler W. and Krückels W., *Chem. Ing. Techn.* 1970 42 1258

9. Krückels W., *Chem. Engng Sci.* 1973 28 1565

10. Carter J.W., *Trans. Instn chem. Engrs* 1966 44 T253

11. Carter J.W. and Barret D.J., *Trans. Instn chem. Engrs* 1973 51 75

12. Sherwood T.K., Pigford R.L. and Wilke C.R., *Mass Transfer*, McGraw-Hill New York 1975

13. Garg D.R. and Ruthven D.M., *AIChE Journal* 1973 19 852

14. Zwiebel I., Gariepy R.L. and Schnitzer J.L., *AIChE Journal* 1972 18 1139

15. Ruthven D.M. and Derrah R.I., *Can. J. Chem. Engng* 1972 50 743

16. Vermeulen T. and Klein G., *AIChE Symp. Ser. No. 117*, 1971 67 65

17. Nordon P., *Int. J. Heat Mass Transfer* 1964 7 639

18. Carter J.W., *AIChE Journal*, 1975 21 380

19. Krischer O. and Kast W., *Die Wissenschaftlichen Grundlagen der Trocknungstechnik*, 3 ed., Springer-Verlag 1978

20. Carslaw H.S. and Jaeger J.C., *Conduction of Heat in Solids*, Oxford Univ. Press 1959

21. Crank J., *The Mathematics of Diffusion*, Oxford Univ. Press 1975

22. Schlünder E.U., *Chem. Ing. Techn.* 1976 3 190

23. Zabeschek G., Dissertation, University of Karlsruhe 1977

24. Keey R.B. and Suzuki M., *Int. J. Heat Mass Transfer* 1974 17 1455

25. Garside J., Lord L.W. and Reagan R., *Chem. Engng Sci.* 1970 25 1133

26. Hallstöm A., To be reported, Dept. of Chem. Eng., Lund Institute of Technology 1980

27 Getty R.J. and Armstrong W.P., *Ind. Engng Chem., Process Des. Develop.* 1964 3 60

28. Cooney D.O., *Ind. Engng Chem., Process Des. Develop.* 1974 13 368

29. Garg D.R. and Ruthven D.M., *Chem. Engng Sci.* 1975 30 1192

IV

CODEN: LUTKDH/(TKKA-3004)/1-19/(1980)

THE DRYING OF A CRYSTALLINE ORGANIC MATERIAL - A CASE STUDY

KENNETH WERLING

DEPARTMENT OF CHEMICAL ENGINEERING
LUND INSTITUTE OF TECHNOLOGY
LUND
SWEDEN

Dokumentutgivare
Lund Institute of Technology
Department of Chemical Engineering

Handläggare
R. Wimmerstedt

Författare
K. Werling

Dokumentnamn
Report

Utgivningsdatum
February 1980

Dokumentbeteckning
LUTKDH/(TKKA-3004)
/1-19/(1980)

Ärendebeteckning

Dokumenttitel och undertitel

The Drying of a Crystalline Organic Material - A Case Study

Referat (sammandrag)

Abstract (IV)

The drying of a wet filter cake of fine crystals in a vibrated fluid bed dryer was studied both in a small-scale batch dryer and in an industrial plant. The experiments showed that only surface moisture existed. Clogging problems of the dried product were caused by a by-product with the melting point 60°C, rather than by water. The bed had to be vibrated properly and a certain pressure drop over the distributor plate was needed in order to reduce channelling. The amount of entrained material increased rapidly as the bed became drier. A literature review is also included.

Referat skrivet av
author

Förslag till ytterligare nyckelord

vibration, entrainment

Klassifikationssystem och -klass(er)

Indextermer (ange källa)

Omfång
26 pages

Övriga bibliografiska uppgifter

Språk
English

Sekretessuppgifter

ISSN

ISBN

Dokumentet kan erhållas från
Department of Chemical Engineering
Chemical Center, POB 740,
S-220 07 LUND 7, Sweden

Mottagarens uppgifter

Pris

DOKUMENTDATABLAD enligt SIS 62 10 12

Blankett LU 11:25 1976–07

SUMMARY

The drying of a crystalline organic material in a fluid bed dryer has been studied both in a small-scale batch dryer and in an industrial plant. Some problems with the industrial dryer were:

- The dried material had tendencies to agglomerate and clog the product transporting system.
- The heat demand was too high (≃ 5 kg steam/kg evaporated water).
- The capacity of the dryer was too low.
- The amount of fines to the bag filters was too high.

Before this investigation it was believed that remaining water in the product caused the clogging problem and therefore the product was over-dried in order to reduce this water as much as possible. This report shows instead that an organic by-product is the most probable cause of the clogging. As the temperature of the dried material should not exceed the meltingpoint of this component (≃ 60°C) the heat demand can be lowered significantly.

The low capacity of the dryer was found to be caused by clogged holes and cracks in the perforated plate. Also the shaking movement of the dryer seemed not to be efficient enough to transport and distribute the material as stationary zones of material were observed.

Several small-scale drying experiments were conducted. These showed that, with proper vibrating (to reduce channelling), even a bed of 20-30 mm in height produces an almost fully saturated outlet air, until the moisture content of ≃ 0.6% is reached in the bed. The wet bed is not fluidizable and the amount of carry over in the first part of the drying is therefore low. The entrainment rate then increases as the bed becomes drier and bubbles are formed. In the industrial dryer the amount of entrained material is approximately twice of what was found in the small-scale tests. The main reason for this is that the industrial dryer has less space above the bed where coarse particles are allowed to settle.

A literature review over some problems encountered in dimensioning flui bed dryers is also given.

CONTENTS

1.	INTRODUCTION	1
2.	DESCRIPTION OF THE INDUSTRIAL DRYING SYSTEMS	2
	2.1 The drying system of 1977	2
	2.2 The drying system of 1979	3
3.	EXPERIMENTAL FINDINGS	5
4.	A LITERATURE SURVEY OF SOME PROBLEMS OFTEN ENCOUNTERED IN THE DESIGN OF A CONTINUOUS FLUID-BED DRYER, COMPARED WITH OWN OBSERVATIONS OF THESE PROBLEMS	10
	4.1 Distributor plate	10
	4.2 Vibrations	12
	4.3 Residence time - mixing	13
	4.4 Heat and mass transfer in fluidized beds	15
	4.5 Entrainment of solids	15
5.	CONCLUSIONS	17
6.	RECOMMENDED FURTHER INVESTIGATIONS	18
	REFERENCES	
	TABLES	

1. INTRODUCTION

The goal of this investigation has been to make preliminary studies of the fluid-bed drying of a crystalline material. The objective of the whole project, to which this investigation belongs, is to learn more about the dimensioning and the actual operation of dryers in order to minimize energy consumption and product damage. The outlines of the project are as follows: First to study the drying kinetics in a small-scale batch dryer. The mechanical transport of the material in the dryer will then be studied in a pilot-plant dryer, which is presently under construction, and together with the knowledge of the drying kinetics a model for the whole dryer can be set up. The model will then be used to simulate different drying conditions in order to optimize the new dryer. The model will of course be tested for some conditions in the pilot-plant dryer and finally scale-up problems can be studied comparing the model, the pilot-plant dryer and an industrial dryer.

This report describes some small-scale drying experiments together with two industrial dryers for drying the crystalline material. A literature review over problems encountered in operating a fluid-bed dryer is also given.

The material investigated is an organic crystalline material (particle diameter 100-700μ). The wet material enters the industrial dryer as a filter cake with a water content of 10-20% (dry basis).

2. DESCRIPTION OF THE INDUSTRIAL DRYING SYSTEMS

In 1977 an energy investigation over some dryers was carried out. The investigation included the drying of this material and some data of the 1977 dryer can be found in section 2.1. As a result of increased production this dryer was later replaced with a dryer of another make. Data for the new dryer are given in section 2.2.

2.1 The drying system of 1977

Figure 1 presents some of the most important data for the dryer. The data given are normal values based on several measurements. The moisture content of the material leaving the vacuum belt filter varies considerably between 10 and 20%, depending on available vacuum, filter cake thickness and size of the crystals, as determined by the conditions earlier in the process line.

The dryer is of a so called fluid-bed type with vibrators (17 Hz) to transport the material through the dryer. The effective area of the dryer is 6×0.8 m and the thickness of the fluidized bed is approximately 0.18 m. The temperature of the outlet air controls the amount of steam supplied to the air heater. Normally the steam valve was fully open.

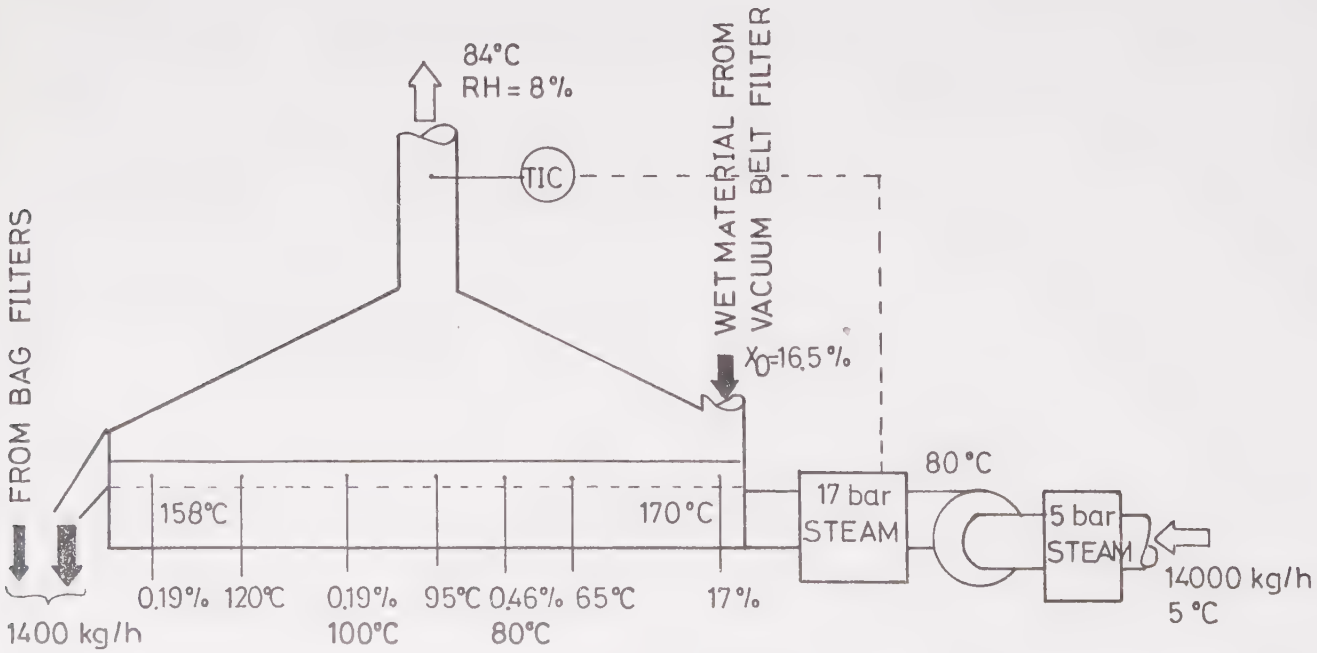

Fig. 1 The drying system of 1977

Some interesting things can be derived from Figure 1.

- The steam consumption is high (approx.5kg steam/kg evaporated water).
- The material reaches the moisture content of 0.5% already after one third of the continuous dryer.
- The temperature of the material rises slowly towards the end of the dryer, indicating considerable heat transport counter-current the drying material.

As a result of the investigation the outlet air temperature was set to a lower value ($60^{o}C$) resulting - together with better insulation of the dryer - in a 30% reduction in steam consumption. As this did not affect the agglomeration properties of the dry material, the outlet temperature was soon set back to the previous temperature.

2.2 The drying system of 1979

As a consequence of increased production the previous dryer was replaced. Figure 2 gives some measured data of the new dryer. Most of these data change considerably with time, so the data given should only be regarded as average values over a short length of time.

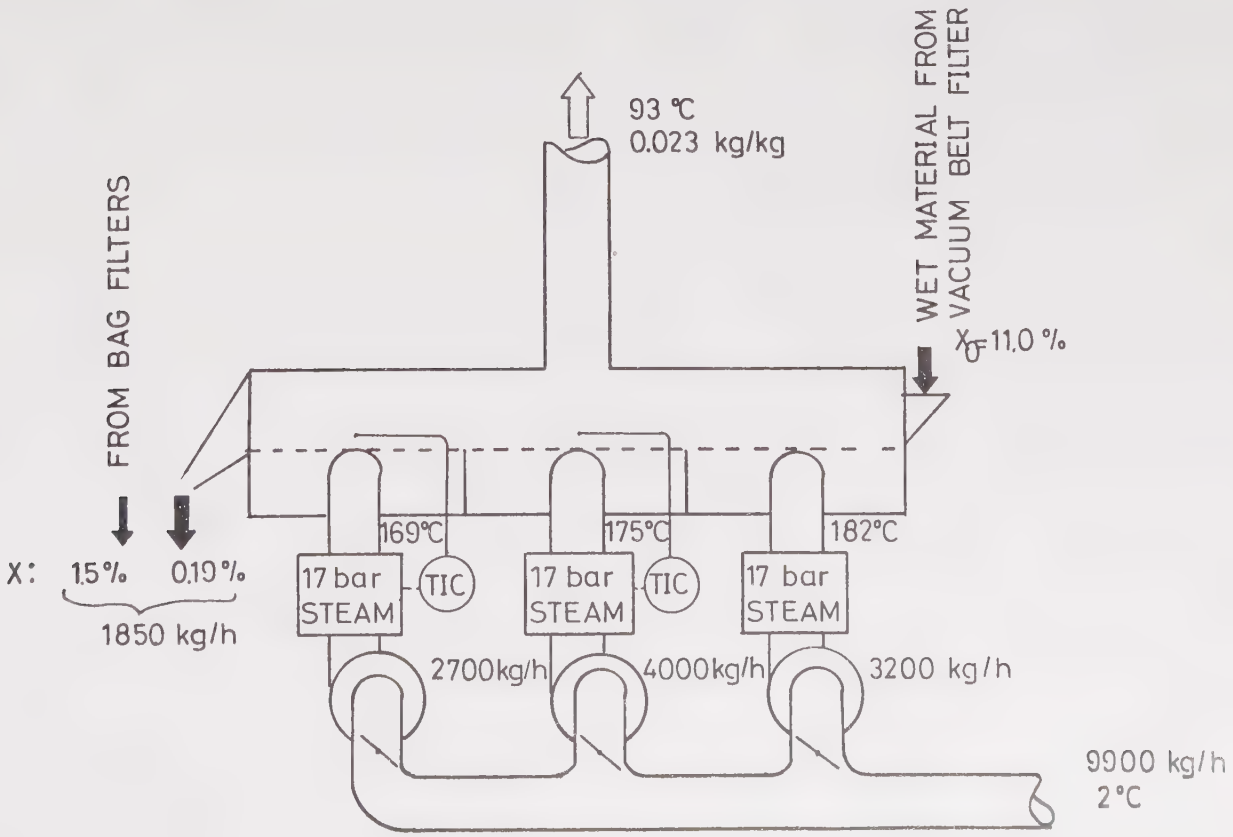

Fig. 2 The drying system of 1979

The basic differences with this new dryer compared to the old one are:

- The new dryer is divided into three sections with separate air supplies.

- The frequency of the vibration or shaking movement is much lower (4.5 Hz compared to 17 Hz) and the amplitude much greater (10 mm compared to approximately 1 mm).

- The bed is only 0.02 - 0.03 m in height (compared to 0.18 m).

To get a better control of the drying process, the temperature of the air over the bed in sections two and three controls the steam supplied to the air heaters. Normally the controllers were set to 90^{o}C. The effective area of the dryier is 6×1 m. The perforated plate has a total open area of 4% and the holes are 0.8 mm in diameter.

On one occasion the temperature and moisture content of the material were measured at a distance of 1 m from the material inlet. It was found that dependent on where in the cross section the samples were taken, the moisture content varied from 0.4 to 10% and the material temperature accordingly from 100 to 28^{o}C. The bad mixing of material could be explained by that stationary beds, sometimes as thick as 0.1 m, were formed due to plugged holes in the bed plate and that the shaking movement could not in itself distribute the material evenly. Sometimes even lumps of wet material reached the dryer outlet. Later, cracks in the bed plate were discovered and these could also explain the poor efficiency of the dryer.

Table 1 reveals another problem. The screen analyses show that approximately 1/4 of the material is carried away by the exhaust air and later is collected in the bag filters. This causes inefficient operation of the underdimensioned bag filters. Note also that particles with a diameter over approximately 120 µm (≃ 85%) have a terminal falling velocity over the superficial velocity of the air.

Another problem with tha bag filters is that after a couple of months of operation the bags are clogged and have to be replaced.

The problem of clogging in the product handling still exists and the steam consumption is still high.

3. EXPERIMENTAL FINDINGS

In a small-scale batch dryer (see Fig. 3) heated air was forced through a perforated plate and through a bed of wet material. The bed temperature, inlet and outlet air temperatures and outlet humidity of air were continuously recorded. It was found rather early that without vibrating the equipment, severe channelling appeared, resulting in low drying efficiency. A frequency of 16-20 Hz and an amplitude of 1-1.5 mm were found to give an even distribution of the wet material without channelling.

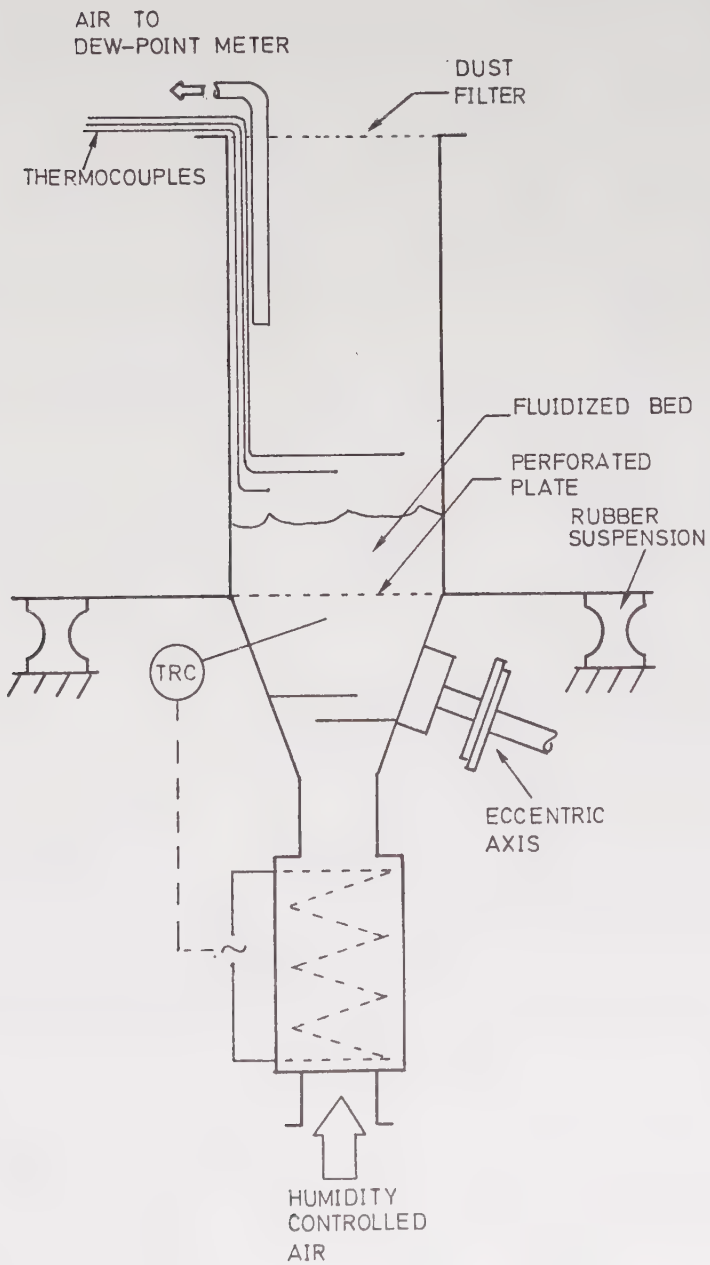

Fig. 3 The small-scale batch dryer

A number of experiments were carried out. In all experiments a perforated plate with a total open area of 1% and with holes of 0.5 mm in diameter was used. The air flow rate was varied from 0.4 to 0.8 kg/m^{2}s, the pressure drop over the perforated plate from 1.5 to 7.0 kPa, the air temperatures from 35 to 110^{o}C and bed heights from 30 to 150 mm. In all these experiments the outlet air was found to be fully saturated until a moisture content of 0.6-0.7% was reached in the bed. A typical drying curve is presented in Fig. 4. The moisture reduction was calculated from the humidity difference between outlet and inlet air. One problem was that fast changes in humidity, as happened at the critical moisture content of 0.6-0.7%, could not be detected accurately. Expressing the slowness of the dew-point meter as a first-order system with a time constant of nine seconds, gave a satisfactory description of the humidity changes for this system. A faster device utilizing infrared technique, is at the moment under development.

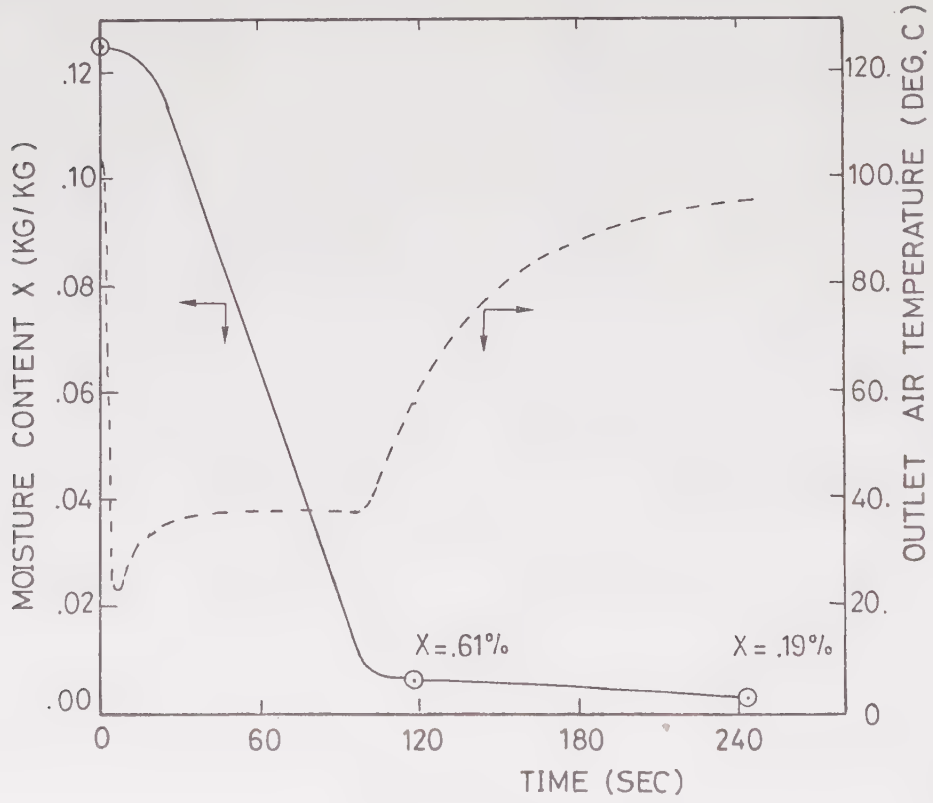

Fig. 4 A typical drying curve

A visual inspection of the bed during a drying run, showed that at moisture contents over 5%, the bed behaved more or less as a fixed bed, i.e. with low mixing of material. Sometimes a channel was formed, which due to the vibration instantly collapsed. The material around this channel was mixed and some was carried away by the air stream. The number of these channels increased as the material became drier and they were gradually

transformed to bubbles of air rising through the material. At a moisture content of approximately 2.5% all material moved around in the drying chamber due to the rising air bubbles. As the bed became drier (0.6-0.7%) dust was released. Similar observations in drying of wet sand has been reported by Kröll[1]. After that the bed reached the moisture content 0.6% the bed temperature rose and its moisture content was reduced to 0.2% after some minutes at 90°C.

The amount of entrained material was measured during three different air flow rates. The results are presented in Fig. 5 as the amount of entrained material versus the relative drying time $\tau = t/t_{cr}$ (t_{cr} is the time to reach the moisture content of 0.6%). The height of the resting, dry bed was in the three experiments 20-35 mm and the freeboard height, i.e. the distance between the upper surface of the bed and the air outlet was 0.30 m. It can be seen that during the first part, the

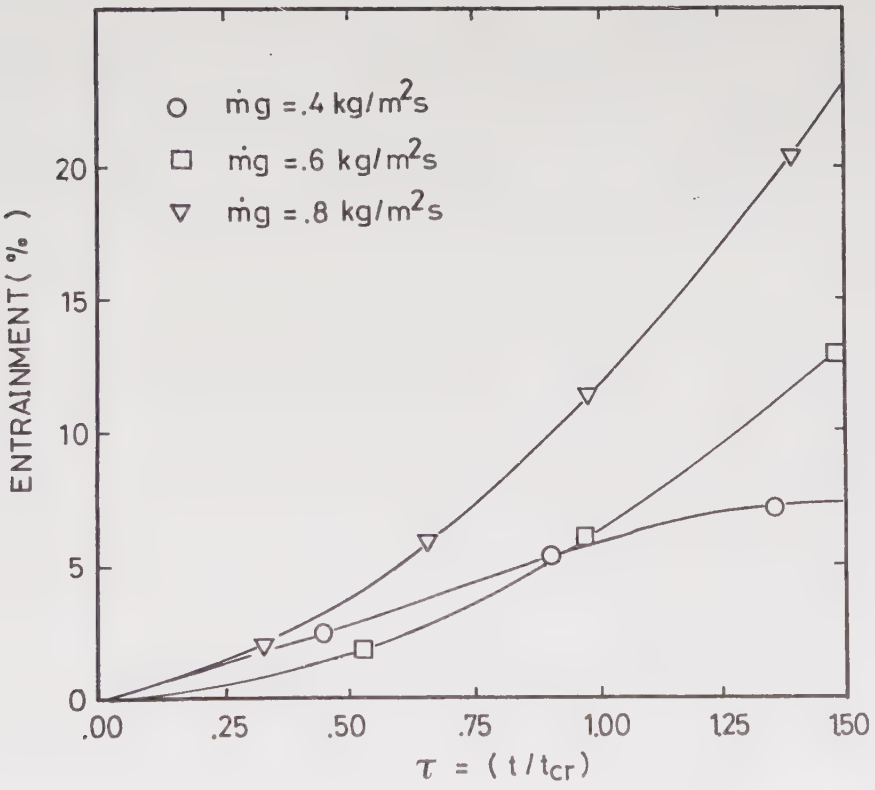

Fig. 5 Entrainment versus relative drying time, τ, with airflow rate as parameter

entrainment is low. Already at 50% moisture reduction (original moisture content 12.6%) the entrainment increases considerably with air flow rate. Finally after the t_{cr} is passed, the entrainment rate seems to be proportional to u_0^4. A rough estimate of the amounts of solids with a terminal falling velocity less than the superficial velocity for the three runs is 8, 18 and 32% respectively.

All moisture contents given so far have been determined by placing a sample of the material in an oven at 105°C for two hours. The question arose whether the slow drying rate below 0.6% moisture content could be explained by the loss of some other component than water. Tests have shown that the dry material increased less than 0.1% in weight when air of 23.5°C and 90% R.H. was forced through a bed of material for one hour. The increase in moisture content can well be explained by errors in moisture content determination, so the question about hygroscopic water could be left behind.

During the study of the industrial drying system it was noted that a waxy material had congealed on the walls beyond the bag filters. A sample of this material was analysed (by liquid chromatography) and 38% proved to consist of a relatively low-boiling by-product called CMF (M.p.: 60°C, B.p.: 144°C). Similar analysis of the separated fines gave 1.7% CMF. The temperature of the fines when sampled was 90°C and the conventional moisture determination method resulted in 1.9% moisture. Only traces of CMF could be found in a sample withdrawn from the dryer outlet, where otherwise the "moisture content" was determined to 0.2%. It is therefore believed that most of this "moisture" below 0.6% in fact consists of the organic compound CMF.

As a consequence the CMF must be the main reason for the problem of agglomerating particles. Much CMF seems to be removed in the dryer, especially in the later zones, where the bed temperature is high (up to 125°C). Much material is entrained before it loses its CMF-content and CMF probably condensates or sublimates on the bag filters, thus resulting in a rather high CMF-content of the fines. As the CMF at temperatures over 60°C is in the liquid state, small particles can easily stick to the CMF and agglomerates are formed. This also explains why the tubes, in which the material from the dryer and from the bag filters periodically is transported to the product silo, are so easily clogged. When no material flows through the tube, the tube cools down below 60°C. When material of 80-110°C is passed through, some "wet" material will stick to the walls, the CMF will freeze, and a deposit is formed. A moisture determination (in oven) of such deposit showed 2%. Unfortunately no CMF-analysis was made for this sample, but there is reason to believe that much of this "moisture" in fact is CMF.

The discussion above gives the guideline that the material and outlet air temperatures should not exceed 60°C. This necessitates a very good control of the drying process so the dryer still fulfills its duty at changing inlet conditions of the material. Another solution is to have a cooling section at the end of the dryer. This will satisfy both requirements since the outlet air temperature to the bag filters will also be substantially reduced. Tests utilizing section three of the dryer as a cooling section were conducted, but because of low drying efficiency in sections one and two this alternative had to be discarded. Table 2 gives some analyses of samples withdrawn from the dryer outlet. As a comparison Karl-Fisher determination of water has also been included. As the material does not dissolve in such an analysis, the technique only analyzes surface water.

4. A LITERATURE SURVEY OF SOME PROBLEMS OFTEN ENCOUNTERED IN THE DESIGN OF A CONTINUOUS FLUID-BED DRYER, COMPARED WITH OWN OBSERVATIONS OF THESE PROBLEMS

The basic ideas behind fluid-bed dryers can be found in several textbooks[1-4]. Here some of the problems in fluid-bed dryer design will be discussed in more detail. Where possible, the literature will be compared with the experience from the studied dryers.

Some of the advantages and disadvantages with fluid-bed dryers are summarized below.

Advantages:

- High drying rates per drying volume. This is also true for pneumatic or flash dryers.
- Low capital costs compared to many other dryers. (Also true for flash dryers.)
- The residence time of the material in the dryer can be chosen relatively freely (in contrast to flash dryers).
- The temperature of the material is uniform. This is essential for heat sensitive products, which in this dryer can be processed with high inlet air temperatures.
- Gentle handling of product in comparison to such dryers as flash or rotary dryers.

Disadvantages:

- High pressure drop. However, some energy supplied to fans is recovered as heat to the drying process.
- The residence time distribution curve can be wide. The curve can be narrowed by internal baffles or using a more shallow bed.
- The carry-over or entrainment can be severe.

4.1 Distributor plate

Although very sophisticated distributor systems sometimes have been used, this section will only discuss the perforated plate. However, much of the

discussions will be applicable to those types as well.

In almost all fluid-bed systems, where particles are fluidized with a gas, a so-called aggregative or bubble fluidization occurs. In this type of fluidization it is believed that all air in excess of that required to fluidize the material will pass in form of bubbles. This means that on the distributor plate bubbles are formed. How bubbles are generated and how they rise are discussed by Zenz[5]. The bubbles form because the air input is greater than what can be passed through the interstices at a frictional resistance less than the bed weight. As a consequence a bubble of air grows until the surface of the walls of the void have increased in size to a degree that corresponds to the incipient fluidization velocity. Further air input will decrease the interface velocity below the incipient and, as a consequence, the walls cave in and cut off the void. As solids slide down, the bubble of air rises. Bubbles grow by merger as they rise through the bed.

The primary role of the distributor plate is to ensure a good air distribution through the bed. The distributor also influences the initial bubble size and this can have an effect on shallow beds[2].

Kunii & Levenspiel[3] claim that for fine solids a well-designed distributor should also act as a stirrer to increase the mixing and reduce channeling tendencies. The aurthors suggest that the kinetic energy of orifice jets should be 50-75% of the resistance of the bed weight. A high kinetic energy is also important to prevent fine solids from falling through the distributor and to prevent clogging of the holes.

Some authors[2,4] state that the resistance should be in the same order as that of the bed to maintain a good air distribution. Even if a channel is created in the bed or when a section of the distributor plate becomes free, the velocity of the air through the other distributors should not fall below the incipient fluidization velocity.

Agarwal et. al.[6] recommend a minimum pressure drop over the plate of about 3.5 kPa. The authors have made studies of the drying of fine coal powder

within a shallow fluidized bed.

Howmand et. al.[7] describe a theory based on experimental work. The theory is based on the observation that only certain holes generate bubbles. The number of active holes increases with increasing pressure drop over the plate, but their analysis also includes the dependence of distance between holes and particle diameters. When calculating the pressure drop over their perforated plates - according to Perry[8] - 3-10 kPa is needed to "activate" more than 90% of all holes.

It can therefore be concluded that, for many materials, a pressure drop over the plate corresponding to the weight of the shallow bed is often enough. Higher pressure drops or other means such as vibrations can be needed when the material easily sticks together or when the holes are easily clogged. To increase the mixing and transport of material, inclined holes have sometimes been used.

The dryer of 1977 had a pressure drop of 4 kPa (originally 2 kPa) with a bed height of 0.18 m. The new dryer has a bed height of 25 mm and a pressure drop over the plate of appr. 0.15 kPa.

4.2 Vibrations

The main purpose in applying vibrations to a dryer is to transport the material[1,9,10]. As a consequence the air rate can be chosen more freely, without affecting the transport rate. When processing a material with wide particle distribution, the air rate can be lowered to minimize entrainment of solids. The vibrations transport and also maintain the particles separated. In a continuous shallow bed dryer the vibrations should also distribute the material evenly over the cross-section.

Another important purpose, as I also noted in my own experiments, is to reduce channelling. This tendency is very pronounced when handling finely divided materials.

Vance[11] mentions a drying process where an unfluidizable centrifuge cake is partly dried in a vibrated plug-flow fluid bed dryer to a fluidizable condition.

Usually the whole dryer is vibrated, but vibrating elements consisting of a frame with cross bars inserted in the bed have also been used[4].

The transporting properties of the vibrations are hard to define theoretically, but Kröll[1] defines a throwing number Γ as:

$$\Gamma = \hat{x} \, (2 \pi f)^2 \sin\beta / g$$

where $\hat{x}$ is the amplitude, f = frequency, β = the direction of impact (normally 20-45°) and g = gravity (9.81 m/s^2). For sliced material Γ should be close to 3.3, whereas for attrition sensitive materials Γ should be around 1.

The dryer of 1977, earlier described, had a frequency of approximately 17 Hz. This frequency was found in the small-scale drying experiments to eliminate channelling and to distribute the wet material evenly over the perforated plate. The new dryer has a rather low frequency of 4.5 Hz. The amplitude is 10 mm and the throwing angle is as high as 70°. The throwing-number then will be 0.77. As discussed earlier it was found that this vibrating or shaking movement could not transport and distribute the material satisfactorily without air support. Looking into the first section of the dryer, where the material was still wet enough not to fluidize, it could be seen that the whole bed was thrown upwards when it fell back by gravity, the air forced it to crack up into smaller pieces.

4.3 Residence time - mixing

The effective mixing of particles in a fluid-bed dryer is the main reason for high heat and mass transfer, temperature equalization etc. In bubble fluidization, particles in the bubble wakes are carried upwards to the surface of the bed, and as a consequence there is a general motion downwards of material in the surrounding dense phase. The degree of mixing increases with velocity i.e. with amount of bubbles flowing through the bed. It should also be noted that the degree of vertical mixing is much higher than the degree of horizontal mixing.

However, the horizontal mixing might be troublesome since this causes a wide residence time spectrum. To narrow the residence time distribution curve from that of an ideal mixing tank, the material is often

dried in a shallow bed.

The continuous dryer is often rectangular in shape and has internal weirs to further narrow the residence time spectrum. Less common is to divide the bed into stages, or to place perforated baffles, sieves or louvres horizontally in the upper portion of the bed. The latter arrangement also reduces the amount of carry-over.

As a result of the fluid behaviour, the mixing of solids also transports the material, but with vibration - to carry out the transport - the air flow can be reduced and thus the control of the residence time can be improved[10].

Many attempts have been made to describe the mixing of solids and thus describe the residence time distribution. The most simple model is that of ideal mixed tank or tanks in series. When all tanks have the same volume, the residence time distribution is as follows:

$$E(t) = \frac{1}{(n-1)!} \frac{t^{n-1}}{T^n} \exp(-t/T)$$

where $E(t)dt$ is the fraction of solids with a residence time between t and t+dt, n is the number of idealised tanks and T is the mean residence time for one tank.

Roeder and Skerhut[12] point out that a model with tanks in series could be applied successfully for long fluid beds. They also state that in cases of bad air distribution the main portion of material leaves the dryer before the mean residence time. Weirs in the dryer were found to narrow the spectrum. It was also found that air pulsation of 20 Hz narrowed the residence time spectrum.

The dispersion model for backmixing has also been used to describe the mixing of solids in a fluid-bed. The change in concentration of a tracer, C_a, is then supposed to follow:

$$\frac{\partial C_A}{\partial t} = D \frac{\partial^2 C_A}{\partial z^2}$$

where D is a "particle" diffusivity, t is the time coordinate and z the length coordinate.

Some state that the dispersion model for backmixing should not be used for bubbling fluidized beds[2], whereas others have had good experimental results. Reay[13] has made some experiments on a shallow bed (0.1 m) and concludes that the longitudinal mixing can be described with a Fickian diffusion process. The particle diffusivity was found to increase with increasing air flow and decreasing particle diameter.

More about mixing models can be found in textbooks by Kunii & Levenspiel[3] and Levenspiel[14]. Experimental findings on the mixing of dry materials in a fluid-bed have been reported by several authors[2,3,13].

In a real dryer the wet material might not even be fluidizable, so the mixing in the first part is negligible. The mixing then increases as the material becomes drier, as also was noted in own experiments.

4.4 Heat and mass transfer in fluidized beds

As a consequence of effective mixing and high heat and mass transfer, temperature equilibration is often reached within a few centimeters of the bed. Experimental data on heat and mass transfer properties - expressed as Nu and Sh-correlations - have been reported by Kunii & Levenspiel[3] and Schlünder[15].

The mixing also explains the high longitudinal "heat conductivities" reported in literature. Peters et. al.[16] report such heat conductivities approximately three to five times greater than that for silver. Such heat conductivities are also discussed by Davidson & Harrison[2].

Due to the movement of particles also the heat transfer to the walls is substantial. This aspect is dealt with by Kunii & Levenspiel[3]. This effect definitely plays an important role when comparing a drying process in a pilot plant dryer to one of industrial size.

4.5 Entrainment of solids

The entrainment or carry-over of solids is due to two processes. First is the elutriation of fine solids, which can be carried away since their terminal falling velocity is less than the air velocity.

When the bubbles of air reach the surface of the bed, they project agglomerates of particles into the space above the bed. With increased air flow this action becomes more violent. Kunii & Levenspiel[3] define a "transport disengaging height" TDH over the bed where the concentration of the coarse solids transported by this second process is zero. When bubbles burst at the surface, sharp velocity fluctuations above the bed have been noted. These fluctuations dissipate with height and the gas velocity approaches to the average velocity at TDH. This also explains why a grid over the bed reduces the amount of carry-over, as such grids smooth out the velocity fluctuations.

Theory and experimental findings of entrainment in general can be found in Kunii & Levenspiel[3]. Interesting to note is that the entrainment rate has been found to be proportional to the air flow rate raised to the power of four. Hanesian[17] has investigated a system of two particle sizes and found that the entrainment could be described as two first-order systems.

The entrainment experiments described earlier resulted in little entrainment with wet material. The entrainment rate then increased rapidly with air flow rate as the bed became drier and the first air bubbles were created. For the dry material it was shown that the entrainment rate increased with air flow rate approximately to the power of four. In the industrial dryer the space above the bed seems to be too small to let larger particles (which are thrown upwards due to the bursting action of the bubbles) settle. At this air flow rate (0.47 kg/m^2s) the amount of carry-over would theoretically be around 14% compared to the 25% measured.

5 CONCLUSIONS

From the investigations carried out it can be concluded that:

- The problems with agglomerates in the product handling are not due to remaining water in the nonhygroscopic material but to an organic by-product with low melting point ($\simeq 60^{o}C$).

- The energy consumption can therefore be significantly lowered from the present value. Before this investigation the policy was to achieve as high a material temperature as possible at the dryer outlet in order to reduce remaining water. The discovered importance of the by-product component indicates that the product and outlet air should be kept below $60^{o}C$. The highest possible limit (fully saturated outlet air) would give energy savings of up to 56%. A more practical value would be 37% (2600 tonnes steam per year). This latter value has been estimated for a dryer with a maximum capacity double the needed capacity in Fig. 2, to account for changing solid flows and moisture contents. The outlet air temperature is assumed to be $60^{o}C$.

- Several visual inspections state that the slow shaking movement (4.3 Hz, amplitude $\simeq$ 10 mm) can not transport the wet or dry material satisfactorily, whereas experiments at 20 Hz (amplitude: 1-1.5 mm) indicate achieving this.

- It is still unclear if the needed pressure drop over the perforated plate has to be much in excess of that of the bed. However, a high pressure drop (as a larger hole diameter) reduces the tendency to clog the holes.

- Much of the carry-over is due to the bursting action of bubbles at the surface of the bed and can be reduced significantly with a higher freeboard and/or an expanding cross section over the bed, where these particles can settle.

6 RECOMMENDED FURTHER INVESTIGATIONS

Further investigations should be carried out in a pilot-plant dryer. Such a dryer is under construction at the Dept. of Chem. Engineering, Lund. Some interesting fields of investigation are given below.

Vibration and distributor plate. These must be chosen to achieve good material and air distribution if the results from the pilot-plant dryer are to be used together with a mathematical model to describe the changing conditions in an industrial plant. Lumps of agglomerates or heaps of material will cause nonstationary results. This is difficult to treat theoretically, but some guidelines for choosing are given in this report and in the references.

Heat conductivity of the fluid-bed. During studies of the industrial dryer, it was revealed that much heat must be transported to the wet material from the warmer dry bed. For this type of material it might be enough to add a longitudinal heat conductivity expression to the normal heat balance of a batch fluid-bed. In the vertical direction the solids can be assumed to be completely mixed. As this "bed heat conductivity" depends on the degree of mixing, it will have a strong dependence on moisture content and airflow. Measurements of temperature and moisture profiles along the bed of the dryer at steady-state conditions would give such information. The air flow rate dependence can be fitted to a correlation described by Kunii-Levenspiel[3].

Residence time distribution. The high heat conductivity in the bed causes the wet particles to dry at a temperature above the wet-bulb temperature. If a still-wet particle is thrown to a bed of warm material, the temperature of that particle will rise and a higher driving force for drying is achieved. This means that particles with a short residence time will have higher drying rates than particles with a long residence time.

The residence time distribution at different distances from the wet material inlet and the influence of weirs and baffles on the distribution curve will explain much of this drying behaviour.

Entrainment. If the entrainment is large this must be accounted for in the mathematical model of the dryer. It has also a great importance when

comparing costs of increasing dryer size to the separation costs. Entrainment experiments can for example be carried out in a small-scale batch dryer with continuous weighing of the entrained solids. Special care must be taken to have the same height of space above the bed as expected in the final dryer.

Multi-stage drying. In the different stages, the inlet air temperatures, air velocities, and bed heights can be changed to optimize the dryer. In a three-stage fluid bed dryer, the air flow can be high in the first section as the entrainment from the wet bed is low. The outlet air temperatures of the last stage (or stages) can control the heat supplied to further improve the energy economy.

REFERENCES

1. Kröll, K., Trocknungstechnik; Trockner und Trocknungsverfahren, Springer-Verlag, Berlin 1978.

2. Davidson, J.F. and Harrison, D., Fluidization, Academic Press, London 1971.

3. Kunii, D. and Levenspiel, L., Fluidization Engineering, John Wiley & Sons, New York 1969.

4. Vaněček, W. et. al., Fluidized Bed Drying, Leonard Hill, London 1966.

5. Zenz, F.A., Chem Engng., p. 81-91, Dec. 19 1977.

6. Agarwal, J.C. et al., Chem. Engng. Progr., Vol. 58, No. 11, p. 85-90, 1962.

7. Howmand, S. et. al., Trans. Instn. Chem. Engrs., Vol. 49, p. 149-162 1971.

8. Perry, R.H. and Chilton, C.H., Chem. Eng. Handbook 5 ed., p.5:34, McGraw-Hill, New York, 1973.

9. Davenport, D., Process Engng.,p. 55, March 1975.

10. Danielsen, D. and Hovmand, S., Paper presented at 1st Int. Symp. on Drying, Montreal 1978.

11. Vance, S.W. and Lang. R.W., Chem. Eng. Progr., Vol. 66, No. 7, p. 92-3 1970.

12. Roeder, H. and Skerhut, R., Chemie-Ing.-Techn., Vol. 45, No. 22, p. 1321-2, 1973.

13. Reay, D., 1st Int. Symp. on Drying, p. 136-144, Science Press, Princeton, 1978.

14. Levenspiel, O., Chemical Reaction Engineering, John Wiley & Sons, New York, 1962.

15. Schlünder, E.U., Chem. Engng. Sci., Vol. 32, p.845-851, 1977.

16. Peters, K. et. al., Chemie-Ing.-Techn., Vol. 25, No. 6, p. 313-6, 1953.

17. Hanesian, D. and Rankell, A., Ind. Eng. Chem. Fundamentals, Vol. 7, No. 3, p 452-8, 1968.

ASTM Mesh	D_p, mean (µm)	Dryer outlet [1] (%)	Bag filter [1] outlet (%)	Final [2] product (%)
+ 18		2.6	0.2	1.3
18/35	750	16.7	0.9	10.3
35/70	356	68.6	27.1	61.3
70/140	159	10.9	62.5	21.0
140/200	90.5	0.9	8.1	4.0
200/270	64	0.2	1.0	1.4
- 270		0.1	0.4	0.9

Table 1: Particle diameter distribution.
[1] Average of 5 samples.
[2] Average of 2 samples.

	CMF-content (%)	Moisture content (%)		CMF-content after oven method
		Karl-Fisher method	oven method	
3 drying zones	0.5	0.2	0.4	0.3
2 drying zones + 1 cooling zone	0.7	0.5	0.8	0.3

Table 2: Analysis of two samples from the dryer outlet.